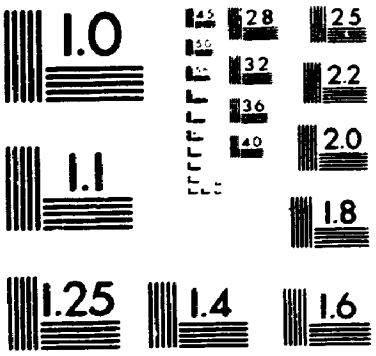

FATIGUE CRACK GROWTH AND COALESCENCE STUDY

by

HONG ZHANG

A thesis submitted to
the Faculty of Graduate Studies and Research
in partial fulfilment of
the requirements for the Degree of
Master of Engineering

Ottawa-Carleton Institute of Mechanical and Aerospace Engineering
Department of Mechanical and Aerospace Engineering
Carleton University
Ottawa, Ontario
August, 1993

ISBN 0-315-89900-X

Name HONG ZHANG

Dissertation Abstracts International is arranged by broad, general subject categories. Please select the one subject which most nearly describes the content of your dissertation Enter the corresponding four-digit code in the spaces provided

Engineering (Mechanical) — SUBJECT TERM

0548 — SUBJECT CODE

U·M·I

Subject Categories

THE HUMANITIES AND SOCIAL SCIENCES

COMMUNICATIONS AND THE ARTS

Architecture	0729
Art History	0377
Cinema	0900
Dance	0378
Fine Arts	0357
Information Science	0723
Journalism	0391
Library Science	0399
Mass Communications	0708
Music	0413
Speech Communication	0459
Theater	0465

EDUCATION

General	0515
Administration	0514
Adult and Continuing	0516
Agricultural	0517
Art	0273
Bilingual and Multicultural	0282
Business	0688
Community College	0275
Curriculum and Instruction	0727
Early Childhood	0518
Elementary	0524
Finance	0277
Guidance and Counseling	0519
Health	0680
Higher	0745
History of	0520
Home Economics	0278
Industrial	0521
Language and Literature	0279
Mathematics	0280
Music	0522
Philosophy of	0998
Physical	0523
Psychology	0525
Reading	0535
Religious	0527
Sciences	0714
Secondary	0533
Social Sciences	0534
Sociology of	0340
Special	0529
Teacher Training	0530
Technology	0710
Tests and Measurements	0288
Vocational	0747

LANGUAGE, LITERATURE AND LINGUISTICS

Language	
General	0679
Ancient	0289
Linguistics	0290
Modern	0291
Literature	
General	0401
Classical	0294
Comparative	0295
Medieval	0297
Modern	0298
African	0316
American	0591
Asian	0305
Canadian (English)	0352
Canadian (French)	0355
English	0593
Germanic	0311
Latin American	0312
Middle Eastern	0315
Romance	0313
Slavic and East European	0314

PHILOSOPHY, RELIGION AND THEOLOGY

Philosophy	0422
Religion	
General	0318
Biblical Studies	0321
Clergy	0319
History of	0320
Philosophy of	0322
Theology	0469

SOCIAL SCIENCES

American Studies	0323
Anthropology	
Archaeology	0324
Cultural	0326
Physical	0327
Business Administration	
General	0310
Accounting	0272
Banking	0770
Management	0454
Marketing	0338
Canadian Studies	0385
Economics	
General	0501
Agricultural	0503
Commerce Business	0505
Finance	0508
History	0509
Labor	0510
Theory	0511
Folklore	0358
Geography	0366
Gerontology	0351
History	
General	0578
Ancient	0579
Medieval	0581
Modern	0582
Black	0328
African	0331
Asia, Australia and Oceania	0332
Canadian	0334
European	0335
Latin American	0336
Middle Eastern	0333
United States	0337
History of Science	0585
Law	0398
Political Science	
General	0615
International Law and Relations	0616
Public Administration	0617
Recreation	0814
Social Work	0452
Sociology	
General	0626
Criminology and Penology	0627
Demography	0938
Ethnic and Racial Studies	0631
Individual and Family Studies	0628
Industrial and Labor Relations	0629
Public and Social Welfare	0630
Social Structure and Development	0700
Theory and Methods	0344
Transportation	0709
Urban and Regional Planning	0999
Women's Studies	0453

THE SCIENCES AND ENGINEERING

BIOLOGICAL SCIENCES

Agriculture	
General	0473
Agronomy	0285
Animal Culture and Nutrition	0475
Animal Pathology	0476
Food Science and Technology	0359
Forestry and Wildlife	0478
Plant Culture	0479
Plant Pathology	0480
Plant Physiology	0817
Range Management	0777
Wood Technology	0746
Biology	
General	0306
Anatomy	0287
Biostatistics	0308
Botany	0309
Cell	0379
Ecology	0329
Entomology	0353
Genetics	0369
Limnology	0793
Microbiology	0410
Molecular	0307
Neuroscience	0317
Oceanography	0416
Physiology	0433
Radiation	0821
Veterinary Science	0778
Zoology	0472
Biophysics	
General	0786
Medical	0760

EARTH SCIENCES

Biogeochemistry	0425
Geochemistry	0996
Geodesy	0370
Geology	0372
Geophysics	0373
Hydrology	0388
Mineralogy	0411
Paleobotany	0345
Paleoecology	0426
Paleontology	0418
Paleozoology	0985
Palynology	0427
Physical Geography	0368
Physical Oceanography	0415

HEALTH AND ENVIRONMENTAL SCIENCES

Environmental Sciences	0768
Health Sciences	
General	0566
Audiology	0300
Chemotherapy	0992
Dentistry	0567
Education	0350
Hospital Management	0769
Human Development	0758
Immunology	0982
Medicine and Surgery	0564
Mental Health	0347
Nursing	0569
Nutrition	0570
Obstetrics and Gynecology	0380
Occupational Health and Therapy	0354
Ophthalmology	0381
Pathology	0571
Pharmacology	0419
Pharmacy	0572
Physical Therapy	0382
Public Health	0573
Radiology	0574
Recreation	0575
Speech Pathology	0460
Toxicology	0383
Home Economics	0386

PHYSICAL SCIENCES

Pure Sciences

Chemistry	
General	0485
Agricultural	0749
Analytical	0486
Biochemistry	0487
Inorganic	0488
Nuclear	0738
Organic	0490
Pharmaceutical	0491
Physical	0494
Polymer	0495
Radiation	0754
Mathematics	0405
Physics	
General	0605
Acoustics	0986
Astronomy and Astrophysics	0606
Atmospheric Science	0608
Atomic	0748
Electronics and Electricity	0607
Elementary Particles and High Energy	0798
Fluid and Plasma	0759
Molecular	0609
Nuclear	0610
Optics	0752
Radiation	0756
Solid State	0611
Statistics	0463

Applied Sciences

Applied Mechanics	0346
Computer Science	0984
Engineering	
General	0537
Aerospace	0538
Agricultural	0539
Automotive	0540
Biomedical	0541
Chemical	0542
Civil	0543
Electronics and Electrical	0544
Heat and Thermodynamics	0348
Hydraulic	0545
Industrial	0546
Marine	0547
Materials Science	0794
Mechanical	0548
Metallurgy	0743
Mining	0551
Nuclear	0552
Packaging	0549
Petroleum	0765
Sanitary and Municipal	0554
System Science	0790
Geotechnology	0428
Operations Research	0796
Plastics Technology	0795
Textile Technology	0994

PSYCHOLOGY

General	0621
Behavioral	0384
Clinical	0622
Developmental	0620
Experimental	0623
Industrial	0624
Personality	0625
Physiological	0989
Psychobiology	0349
Psychometrics	0632
Social	0451

The undersigned hereby recommend to the Faculty of

Graduate Studies and Research acceptance of the thesis

Fatigue crack growth and coalescence study

submitted by

Hong Zhang

in partial fulfilment of the requirements for

the degree of Master of Engineering.

Chairman,

Department of Mechanical and Aerospace Engineering

Thesis Supervisor

Carleton University

August, 1993

Abstract

This thesis presents an investigation on the interaction and coalescence of twin coplanar semi-elliptical cracks under bending loadings of flat plates using numerical prediction methods. For comparison, fatigue crack growth data were obtained from a 4-point bend specimen calibrated by the direct current potential difference method and beachmarking technique. An empirical formula to simulate the coalescence process was also obtained. Good agreement between experimental fatigue crack growth data and prediction is demonstrated.

In addition, the coalescence criteria of international design codes and the Iida proposal are included in the computer program. The comparison of predicted life with the different models will be shown for flat plate and welded specimens.

Acknowledgments

I would like to express my greatest appreciation to my supervisor, Professor R. Bell, for his support, insight and general guidance and extreme patience given me throughout the last two years. Without his encouragement and enlightenment, this thesis could not have been completed. Also thanks to Professor P. Frise for his providing the fatigue testing information and graphics, and many useful discussions. I would also like to thank my fellow student, Mr. Harrington, for using his experimental results and his helpful assistance.

Thanks to many of my colleagues in this department and Mrs. Lois Whillans who have given advice and great help whenever they were asked.

Finally I would like to thank my husband C.J. Liu for his patience and understanding.

Table of Contents

CHAPTER III: Computer Program for Calculating of Fatigue Life

CHAPTER IV: The Coalescence Study

List of Tables

List of Figures

List of Symbols

N_t	Total fatigue life
N_i	Initiation life
N_p	Propagation life
σ_{xx}, σ_{yy}, σ_{zz}	X,Y,Z direction stresses
σ_{xy}, σ_{yz}, σ_{xz}	Shear stress components
K_I, K_{II}, K_{III}	Modes I, II and III stress intensity factors
r, θ	Cylindrical coordinates at the crack tip
ν	Poisson's ratio
E	Young's modulus
r_y	Plastic zone size
σ_y	Yield stress of material
σ	Remote stress normal to the crack
a	Crack depth
c	Crack half surface length
T	Plate thickness
B	Half plate width
Q	Shape factor for an elliptical crack
S_t	Uniform tensile stress
S_b	The bending stress of outer fiber

H	The boundary correction factor
F_s	The free surface correction factor
F_T	The finite thickness correction factor
F_w	The finite width correction factor
F_E	The crack shape correction factor
F_G	The geometry correction factor
F_p	The plasticity correction factor
ΔK	Stress intensity factor range (mode I)
K_{max}, K_{min}	Maximum and minimum stress intensity factor
ΔK_{th}	Threshold stress intensity factor range
K_{Ic}	Fracture toughness of material in state of mode I
C	Material growth rate constant
C_c, C_a	Material growth rate constant at breaking the surface points and deepest points of crack
m	Material growth rate exponent
ΔK_c, ΔK_a	The stress intensity factor range at breaking the surface points and deepest point of crack
R	Stress ratio ($\sigma_{min}/\sigma_{max}$)
da/dN, dc/dN	Crack growth rate in the depth direction and surface breaking point
S_p	Weld toe peak stress
γ	Interaction factor
t_s	Distance between the inner tips of two cracks
ss	Spacing between the centers of two adjacent cracks

M_k	Magnification factor for accounting weld attachment plate effect on stress distributions along weld toe
da/dN*, da/dN'	The growth rate during the coalescence using the kSC1, kSC2 and interaction model
k	The coalescence coefficient
a_t	The crack depth at inner tips of two crack touching
N_{coal}	The coalescence life calculated by computer program at k = 1.0
$N_{exp.}$	The coalescence life obtained from the experimental results
d_i	Interaction distance

CHAPTER I: Introduction

1.1 General Introduction

From an engineering point of view, a material can fracture either due to excessive plastic deformation or to propagation of cracks in the body. Most engineering materials fail in service because of the latter process. The fracture can be classified into two types: brittle and ductile. Brittle fracture gives rise to fast growth of cracks in the body and often occurs catastrophically without any excessive deformation of the material. On the other hand, plastic instability or necking in metals is ductile fracture by plastic deformation.

The progressive fracture of engineering materials by the initial growth of flaws under cyclically varying stresses is called fatigue. Fatigue is a process of cycle by cycle accumulation of damage in a material undergoing fluctuating stress and strain. A significant feature of fatigue is that the load is not large enough to cause immediate failure. Instead, failure occurs after a certain number of load fluctuations have been experienced. When the crack size becomes critical, an unstable fracture occurs. This type of failure can happen in structures or components in aerospace engineering such as aircraft structures, in civil engineering such as buildings and bridges or in mechanical

engineering such as shafts, rotors and turbines. Fatigue is a major consideration in the design, manufacturing and operation of these structures and depends on the materials, environment, service temperature, and types of loading.

The total fatigue life of a structure, referred to in engineering terms as the number of cycles to failure (N_t), is the sum of the number of cycles to initiate the microcracks (N_i), and the number of cycles to propagate them to final failure (N_p), that is

$$N_t = N_i + N_p \tag{1.1}$$

The distinction between crack initiation and crack propagation becomes critical when using data from laboratory-sized specimens to predict the life of more complex components in service.

Some components contain crack-like flaws produced in the fabrication processes. In these components, the flaws begin to grow almost immediately so that the life prediction in such cases is dominated by the crack propagation phase. Other components, that are made from high quality materials and are produced by carefully controlled fabrication processes, do not contain significant initial defects. These components may spend most of their lives initiating cracks. Life prediction in these cases is dominated by the crack initiation phase and is usually termed low cycle fatigue.

Offshore structures are subject to severe fatigue loading due to environmental waves and wind loading. This leads to fatigue damage at the area of stress concentration, such as at the weld toe of joints. In the case of offshore structures, the variable amplitude loadings which are applied to the structures by waves are about 3×10^6 cycles per year of stress variation in addition to storms, currents, iceberg collisions and winds. It is the main

reason for fatigue cracking in offshore structures.

The loading spectrum acting on offshore structures is extremely complex and the prediction of the loading history is very difficult. In order to determine the fatigue stress range at crack sites, a typical global analysis is required and it includes:

(1) structural modelling
(2) wave-load modelling
(3) fatigue crack analysis

In this thesis, fatigue crack analysis is the main subject. Several crack modelling procedures will be analyzed and compared to each other. Also, a new approach will be proposed and the available data and predicted models will be examined, so that a suitable methodology can be defined for fatigue crack growth analysis in offshore structures. In particular, the crack shape development and coalescence of linear arrays of cracks will be considered. As a result, a computer software program (called COALESCE) has been developed to predict the fatigue crack growth of multiple cracks for flat and welded flat plates.

This thesis is divided into five chapters. Chapter II contains a literature review of the concept of the linear elastic fracture mechanics and its application to offshore structures. The crack shape development and modelling of the crack coalescence process outlined in the international codes are also presented in this chapter. In Chapter III, the development of the computer program is described. The comparison of experimental data to the international standard solutions in flat plate and welded 'T' joints will be shown. A new coalescence model is introduced in Chapter IV, with comparison and discussion of the predicted results with the experimental data. Finally Chapter V includes some

conclusions from this work and suggestions for future studies.

1.2 Objectives

The objectives of this thesis can be summarized as follows:

(1) Develop computer software which will permit the modelling of multiple arrays of collinear cracks.

(2) Calculate the fatigue life of multiple cracks using the ASME, BSI and Iida coalescence models and assess the accuracy of the international standard solutions by comparing experimental with predicted crack shape development.

(3) Develop a graphical output which will present the predicted development of crack shape during the fatigue life and coalescence process.

(4) Investigate new models for predicting the coalescence process based on experimental observations.

CHAPTER II: Literature Review

2.1 Introduction

This chapter describes the literature and background information used as a basis for the thesis. The fracture mechanics method is based upon linear elastic fracture mechanics which relates the stress distribution in vicinity of a crack tip to other parameters such as the nominal stress applied to the structure and the size, shape and orientation of the cracks. This method can be applied to predict fatigue propagation life in offshore structures.

It has been observed from experimental studies that the development of crack shape and, in particular, crack coalescence has a significant effect on the fatigue life of structural and welded components. Therefore, this effect must be accounted for in any life prediction software package if results are to be comparable with experiments. With this goal in mind, the literature on crack shape development and coalescence has been reviewed. The procedures for numerical modelling of these processes will be discussed in the section 2.4.

2.2 Linear Elastic Fracture Mechanics (LEFM)

Fatigue is a progressive failure under repeated, cyclic or fluctuating loads. If a structure is subjected to this kind of loading, it may fracture at a stress level less than that required to cause failure under static loading conditions.

Fatigue cracks in a solid can be stressed in three different fracture modes, shown in Figure 2.1. Mode I - opening mode is the most common mode where the applied load is perpendicular to crack direction. It is the dominant fracture mode in offshore structures. Modes II and III are known as the sliding mode and the tearing mode, respectively. The superposition of the three modes describes the general cases of cracking.

The basic concept for fracture mechanics was developed by Griffith in the 1920's. He found that all materials contain some measurable defects (e.g. very small voids). He pointed out that the fracture behaviour of materials is controlled by an energy balance which contains three parts: strain energy without a void; surface energy which is related to the creation of new surface and released energy when a crack moves. Thus, he suggested the energy equation can be stated as:

$$\textit{Total energy} = \textit{Strain energy} + \textit{Surface energy} - \textit{Released energy} \qquad (2.1)$$

As the crack extends, strain energy is released, but surface energy is consumed. If there is a balance, the crack is stable. If there is an unbalance, the crack is unstable and crack propagation will occur, either in a brittle or a ductile manner depending on the degree of constraint (plane stress or plane strain condition).

The practical application of the above concept known as fracture mechanics started with Irwin {1} and Westergaard {2}. In their analysis of the strains and stresses at the

tip of a crack, they derived a parameter called the stress intensity factor (SIF), K, which characterises the crack tip stress field. The general form of SIF equations depends on loading and geometric boundary which will be discussed latter.

The elastic stresses near the crack tip for the mode I type of crack given by Irwin and Westergard are as follows:

$$\sigma_{xx} = \frac{K_I}{(2\pi r)^{1/2}} \cos\frac{\theta}{2} \left(1 - \sin\frac{\theta}{2} \sin 3\frac{\theta}{2}\right) + \ldots\ldots$$

$$\sigma_{yy} = \frac{K_I}{(2\pi r)^{1/2}} \cos\frac{\theta}{2} \left(1 + \sin\frac{\theta}{2} \sin 3\frac{\theta}{2}\right) + \ldots\ldots \qquad (2.2)$$

$$\sigma_{xy} = \frac{K_I}{(2\pi r)^{1/2}} \sin\frac{\theta}{2} \cos\frac{\theta}{2} \cos 3\frac{\theta}{2} + \ldots\ldots$$

Where $\sigma_{zz} = \sigma_{xz} = \sigma_{yz} = 0$ for plane stress, and $\sigma_{zz} = \nu(\sigma_{xx} + \sigma_{yy})$, $\sigma_{xz} = \sigma_{yz} = 0$ for plane strain. K_I is the stress intensity factor for mode I loading and ν is Poisson's ratio. The co-ordinate system is defined in Figure 2.2. Similar expressions exist for the mode II and III.

The important point of the above equations is that stresses near the crack tip are a function of local coordinates r and θ and a function of the stress intensity factor K which is given by the expression for the given geometry.

The stresses at the crack tip are higher than the nominal stresses due to the stress concentration caused by the cracks. According to the equations (2.2), the stresses are infinite at the crack tip, which for real materials is impossible. In reality, such large stresses are limited by the local crack tip yielding. It occurs over a region ahead of the

crack tip known as the plastic zone, where the amount of plastic deformation is restricted by the surrounding material which remains elastic. The size of the plastic zone (r_y) varies depending upon the stress conditions and the geometry of the body. For a cyclically loaded crack in the plane strain condition an approximation for r_y can be taken as:

$$r_y = \frac{1}{24\pi} \left| \frac{K_I}{\sigma_y} \right|^2 \tag{2.3}$$

Where σ_y is the yield strength of the material.

The cyclic plastic zone size is four times smaller than the comparable monotonic value. Under cyclic loading the plastic zone size of plane strain condition is three times smaller than that developed under plane stress condition. Therefore, linear elastic fracture mechanics concepts under cyclic loading and plane strain conditions can be used in the analysis of fatigue crack growth problems even in the materials that exhibit plastic deformation as long as the plastic zone size is small compared to the crack and cracked body.

2.2.1 Stress Intensity Factor K_I

Clearly the usage of LEFM concepts is limited by the ability to evaluate the stress intensity factor. Classical solutions for through-thickness crack geometries can be obtained from data handbooks {3,4,5}. However, the problems of surface cracks are much more complicated. The loading is usually complex and far from being uniform tensile or bending loads. The component geometries are another complicating factor. In most cases, the state of stress at the crack tip varies from almost plane stress at the intersection of the

crack with the free surface to a three-dimensional plane strain state along the deep parts of the crack front. Because of these problems, exact solutions of surface cracks are virtually non-existent. Stress intensity factor solutions have been solved by analytical methods {6}, experimental methods such as photoelasticity {7}, and numerical methods such as the finite element method {8,9,10,11}. Of these methods the finite element method is popular since it can accommodate almost any type of geometry and any combination of loading conditions. It is also accurate and relatively inexpensive.

Many authors have studied SIF solutions both analytically and empirically. Irwin {12} obtained approximate SIF equations for surface flaws, using the solution of an elliptical crack in an infinite body. Smith *et al* {13} considered a circular and a semi-circular crack in an infinite body. Carpinter {14} used a model with finite strips arranged in series to calculate the stress intensity factor along the crack front. Bell {15,16,17} calculated SIFs for semi-elliptical surface cracks in butt-welded T-joints using FEM by accounting for weld geometries. Niu and Glinka {18} calculated SIFs using the derived weight function method for the same geometries in a welded structure.

In their widely accepted work, Newman and Raju {19} developed empirical SIF equation for a semi-elliptical surface crack in a finite plate by means of FEM under tension and bending condition, given by

$$K(\theta) = (S_t + H*S_B) \sigma\sqrt{\frac{\pi a}{Q}} F (\frac{a}{c} , \frac{a}{T} , \frac{a}{B} , \theta) \tag{2.4}$$

for $0.0 < a/c \leq 1.0;\ 0.0 < a/T \leq 1.0;\ c/B < 0.5;\ 0.0 \leq \theta \leq \pi$.

Where

$K(\theta)$ is the stress intensity factor at a point of a semi-elliptical crack front (MPa$\sqrt{}$ m).
σ is the remote stress normal to the crack applied to component (MPa).
a is the crack depth (mm).
c is the crack half surface length (mm).
T is the plate thickness (mm).
B is the half plate width (mm).
Q is the shape factor for an elliptical crack.
θ is the angle of an ellipse that defines the position of the point under consideration.
S_t is the uniform tensile stress (MPa).
S_b is the bending stress of outer fiber (MPa).
H is the boundary correction factor.

$F(a/c, a/T, a/B, \theta)$ is a correction factor that depends on the specimen and crack geometries.

It can be written as:

$$F\left(\frac{a}{c}, \frac{a}{T}, \frac{a}{B}, \theta\right) = F_S * F_T * F_W * F_E * F_G * F_P \qquad (2.5)$$

The various factors account for particular features of the geometries.

F_S is the free surface correction factor
F_T is the finite thickness correction factor
F_W is the finite width correction factor
F_E is the crack shape correction factor
F_G is the geometry correction factor
F_P is the plasticity correction factor

In a refinement of these sets of equations, Scott and Thorpe [20] have proposed polynomial fitted equations of SIF solutions based on original work by Irwin, with the front free surface correction by Hartranft and Sih [21], the finite plate thickness correction by Raju- Newman [19] and Koterazawa-Minamisaka [22] and the finite plate width correction by Holdbrook and Dover [23]. The work of Scott and Thorpe is based on the premise that the best SIF solutions were those that predicted most accurately the

changes in the shape of the growing cracks.

2.2.2 Fatigue Crack Growth

The geometry of a surface crack is defined by the crack length along the front surface $2c$ and the crack depth through the plate thickness a. Rather than specifying these dimensions along with the plate thickness T, it is more convenient to define dimensionless ratios of crack depth to half surface length (aspect ratio a/c) and crack depth to plate thickness (a/T), shown in Figure 2.3, as well as straight-fronted crack that is characterised by a single depth dimension.

The fatigue fracture process may start from macroscopic cracks already present in the component during the manufacturing stage. The initiation can start in slip zones adjacent to the outer surface or at internal voids or inclusions in the material. Then the mechanism is a process of cumulative plastic strain between slip planes until small crack-like defects are produced. Among these initiated cracks, which are greater at a free surface than in the bulk of material, only a few may develop further when the stress concentration is high enough. This phenomenon, in general a surface phenomenon, is termed stage I - crack initiation. In stage II, the cracks propagate in a direction normal to the maximum principal stress direction. This stage of crack growth has been subjected to many detailed analyses using the linear elastic fracture mechanics {24,25,26}. Finally, a dynamic crack propagation may complete the failure process - stage III. The three stages of fatigue process are not completely separable but must be considered since the fatigue accounts for about 90% of all service failures.

The fact that the fatigue crack growth rate da/dN is related to the stress intensity factor range (ΔK) is well established and can be described by the sigmoidal shape curve shown schematically in Figure 2.4. The crack growth rate decreases sharply near the threshold ΔK_{th} and increases rapidly when ΔK is close to K_{Ic} which is known as fracture toughness of material. The crack growth threshold ΔK_{th} is an important factor governing the fatigue crack growth rate in the near threshold region. Unfortunately, the experimental determination of ΔK_{th} is rather difficult and expensive {28}.

Since fatigue crack propagation is clearly a phenomenon which depends on stresses, it was suggested by Paris & Erdogan {27} that the stress intensity concept which describes the stress condition adjacent to the tip of a crack could also be used as a basis for defining quantitative values of crack propagation rate. The relevant parameter was the range of stress intensity factor: $\Delta K = K_{max} - K_{min}$, where K_{max} , K_{min} are the values of K at the upper and lower limit stresses of the loading cycle. The Paris law which refers to the stage II of crack growth, in simplest mathematical terms, is given by

$$\frac{da}{dN} = C\ (\ \Delta K\ )^m \tag{2.6}$$

Where C and m are "constant" for a certain material and certain testing conditions. C is considered to be a material property that is slightly influenced by yield strength and fracture toughness of the material {29}. m is material growth rate exponent. Experiments show that the exponents of most metallic materials range from 2.0 to 4.0 {30}.

Paris law can be used to calculate the crack growth rate in the surface and through the thickness directions. The crack growth at the deepest point of the semi-elliptical

surface crack ($\alpha = 90^o$) can be calculated by the stress intensity factor from equation (2.4) represented by ΔK_a and crack growth constant represented by C_a while at the surface intersection point is expressed by ΔK_c and C_c.

$$\frac{da}{dN} = C_a \, (\Delta K_a)^m \qquad \frac{dc}{dN} = C_c \, (\Delta K_c)^m \tag{2.7}$$

Using the above equations, Newman-Raju [19] indicated that the variation in fatigue resistance along the crack front due to the variation in the stress field is the main reason for accounting the different crack growth coefficients C_a and C_c. They are related by the formula:

$$C_c = 0.9^m \, C_a \tag{2.8}$$

Where C_a, C_c are the crack growth coefficients at the deepest point and surface points, respectively. The Paris exponent m is assumed to be the same for the growth in the both directions.

This approach allows for the fatigue crack growth calculation to any type of geometry and provides a crack growth rate curve established by simple specimen tests. For the particular material, the Paris law provides an adequate description of crack growth at an intermediate range of growth rates, typically between 10^{-6} and 10^{-3} (mm/cycle) in which region most offshore structure components operate. However, it underestimates crack propagation rates at higher stress intensity levels as instability is approached, that is, ΔK approaches K_{Ic}. It also overestimates crack propagation rates at lower stress intensity levels approaching the ΔK_{th} below which the crack does not propagate.

In particular the Paris law does not model:

(1) The mean stress effect

The mean stress dependence is seen in some materials at the intermediate rates. The higher mean stress may lead to higher growth rates. Forman *et al* {31} give the modifications to Paris law. They proposed

$$\frac{da}{dN} = \frac{C\,(\,\Delta K\,)^m}{(\,1 - R\,)\,K_{Ic} - \Delta K} \tag{2.9}$$

Where R is the stress ratio of $\sigma_{min}/\sigma_{max}$ (= K_{min}/K_{max}). K_{Ic} is fracture toughness of material in state of mode I.

(2) The threshold effect

The threshold effect is the deceleration of crack growth to infinitesimal rates at low values of ΔK. The threshold is the point below which cracks do not grow. Empirically, the growth curve in the near-threshold region can be described by an equation of the form {32}:

$$\frac{da}{dN} = C\,[\Delta K^m - \Delta K_{th}{}^m\,] \tag{2.10}$$

(3) Schutz {33} considered both the above effects by the expression

$$\frac{da}{dN} = \frac{C\,(\,\Delta K^m - \Delta K_{th}^m\,)}{(\,1 - R\,)\,K_{Ic} - \Delta K} \tag{2.11}$$

In addition, stress ratio, crack closure effects, environment effects such as frequency of loading and operating temperature can also affect the crack growth rate.

By integrating the growth law, the predicted fatigue life and crack shape development can be obtained. With respect to a, the number of cycles N to propagate a crack from an initial crack length (or depth) a_i to final (critical) crack length (or depth) a_f can be calculated as follows:

$$N = \frac{1}{C} \int_{a_i}^{a_f} \frac{da}{\Delta K^m} \tag{2.12}$$

2.2.3 Advantages and Limitations of LEFM

The fatigue life can be determined either by the S-N method or by the fracture mechanics approach. The traditional S-N method is based on the experiments, resulting in graphs with the stress range $\Delta\sigma$ versus the number of cycles to failure N_f. On the other hand the fracture mechanics approach is based on a theoretical fatigue crack growth model.

The sophisticated fracture mechanics approach has great advantages to the engineers. It provides the essential relationship between the defects, the stress conditions and the material properties for the fracture. LEFM describes this relationship with mathematical formulae which can be applied to service conditions. For example, if the applied stress or strain in a structure can be fixed, i.e. the design is fixed, then the size of acceptable defects can be calculated in the structure. Alternatively, with a known defect size and a known material, operating conditions can be adjusted to ensure that the stress level is acceptable. LEFM can also be used to investigate the effect on the fatigue crack growth of various parameters such as thickness effect, size effect, surface residual stress effect, crack closure effect, etc.

The limitation of LEFM is that it can not take plasticity into account. For improvement, Dugdale {34} showed that the crack tip opening displacement (CTOD) approach gave more reliable prediction to much higher stress levels. Also the path-

independent J integral containing crack tip parameters, proposed by Rice {35}, can describe crack tip conditions with small scale to large scale yielding.

2.3 Applications of LEFM to Offshore Steel Structures

The above discussion of crack growth rates and fatigue life has dealt only with fatigue of flat plates. One current and interesting applications of LEFM is that of tubular connections in offshore structures {65, 66}. Testing of full tubular welded joints is time consuming and expensive, therefore, most experimental testing has been carried out on welded T plate joints.

Some features are to be noted for typical high cycle fatigue of offshore structures:

(1) The structure components are welded T-plates or Tubular joints. The initiation of multiple surface defects are present in the areas of high local stress concentration such as the weld toes. These stress concentrations will influence the crack growth rate and the development of crack shape.

(2) The material has undergone only minor plastic strain, i.e. the strains have been essentially elastic. The fracture surface is smooth, with characteristic beach marks reflecting the variations in load intensity through interchanging periods of storms and calmer weather.

(3) Semi-elliptical surface cracks are common types of the crack shape in offshore structures. The multiple cracks grow and coalesce to form a dominant semi-elliptical crack during propagation process.

(4) Offshore structures are in the aggressive corrosive environment of the salt water of varying temperature.

The crack growth of the welded joint has the same three growth stages: initiation, crack coalescence and growth of a dominant crack until failure. In the first stage, usually refers to as the initiation of very small cracks on a microscale, with crack depth less than 0.5mm. In the second stage, the cracks grow with a high aspect ratio and coalesce into

fewer cracks of lower aspect ratio. These cracks continue to grow and coalesce into a single dominant semi-elliptical crack. In the last stage of the life, this crack becomes an edge crack or straight fronted crack which only grows in the thickness direction until final failure. A large proportion of the total life of a welded structure is spent in the propagation of a crack initiated at the weld toe. Thus, the prediction of the fatigue life for a weld joint requires accurate fatigue crack growth calculations in the highly stressed region near the weld toe using the LEFM approach. The stress intensity factor for semi-elliptical cracks at weld toe was reported by Bell {15} from three-dimensional finite element calculations.

The fatigue crack growth behaviour of welded joints is influenced by some important factors such as the material property, the loading condition, the weld dimensions, plate thickness, weld toe grinding, and welding process, etc. The geometric configurations of the weld and plate are described as the attachment thickness (t), main plate thickness (T), the radius (r) of curvature of the weld toe and the weld angle as shown in Figure 2.5. Welding also introduces residual stress and in addition, small variations in geometry will cause the stress gradient to be very steep near the surface. The magnitudes of the stresses are controlled by the weld toe leg length L, the angle of intersection between the weld and main plate θ, and the weld toe radius γ. These parameters are expressed as the terms of L/T, γ/T, and θ {36}.

The growth of cracks in the severe stress gradient of the weld toe region can be described in terms of the thickness effect in fatigue. The thickness effect is the phenomenon of the reduction in fatigue life which occurs when the thickness of the main

plate of a T-joint is increased. The effect on geometrically scaled-up joints can be described as:

(1) The higher probability of finding a large defect in a large volume of material will result in lower strength for the thicker part.

(2) The fact that through thickness stress distributions scale up if the joints are geometrically similar. The magnitude of the stress is dependent on the non-dimensional a/T values. Thus a crack of absolute depth a will experience a higher stress in a thicker plate than a thinner plate.

(3) The magnitude of the notch radius r at the weld toe is independent of the plate thickness. The value of r/T decreases as T increases which correspondingly increase the magnitude of the weld toe effect.

Experimental and theoretical studies have yielded design recommendations which take the form of a thickness correction factor. The full thickness correction for fatigue strength is stated by Gurney {70} as:

$$S = S_0 \left[\frac{t_0}{T} \right]^{0.25} \tag{2.13}$$

Where S_0 is the fatigue strength for a section of reference thickness t_0 (t_0 is equal to *22 mm* for the flat plates and *32 mm* for the tubular joints).

It is very difficult to study the T-plate welded crack growth in actual welds since about 100-200 crack initiation sites per meter of weld occur during fatigue cycling. For this reason Frise {30} proposed that the weld geometry be simulated by a 135^0 V-notch with a representative root radius (*0.2mm*). The T-plate SIF equations of Bell *et al* {15} were used to model the growth of the V-notch specimen. The validity of using the 3-D SIF solutions for weld toe was determined by comparing the through thickness stress distribution of the V-notch specimen to that of the T-plate. It was found that they are

virtually identical.

2.4 Crack shape development

Crack shape development describes the changes of the shape of fatigue cracks during the fatigue growth. It is the most interesting subject in recent years {67,68,69}. Many factors can significantly alter crack shape such as stress fields (tension or bending, linear or non-linear stress distribution), local stress concentration, multiple crack interaction and coalescence, and environment. An accurately evaluated crack shape and probable shape change during fatigue is invaluable as an aid to predicting the fatigue life of structures. In several experimental studies {8,9,10,11,38,39}, crack shape development of single and multiple defect arrays was monitored by potential drop measurements and by beachmarking the fracture surface. Then crack shape development is compared to current predictive techniques and also to current design and assessment codes.

In the experimental tests, crack shape development has been measured using alternating current potential drop method (ACPD), direct current potential drop method (DCPD) and beachmarking method.

In the ACPD method, an alternating current is passed through a thin layer at the specimen surface. The crack shape is inferred from the ratio of the potential drop across the crack and the reference potential drop remote from the crack. A small current is required to generate the electric field, {30}.

In the DCPD method, a direct current is applied to the body and the crack depth and shape is obtained from potential readings across the crack. For detailed information

involving the calibration procedure the reader is referred to in reference {40}. Much larger currents for the DCPD method are required than for the ACPD method. A variation on the DCPD method is localized DCPD where the input current is applied close to the crack plane and creates the electric field in this region. It only needs a small amount of direct current and obtains good results, indicated by Harrington and Bell {41}. Some of these results will be referred to in the later section of this thesis.

In addition, a beachmarking technique is used to show the cycle counts relative to crack shape change and to provide a record of the fatigue crack profile. After completion of each test, the specimens are broken and the surface length and maximum depth are measured to determine crack shape. Beachmarking is achieved by reducing the load by 50% and doubling the frequency of load cycling for an appropriate number of cycles.

Many publications in the literature describe a large amount of testing and analysis concerning the shape change of a surface crack during fatigue growth {42,43,44,45}. The analysis of shape change generally assumes that a crack is semi-elliptical and its depth a and half surface length c grow according to the Paris or other fatigue crack growth laws.

Several topics which have a great effect on crack shape development are crack interaction and coalescence. So far the crack coalescence phase is not well understood. Since it encompasses a portion of the total fatigue life, it is necessary to understand this behaviour and to develop design rules and safety criteria. Design codes exit that provide a simple assessment to deal with the analyses of crack interaction and coalescence

problem, such as ASME Section XI Code {46} and BSI PD6493 Code {47}. They define the coalescence of cracks as recharacterization, that is, the resulting single crack was recharacterized as a semi-elliptical crack with a combined surface length of the two interacting cracks, and the depth equal to the maximum depth of the two coalescing cracks. The codes also propose to account for accelerated growth in the length direction when the two crack tips approach each other and this is known as interaction effect. Recharacterization and interaction are two phenomena of coalescence and will be discussed below.

Crack coalescence is the process of shape development where several small semi-circular or semi-elliptical cracks gradually lengthen and join together to form large semi-elliptical cracks. This continues until there is one single crack. There are three stages of crack coalescing growth before, during and after coalescence as shown in Figure 2.6.

Before coalescence, the cracks grow independently until the distance between them has reached a certain value, Figure 2.6 (a) and (b). Deviations of the adjacent crack-tip A and A' are observed just before coalescence, Figure 2.6 (e). It shows adjacent crack tips generally grow past each other across the region of high stress intensity between them. During the coalescence period of Figure 2.6 (c), parts of the crack front of the two cracks merge and inner tips of the crack grow fast through the thickness. The end of coalescence stage was assumed when the center portion of the crack profile becomes flat. After coalescence, the resulting single elliptical shape maintains until it reaches the specimen boundaries or back surface, as shown in Figure 2.6 (d).

Experimental results {8} showed that the highest crack growth rates were observed

during coalescence. The growth rates at the concave point A, A' were about twice those at the surface point C, C' and about three times those at the deepest point B, B'. The higher growth rates decreased as the crack shape changes from a concave profile to a smooth convex profile.

Kishimoto *et al* {11} proposed that the stress intensity factors are affected by the local curvature of the crack front. It was pointed out that when the inner tips of the twin cracks approached each other, SIFs began to increase. The maximum stress intensity factor was reached during the coalescence period while the profile of the combined single cracks was sharply concave and subsequently decreased as a smooth concave-to-convex shape was reached. On the other hand, the SIFs at deepest point B, B' and surface point C, C' increased monotonically with increasing crack area. They did not appear to be influenced by the rapid change of the crack shape.

The ASME section XI and BSI PD6493 Codes gives guidance on the LEFM approach to fatigue life assessment providing methods for the assessment of defects, planar and non-planar, on a fitness-for-purpose basis. The principle of the assessment is based on first defining a limiting size for the defect and then assessing whether it could grow to this limiting size in the required service life.

In the ASME approach, the analytical procedure of fatigue crack growth evaluation contains several assumptions to simplify the analysis. Surface cracks are regarded as a semi-circular or semi-elliptical. A crack is assumed to grow to a geometrically similar larger crack, that is, growth with a constant aspect ratio. Adjacent cracks are regarded as a single coalesced crack when the distance between the inside defect tips is less than or

equal to twice the depth of the deeper defect.

The BSI PD6493(1991) document suggests that if the bending component exceeds 20 percent of the total stress, the cracks are assumed to be recharacterised as an edge crack or a straight-fronted crack. If the bending component is less than or equal to 20% of the total stress, the surface length of the defect is held constant and the defect depth is continuous grown through the thickness. The crack aspect ratio increases to *1.0* where a semi-circular shape is obtained and maintained until the defect penetrates through the thickness or the coalescence criteria are reached. Adjacent defects are replaced by a single crack when the distance between the inside tips of the cracks is less than twice the smaller surface length of cracks.

For both approaches, the final dimensions after coalescence are that the depth is equal to the deeper crack and surface length is equal to sum of two crack surface lengths plus the distance between the inside of crack tips. As can be seen, the recharacterisation rules are broadly similar in both codes, those in the ASME code being based on defect depth and in the BSI PD6493 code on defect length. Recharacterisation can also be performed on co-planar and non co-planar surface defects. These assumptions greatly simplify the fracture mechanics analysis of fatigue crack growth.

The predictions of these design codes resulted in relatively large over-estimation or under-estimation of the actual crack growth. One reason for this is the interaction effect due to the premature recharacterisation of the two cracks before their adjacent tips come into contact [8,9,10,11,38]. Another shortcoming is that the recharacterisation does not allow for sub-critical growth during the coalescence. This is unrealistic.

In Japan Iida *et al* {10} studied their experimental data on the coalescence of multiple crack arrays and found out that interaction between adjacent cracks was not apparent and that the crack shape development observed from the experiment was quite different from that described by the two international design codes. They have reported empirical formulas to predict the aspect ratio change of growing semi-elliptical cracks. They proposed that crack shape development may be adequately described by assuming the cracks are independent until they contact, at the same time they instantaneously adopt a smooth semi-elliptical shape whose surface length is the sum of their separate surface lengths and whose depth is equal to that of the deepest crack.

At the point that two individual defects coalesce at a free surface, all three proposals above indicate that there is a greatly enhanced stress intensity factor in the ligament region of the coalesced crack causing it to propagate rapidly through the plate thickness. They suggest that the coalescence process occurs so rapidly that it can be generally ignored in the development of predictive models.

Graphically, the crack shape development in terms of a/c *vs.* a/T will take the shape of curve I for a single crack growth and the curve II for double crack coalescing as shown in Figure 2.7. During the initial stages of the growth both give similar results as a single crack develops independently. After coalescence, curve II shows a sharp drop in the value of aspect ratio and a dominant crack with lower aspect ratio is formed. The shallow crack is then allowed to propagate until failure.

As mentioned above, when growing from initial defects, cracks show a tendency to deviate slightly away from the common plane of the cracks resulting in a small

divergence of the crack tips. Contrary to the expectations this divergence does not correct itself as the crack tips approach each other, and in fact the cracks grow some considerable way past each other before tearing of the ligament between them occurs. This type of behaviour was also described by Iida and many other researchers {9,10,38,42}.

Melin {43} declared this behaviour as introducing a disturbance that forces the cracks to deviate from a straight path. It is shown that the straight crack path is unstable, so that tip to tip coalescence will not take place.

Morgan {47,48} Scott and Thorpe {20}, Hodulak *et al* {49} and Kawahara *et al* {50} showed that semi-elliptical surface cracks subjected to tensile and bending loads will adopt preferred shapes. Morgan suggested that as the crack depth increased, defects are assumed to grow towards a preferred aspect ratio - representing the stable crack shape under the particular loading condition. He called this stable shape the ***Preferred Propagation Path***. This agreed with Scott and Thorpe who calculated the shape changes by considering a wide range of initial aspect ratios under tension and bending. The diagram with preferred propagation path are shown in Figure 2.8.

Figure 2.8 indicates that under tensile loads fatigue cracks in finite thickness plates grow preferentially to the nearly semi-circular shape when the depth is less than half of the plate thickness and then elongate a little as they grow toward the back surface. Under bending loads, cracks will grow with a rapidly decreasing aspect ratio. But even the initial crack shape is very different from the "equilibrium" shape, they will adjust their shape rapidly to achieve the "equilibrium" shape. Therefore, when the initial aspect ratio of the crack is low, it will first grow in the thickness direction with slow growth in the surface

direction to adjust its shape and to achieve the "equilibrium" shape.

Wu Shang-Xian {51} and Mahmoud {7,52,53} have shown that defects in materials of high growth rate exponent (m) have a slightly reduced equilibrium aspect ratio. Scott and Thorpe {20} stated that the stress ratio (R) partly influences the equilibrium shape of defects. Gilchrist *et al* {54} found that the initial relative crack depth(a/T) and initial aspect ratio(a/c) influence the defect aspect ratio which tends towards an asymptotic value. Hodulak *et al* {49} described the calculation of the preferred crack propagation path, that is, shape is a function of aspect ratio and the stable crack shape will be achieved during fatigue crack growth.

Studying the coalescence of two cracks, Heath and Grandt {55} introduced the interaction factor (γ) which is defined as the ratio of the stress intensity factor for two cracks to the stress intensity factor for a single crack. Soboyejo *et al* (9} and Otegui *et al* {38} studied the variation of γ against ts/c, where ss is the distance between the inner tips of two cracks and c is the half surface length of the crack. They found that K_I at the positions of the crack fronts near the surface tended to increase, accelerating crack growth and coalescence. However, K_I at the deepest point of crack front slightly decreased and in-depth growth rates remained stable or slightly decreased. This was similar to Morgan {48} who suggested that during the coalescence period the maximum depth of the crack was constant over a significant portion of the fatigue life. The depthwise growth in fact had been retarded by the need for the crack to grow through the cusp region.

Vosikovsky, Bell *et al* {56,57} have developed an empirical forcing function to model crack shape development and coalescence in welded T-plates. This function was

developed from experimental measurement. The function assumed that fatigue cracks at the weld toe are initially semi-circular under cyclic fatigue loading. As the cracks grow deeper, they coalesce and form a dominant semi-elliptical crack. Then they grow to become an edge crack or straight fronted crack. The forcing function simulated this process based on the single crack. The function is a simple exponential relationship shown as:

$$\frac{a}{c} = e^{-ta} \tag{2.14}$$

$$t = 2.09*10^{-6} \ (S_p)^{1.95} \tag{2.15}$$

Where a/c is the aspect ratio of the crack, t is given by equation (2.15). S_p is the weld toe peak stress which reflects both geometry and test conditions.

Bell *et al* [58] found that multiple crack model based on above forcing function gave good life prediction results when compared to their T-plate test results. Frise *et al* [30] modified this model into two regions to predict the coalescence of two growing cracks. The model is described mathematically by

$$\frac{a}{c} = e^{t_I a + b_I} \qquad \textit{for } a < a_{coal} \quad \textit{before coalescence} \tag{2.16}$$

$$\frac{a}{c} = e^{t_{II} a + b_{II}} \qquad \textit{for } a \geq a_{coal} \quad \textit{after coalescence} \tag{2.17}$$

Where a_{coal}, t_I, t_{II}, b_I and b_{II} are determined from the crack shape and depth of experimental data, and a_{coal} is the depth of the single semi-elliptical crack after it has coalesced from the two starters. This model does not account for shape development

during coalescence process.

The experimental results from Frise show that the cracks did not grow significantly in the deepest point of the starter as expected while coalescence occurred, and also the cracks did not grow much in the surface direction during this period. He found that the coalescence life may range from 28% to over 87% of the total life of the specimen.

In the next chapter, the computer program modification and the fatigue life prediction using different predictive models will be discussed. The comparison to the experimental results will be also discussed.

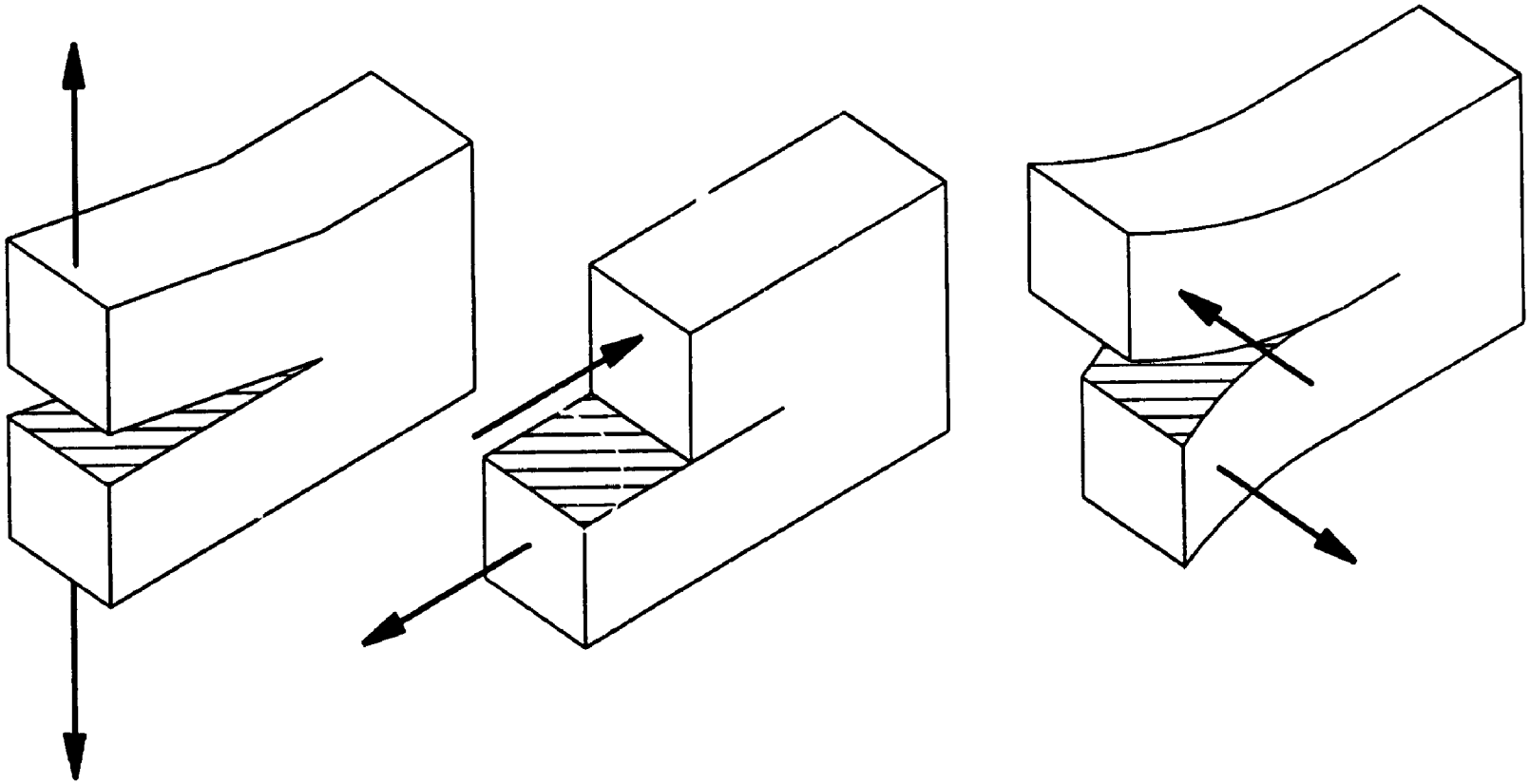

(a) model I, opening (b) mode II, sliding (c) mode III, tearing

Figure 2.1 The three loading modes for fracture analysis of a cracked body

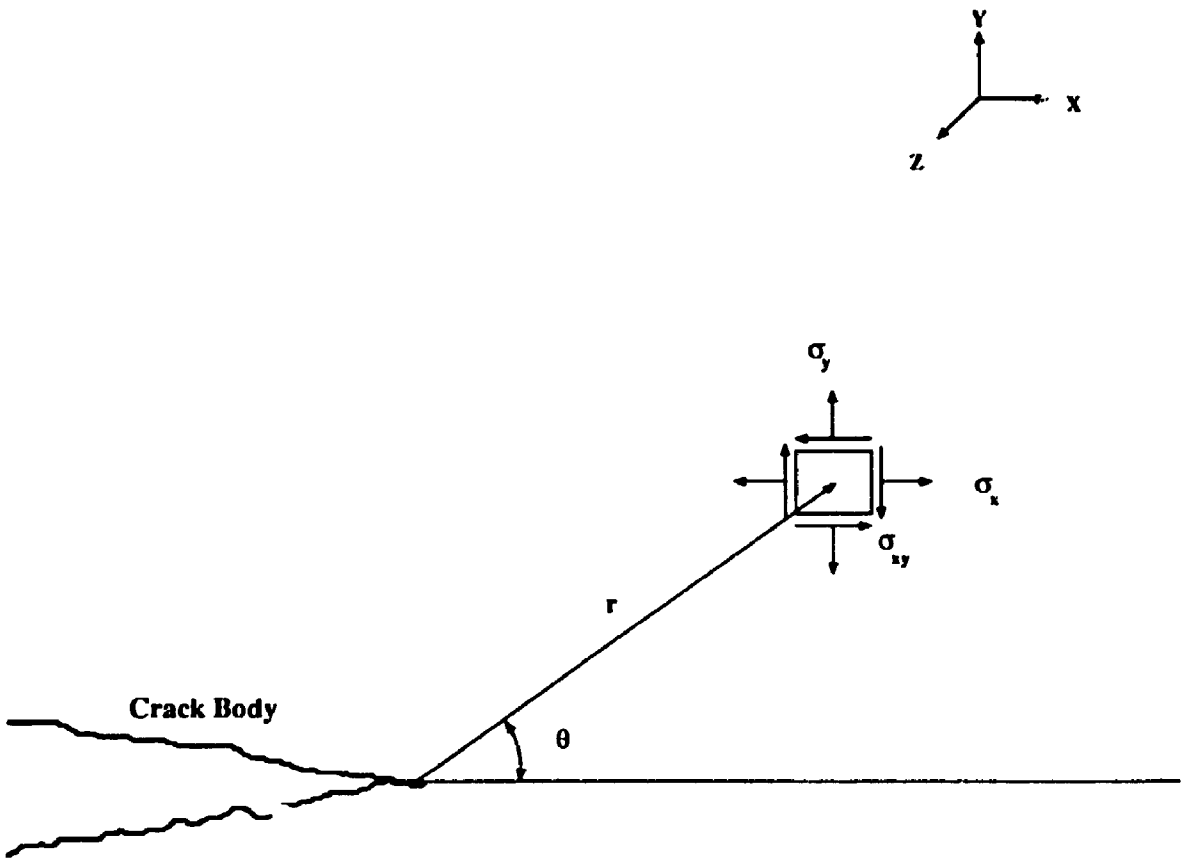

Figure 2.2 Location of local stresses near a crack tip in cylindrical coordinates

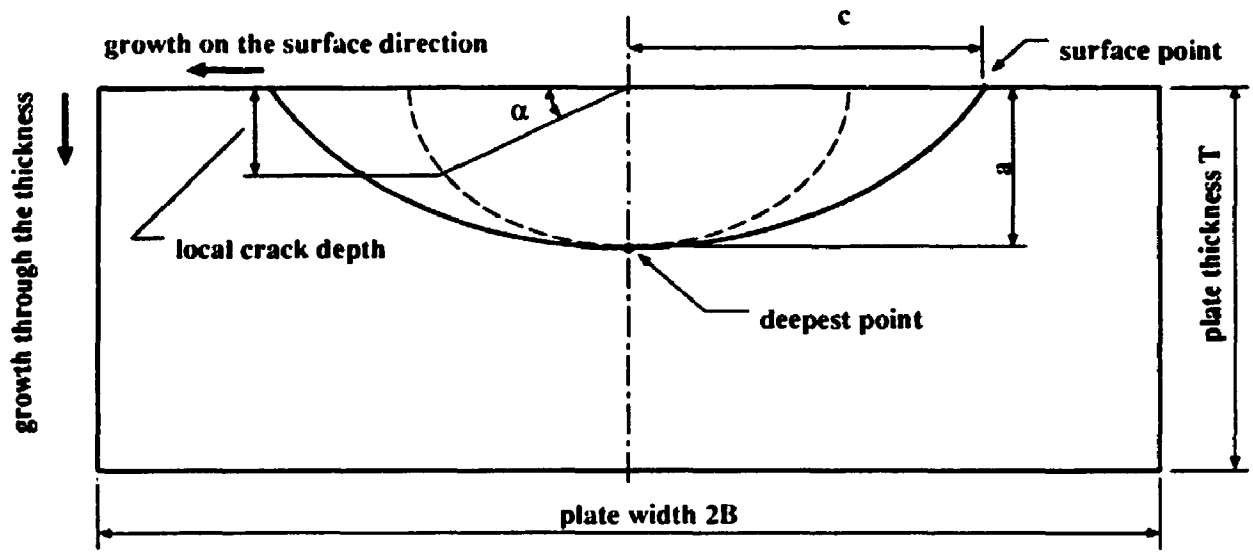

(a) Semi-elliptical surface crack (3-D)

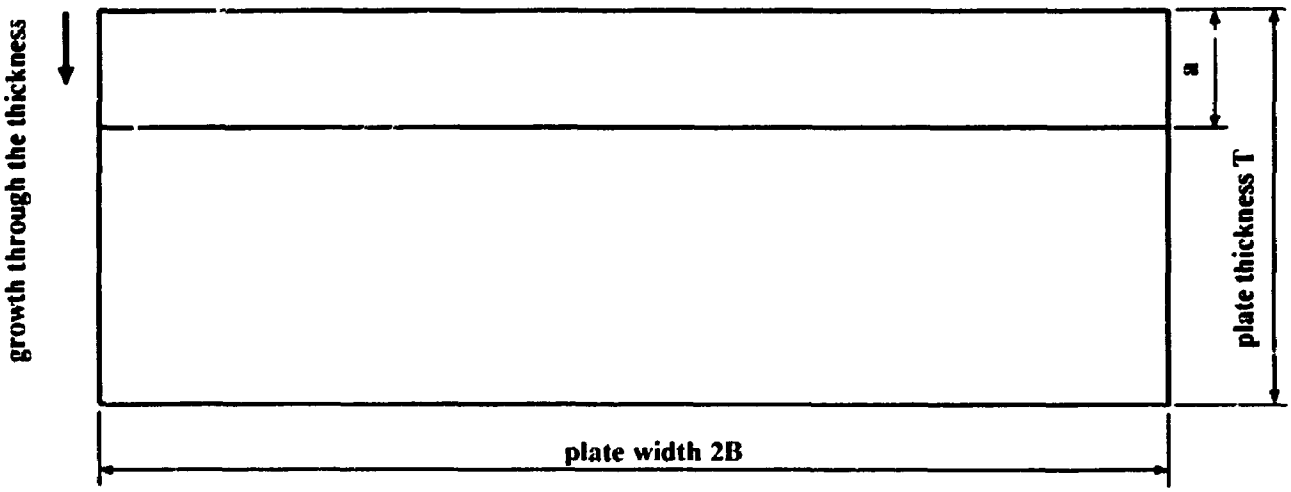

(b) Straight-fronted crack (2-D)

Figure 2.3 Cross-section of finite plate with various crack geometries

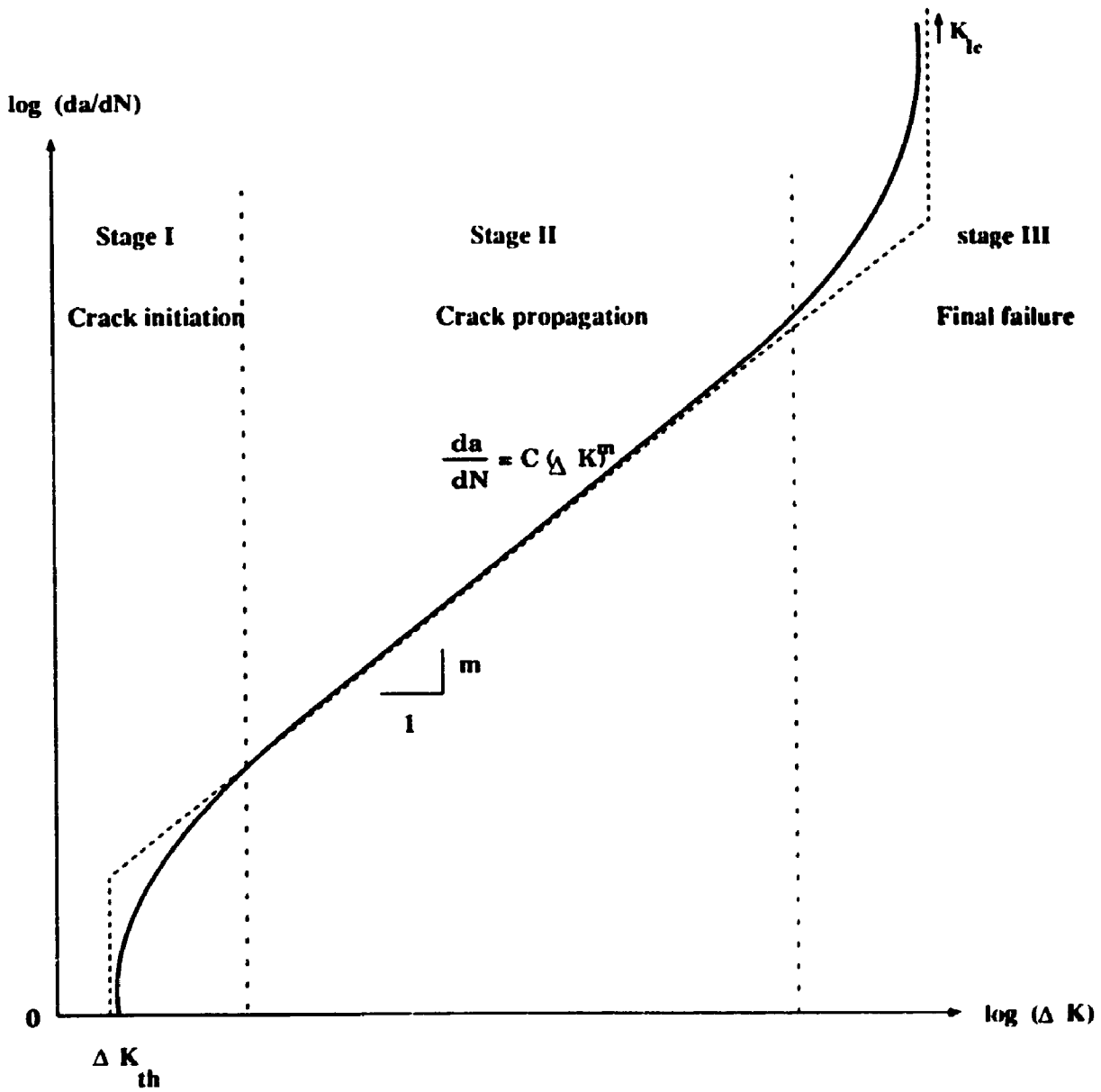

Figure 2.4 Schematic crack growth curve in three stages
ΔK_{th} is the threshold stress intensity range of crack growth
K_{Ic} is the fracuure toughness of material for mode I

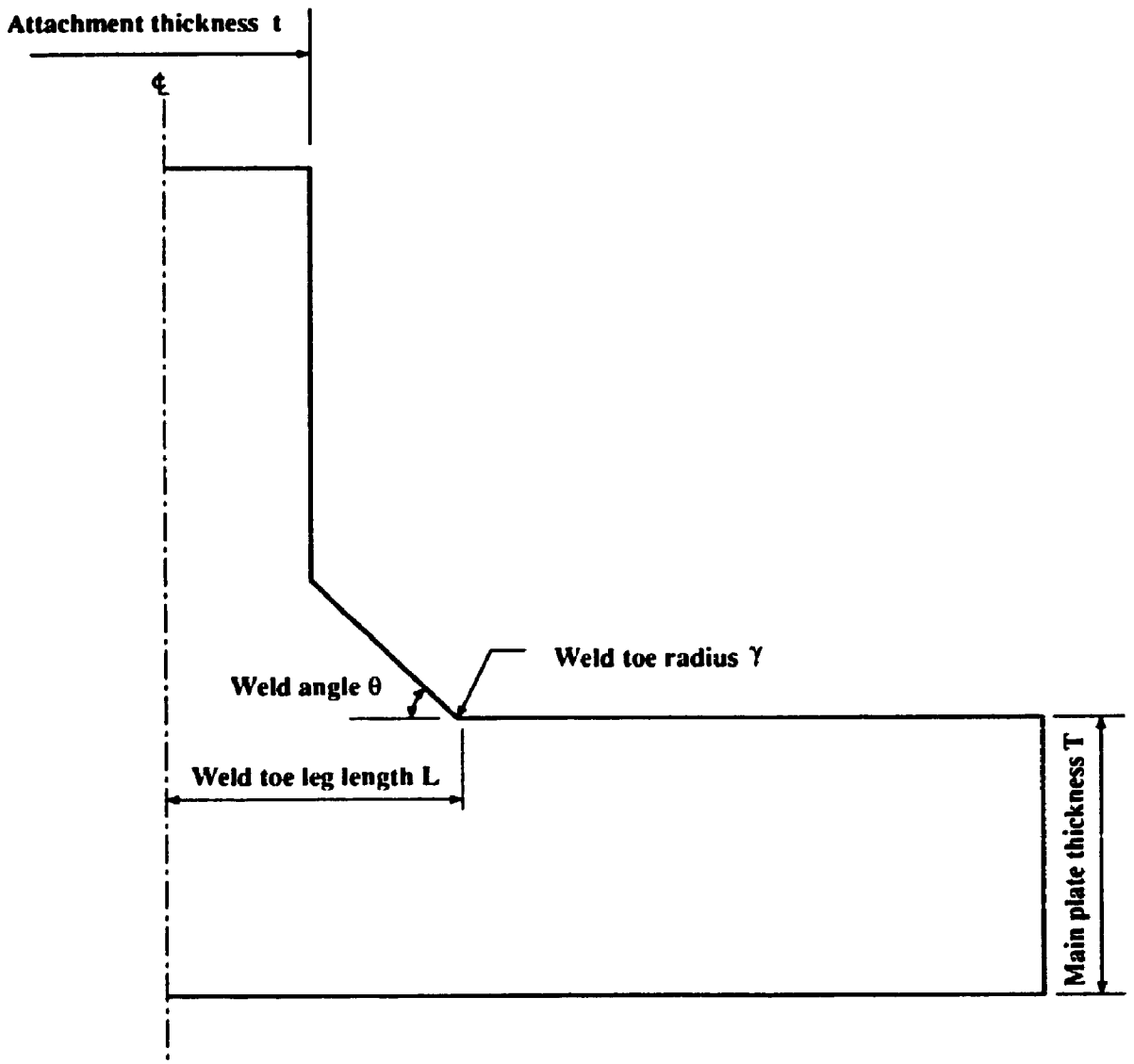

Figure 2.5 Weld toe geometry parameters

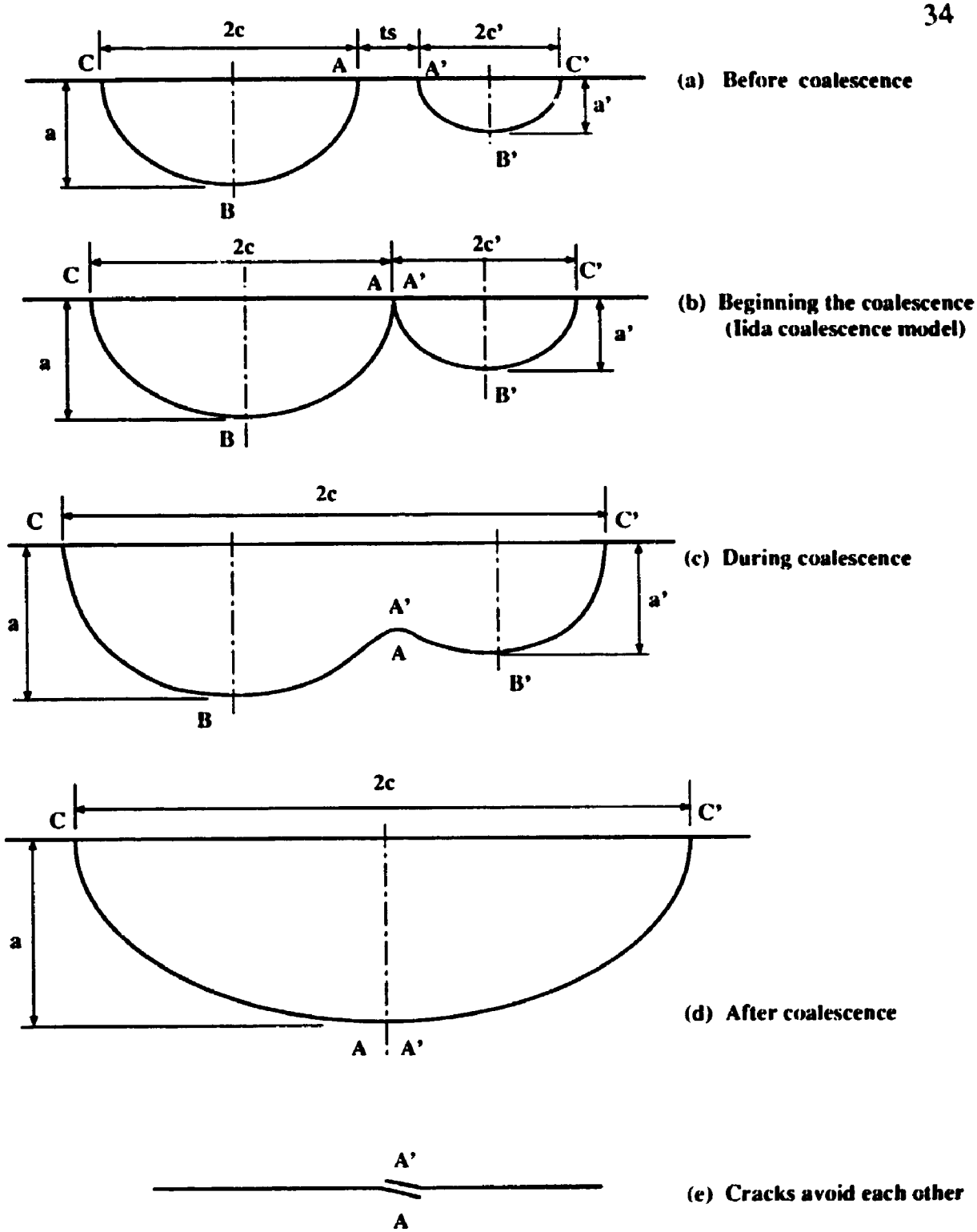

Figure 2.6 Crack coalescence phases

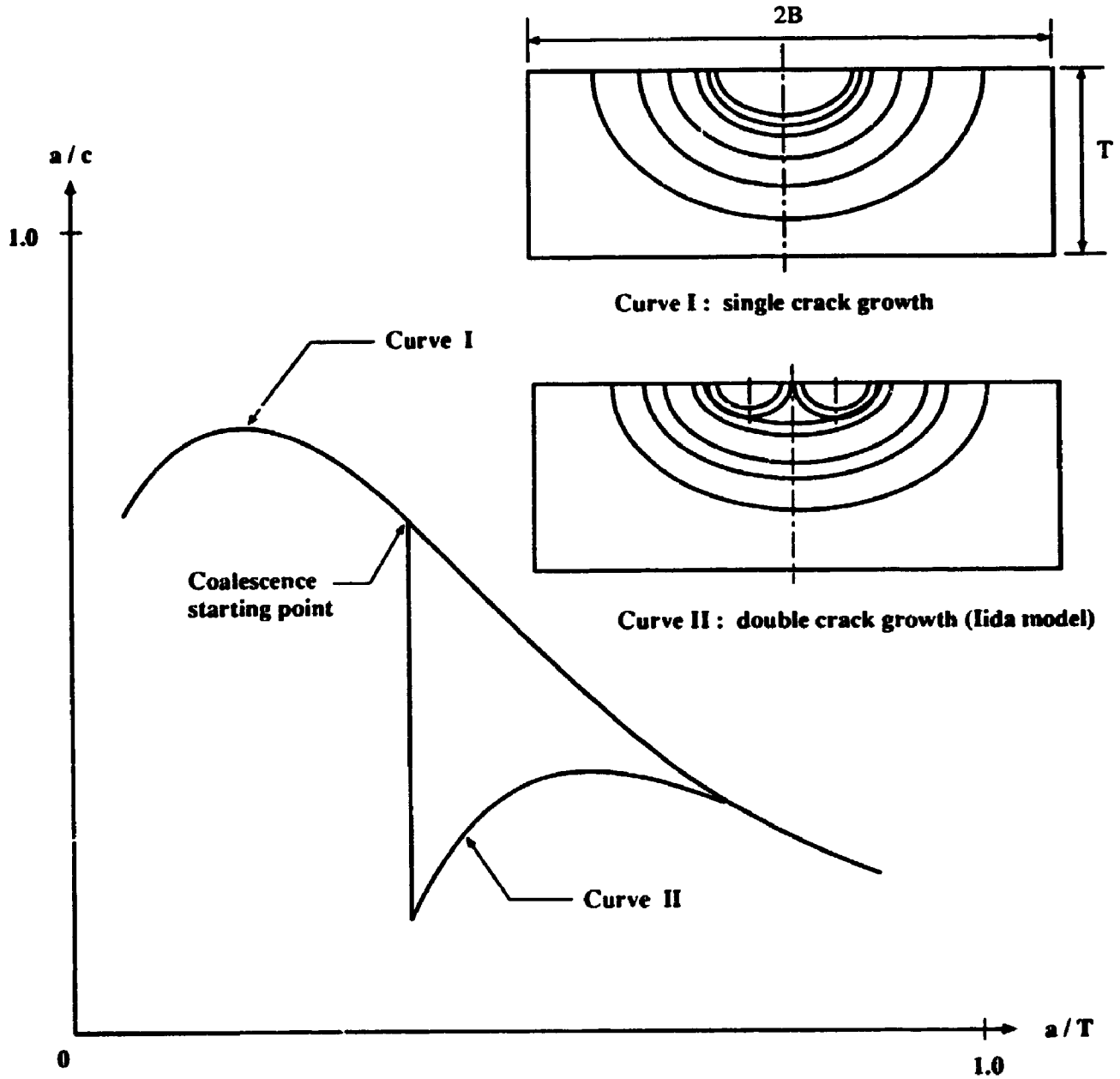

Figure 2.7 Comparison of crack shape development curve for single and double cracks, schematically

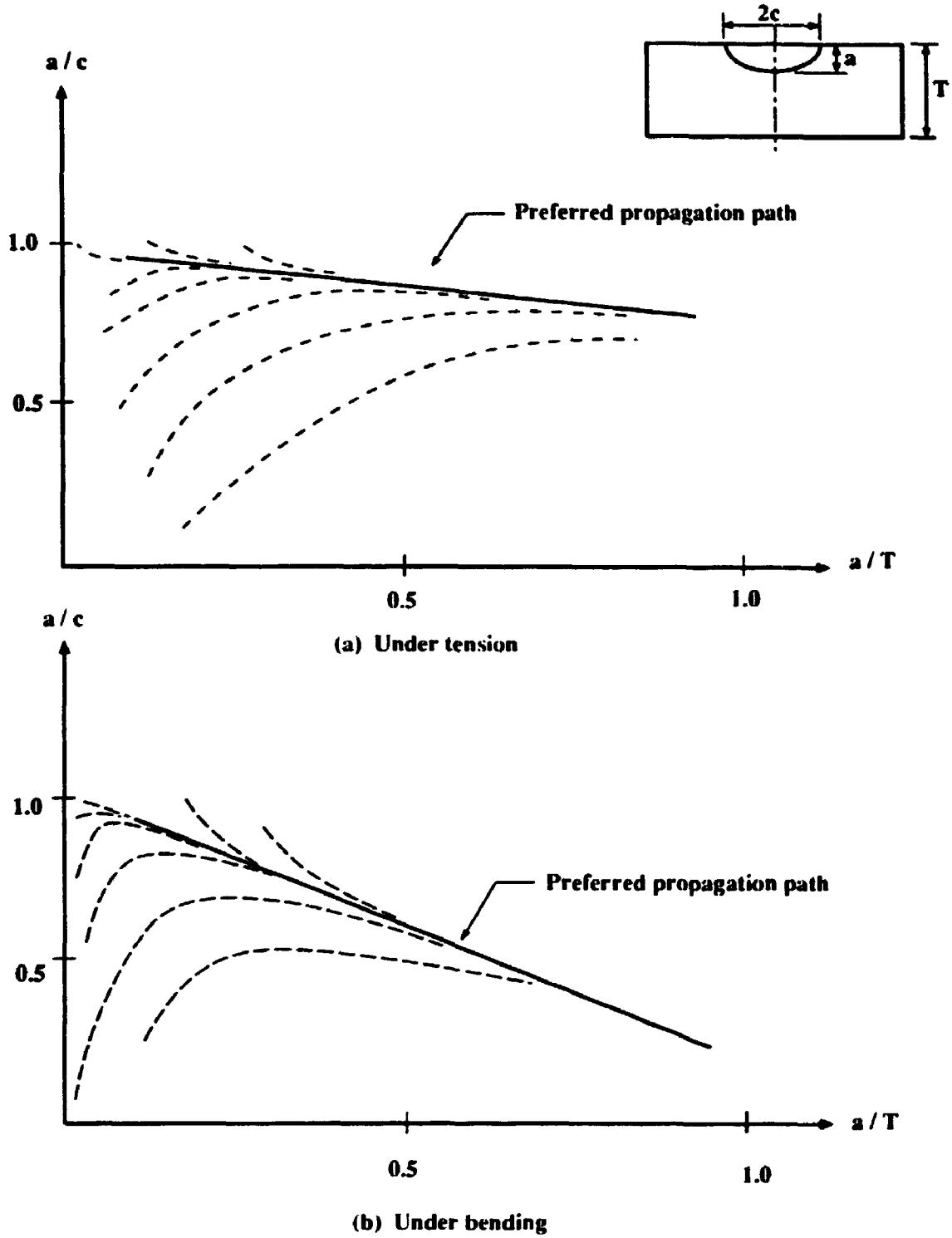

Figure 2.8 Predicted crack shape change for single crack loaded under tension or bending, schematically {Ref. 20}

CHAPTER III: Computer Program for Calculating Fatigue Life

3.1 Introduction

The fatigue life prediction program is based on the number of cycles, N, to propagate a crack from an initial size a_i to final size a_f calculated by a cycle by cycle integration of the growth laws using Runge Kutta numerical integration technique. In this chapter, the fatigue crack growth analysis including various input and output information and the descriptions of the crack shape development models will be introduced. The development of a fatigue analysis software can model single crack growth, multiple crack initiations and coalescence at the weld toe, and multi coplanar cracks with their shape development and coalescence. Also the prediction of the fatigue life of flat plate or welded 'T' joints using stress intensity factor data will be presented. The fatigue life calculated using the ASME {46}, BSI PD6493 {47} and Iida {10} coalescence models and the accuracy of their solutions under pure bending case is shown by comparison with experimental results.

3.2 Fatigue Life Prediction Program for Single Crack Growth

A computer program (called FATCRACKS) was written to predict the fatigue propagation life of a semi-circular, a semi-elliptical or a straight-fronted crack in flat plates or at the weld toe of 'T' plates using LEFM theory. It has two separate data systems: an input system and graphic data output system. The computer input system consists of a set of parameters which describes the configuration of an initial flaw, the stress range, the types of loading and several other parameters which describe the SIF equations and crack growth laws. The program for the constant amplitude loading option needs the following information:

3.2.1 Initial input

The computer program requires initial size of a crack and plate geometries in order to calculate stress intensity factor and crack growth rate. The initial input data are as follows:

Main plate thickness T
Plate width $2B$
Initial crack depth a
Initial crack half surface length c
Final crack depth (option)
Weld angle θ
Weld toe radius ρ
Loading conditions, e.g., tension, tension plus bending, 3-point bending or 4-point bending Stress range ΔS_t , ΔS_b
Stress ratio R
Material toughness ΔK_{Ic}
Fatigue crack propagation threshold ΔK_{th}
Material growth law constants C_a and m for the a direction
Material growth law constants C_c and m for the c direction

3.2.2 Crack growth laws

This program is used to predict fatigue crack growth rate according to six growth laws. The laws included are the Paris law {27}, the Forman law {31}, the Collipriest law {32}, the Paris law with two regions, the Klensnil law {59} and the Schulz law {33}, as detailed in Section 2.2.2.

3.2.3 Stress intensity equations

The stress intensity equations for a semi-circular, a semi-elliptical or a straight-fronted cracks are derived from empirical, numerical and finite element methods. The equations are:

(1) Elliptical Crack in an infinite body SIF equations by Irwin {12}.

(2) Elliptical surface crack in a plate of finite width and thickness SIF equations by Newman-Raju {19}.

(3) 2-D surface crack at weld toe of a 45°, non-load carrying fillet weld SIF equations by Gurney and Johnston {60}.

(4) 2-D crack at weld toe of a fillet weld SIF equations by Bell and Kirkhope {16,17}.

(5) 3-D surface crack at the toe of fillet weld SIF equations by Bell {15}.

(6) 3-D surface crack at the weld toe of plates with using varying attachment thickness SIF equations by Newman-Raju {19}.

It is noted that the Newman-Raju equations describe the SIF of flat plates containing surface cracks subjected to the tension and bending loads and Bell's 3-D equations describe stress intensity factors of weld toe cracks in the welded T-plates. The effect of the attachment plate on the SIF is presented as a magnification factor M_k. When M_k is multiplied by the SIF for a single surface crack in a flat plate under tension and

bending loads, it gives the stress intensity factor for a surface crack at the weld toe as shown below:

$$K_{I\ weld} = M_k * K_{I\ flat\ plate} \tag{3.1}$$

Where M_k is determined from finite element solutions by Bell {15} and Maddox {61}.

The SIF equations of two dimensional surface crack, derived by Gurney *et al* and Bell *et al*, are used to calculate the straight-fronted crack growth through the thickness.

3.2.4 Crack shape growth models

Under fatigue loading of offshore structures, cracks tend to grow as a semi-elliptical shape. The growth of a single semi-elliptical crack can be described by integrating the growth law in the depth direction to obtain the change in crack depth a and in the surface direction to obtain the change in a half crack length c, designated as SC1 model. Or alternatively one of the a or c values are calculated by the normal way described above and the other is obtained through the constant aspect ratio, designated as SC2 model. With these calculated values, a new elliptical crack shape is obtained. This work is designated as the single crack solution (SC). To predict the development of the crack shape, the mathematical models will be briefly described below:

(1) The SFC model
The SFC model is the growth of a straight-fronted crack using the SIF equations developed by Bell-Kirkhope using 2-D finite element methods and by Gurney *et al*. It is assumed that the crack only grows through the thickness of a plate with a long surface length and the aspect ratio of SFC is 0.0.

(2) The SC1 model

The SC1 model is the natural growth of a single semi-elliptical crack. In this model the crack growth in the *a* and *c* directions are calculated by independently using the crack growth law with SIF values at the deepest and surface points of the crack. The SIF data were obtained by using 3-D finite element methods.

(3) The SC2 model
The SC2 model permits the crack to grow as a single semi-elliptical crack but the crack shape is maintained as a constant aspect ratio throughout the propagation life. One of the surface length and depth of the crack is controlled by the other and by constant aspect ratio *a/c*. The SIF data was produced from 3-D finite element methods. This model allows a crack to grow towards a geometrically similar larger crack.

The program is very flexible in the treatment of a single crack by permitting the selection of the SIF equations, crack growth laws and the crack shape growth models. However, it is unusual to find that only a single crack initiates and propagates during the fatigue processes of offshore structures. An experimental study of welded T-joint specimens under bending loads, Yee *et al* {62}, showed that there were multiple flaws initiated along the fracture surface. As the cracks grew deeper, the value of aspect ratio decreased and the cracks coalesced. Then they continued to grow as a straight-fronted crack or a crack with a very low aspect ratio. From this point of view, the actual shape of the growing cracks and progress of coalescence along the weld toe should be governed by the coalescing rate of multiple cracks rather than the growth of a single semi-elliptical crack.

Therefore, still based on the growth of a single surface crack, the computer program was modified to allow the multiple crack initiations and coalescence which is handled by an empirical forcing function to model crack shape development. The forcing functions are an empirical relationship described in Section 2.5. In this procedure the

initial crack shape is chosen to be semi-circular. The crack growth in the depth direction a is calculated in the normal way. The change in the crack shape is prescribed by updating the half surface length c which is obtained by the empirical relationships at each growth increment. It results that the surface length of multiple cracks is always longer than that of a single crack and simulates the multiple crack initiation and coalescence at the weld toe. The crack tip stress intensity factors at the surface and deepest points are obtained by Bell using finite element analysis. This work has been designated as the multiple crack solution (MC).

The descriptions of these methods for multiple weld toe cracks are:

(1) The MC1 model
The MC1 model is a single crack model with a forcing function for aspect ratio to account for multiple initiation and coalescence of cracks along the weld toe. When the aspect ratio of the crack reaches a value of 0.2, the crack shape is then assumed to be constant aspect ratio as $a/c = 0.2$ of the SC2 growth model. The crack is treated as a single semi-elliptical crack using a three-dimensional stress intensity solutions until the end of the propagation life.

(2) The MC2 model
The MC2 model is also based on a single crack model with a forcing function for aspect ratio to account for the initiation and coalescence of multiple cracks as described above. As the aspect ratio of the cracks reaches 0.2, the crack shape is assumed to be straight-fronted ($a/c=0.0$). After this point the crack growth calculation is changed from 3-D to 2-D in the SIF relationships. This simulates the crack breaking through the edge of the plate.

The growth of the crack terminates when the crack breaks through the edges of the plate, or reaches the specified crack depth, or to final failure ($K > K_{Ic}$). This program has been found to give a good prediction of the multi crack initiations and coalescence at the weld toe.

3.3 Modifications to Computer Program for Multiple Coplanar Crack Coalescence

According to the discussion earlier, predictive models of the MC1 and MC2 can be used to treat multiple crack growth with empirical formulas at the weld toe, but could not provide a good indication of the coalescence effect of multiple coplanar cracks in the flat plate. For a better understanding and modelling the coalescence behaviour of the real cracks, the computer program has been modified and named COALESCE. In this case up to nine semi-elliptical or semi-circular individual coplanar cracks are allowed to grow independently in the depth and the surface directions. At every crack growth interval, the surface positions of each crack are calculated to find out the distance between the inner tips of adjacent cracks. When this distance reaches a certain value which the international design codes recommend, the two cracks are assumed to be re-characterized into a single crack.

Crack shape development is modeled by using multiple cracks, which may initiate anywhere along the plate or weld toe, grow independently and then coalesce. Such a model has provided more flexible prediction than a single model provided. The advantage of this program is the capability of predicting the change in shape of arrays of fatigue cracks and simulating the coalescence stages by using international design codes and crack shape growth models.

3.3.1 International coalescence models

Two major design codes, the ASME Boiler and Pressure Vessel Code Section XI

{46} and the British Standards Institution PD6493 {47} and the Iida proposal {10} which address how to deal with the coalescence process were discussed in Chapter II of this thesis. In order to examine the approach of each code, the coalescence models were added to the computer program for investigating and evaluating the crack coalescence process.

The additional input required is the number of initial cracks, initial crack sizes and the initial crack positions. The coalescence will start according to the following criteria:

(1) The Iida model
The multiple cracks can grow independently with the SC1 or SC2 shape models before the coalescence. When the inner tips of two cracks contact, they will immediately coalesce into a large semi-elliptical crack. The width of the new crack is assumed to be equal to sum of the width of two previous cracks while its depth is equal to the depth of deeper crack. After the coalescence processes, the crack will continue to grow with the same shape it had before the coalescence. But for the SC2 model the aspect ratio changes to a new constant value depending on the new coalescing crack geometries.

(2) The BSI model
The BSI coalescence model depends on the ratio of tensile and bending loads. When the bending component is more than 20% of total loading, the individual cracks are assumed to be the straight-fronted crack with a long surface length throughout the propagation life. When the bending stress is equal or less than 20% of total applied stresses, the cracks will first grow toward semi-circular cracks and then keep the constant value of $a/c = 1.0$. This means that cracks will keep the surface length constant while growth in the through-thickness direction continues until the aspect ratio reaches 1.0 and then continues to grow with a constant shape of $a/c = 1.0$. When the distance between the inside tips of adjacent cracks is less than the smaller of the surface lengths, the two cracks are assumed immediately to coalesce to a single semi-elliptical crack. Its surface length is equal to the sum of the surface lengths of two previous cracks plus the distance between their inner tips. Its depth is equal to the depth of deeper crack. The crack then continues to grow towards a semi-circular shape.

(3) The ASME model
The ASME model assumes the crack shape as a constant value of the aspect ratio a/c throughout the fatigue life. The crack shape model is the SC2 with a known initial value of a/c. The cracks grow until the distance between the inner tips of the cracks is less than or equal to twice the depth of deeper crack. Then

the two adjacent cracks are replaced instantaneously by a single semi-elliptical crack where the surface length is equal to the sum of widths of the two previous cracks plus the distance between the inside tips of the cracks. The depth is equal to the deeper depth of two original cracks. After the coalescence, the constant aspect ratio is maintained. This results in a larger and deeper crack which continues to grow with the constant aspect ratio.

The ASME and BSI approaches imply a strong interaction effect since the coalescence is assumed to begin when the two cracks have significant distance between their inner tips. But the Iida model ignores the interaction effect of the two adjacent cracks.

It should be noted that the coalescence models of the ASME, BSI and Iida are used to predict when the coalescence will start and what the crack shape is after the coalescence. On the other hand, the shape growth models of the SC1, SC2, MC1, MC2 and SFC are used to simulate the change of the crack shape during each of crack growth interval. These two different approaches together describe the whole fatigue propagation process of the cracks. The program COALESCE will be used in the current study of evaluating the fatigue life.

3.3.2 The computer output

The program output system can provide several output files for different purposes. For example, one of the output files includes all crack depths and widths with related cycle count data, other files contain information such as the aspect ratio of the crack, the ratio of a/T, the crack growth rate and stress intensity factor information. This allows the crack shape changes to be plotted as follows:

(1) a versus N

(2) c versus N

(3) a/c versus a/T

(4) graphical output shows the prediction of crack shape development in the variable coalescence models. Examples of this option are shown in Figure 3.1 to 3.4 for SC1, SC2, MC1 and SFC growth shape models along with the different coalescence models.

From the output data, the coalesced crack dimensions and the dimensions during each growth interval, the coalescence life and the propagation life can be determined.

3.3.3 Summarizing the modifications to the program

(1) The major change to the prediction program is the inclusion of new coalescence models to simulate the coalescence processes which will be described in detail in Chapter IV.

(2) Several changes have been made in the output data files to make the presentation of information on various crack geometries and growth laws more consistent.

(3) Several auxiliary programs have been written to enhance the output and plotting capabilities of the software. For example, graphical outputs show the crack shape development with single crack growth, multiple crack growth or shifted to straight-fronted crack growth with different coalescence codes.

(4) Stress intensity superposition is added for the specimen subjected to both tension and bending loads. For example, in the BSI model the superposition of tensile and bending stresses was developed as a new option in order to account for different loading conditions. It also added the SIF equations of the straight-fronted crack on the flat plate.

(5) The coalescence models as described by the international design codes are included.

(6) Changing the SC2 model from the computer program, that is, after the coalescence the constant aspect ratio is changed to a new constant shape depending on the geometries of the coalescing cracks.

3.4 Comparison of Coalescence Models on Flat Plates for Different Loading Conditions

In this section the fatigue life of flat plates is predicted by the computer program. It needs to be pointed out that the predicted life using the computer program is the propagation life and there is no initiation life included. The crack growth will be calculated using the Paris law and Newman-Raju equations for SIFs. In the following plots, computer predictions are based on two identical cracks, only the growth data on one crack is presented in each plot for purposes of clarity.

The material constants are chosen to be $C_a = 5.36x10^{-12}$ [m/cycle] and $C_c = 0.9^m * C_a = 3.91x10^{-12}$ [m/cycle]. The experimental results of McFadyen {63} have verified that these values can better predict the crack growth in the surface direction. The constant $m = 3.0$ [MPa $m^{0.5}$] is also chosen for all calculations.

To investigate the effect of loading conditions on the propagation life and the coalescence processes, a series of computer runs are carried out under the four types of loading cases:

(1) 100% bending

(2) 50% bending plus 50% tension

(3) 20% bending plus 80% tension

(4) 100% tension

The experimental results (specimen FPB6-6) under pure bending load were also chosen from Harrington {71} for comparison. The results described the flat plate with initial two semi-elliptical starter cracks. The plate was loaded in the four-point bending

test machine and the total loading is 175 MPa. The fatigue crack growth was monitored by the DCPD methods and beachmarkings technique. To be consistent with experimental data, the initial crack dimensions and plate geometries were selected according to experimental parameters. The initial value of constant aspect ratio for the SC2 growth model is chosen to be 0.55, the average aspect ratio of the experimental results before the coalescence. The detailed experimental result analysis will be discussed in the section 4.2.

3.4.1 20% bending plus 80% tension, and 100% tension cases

In the plots of Figures 3.5 and 3.6, there were four different linetypes. Each of them represented the Iida model with the SC1, the Iida model with the SC2 ($a/c=0.55$), the ASME model with the SC2 ($a/c=0.55$) and the BSI model. For both loading cases, all predicted crack shapes initiated and grew in the semi-elliptical or semi-circular shape pattern. The numerical data is also presented in Table 3.1. The figures show that as the cracks begin to coalesce, the instantaneous growth at the crack surface is described by the straight vertical lines on the diagrams of *c versus N* and *a/c versus a/T*. The slope changes on the growth rates through the thickness were also observed in the diagrams of *a versus N*.

In Figure 3.5 of *a/c versus a/T*, the predicted crack shapes of different models have great difference. The BSI predicted shapes changed sharply before and after coalescence. The aspect ratio drops from 1.0 to 0.3. On the contrary, the ASME model has no aspect ratio change at all except at initiation. But the crack shapes did jump to a large semi-ellipse at the coalescence time and the vertical lines in *a* and *c* directions

represent this change. The Iida model with the SC1 and SC2 shape development showed their shape changes smoothly before and after the coalescence. Unfortunately, it is difficult to say with confidence which one gave the best predicted shape due to the lack of experimental data under such loading cases.

Comparing of the figures of *a versus N* and *c versus N*, the predicted growth rate for all models agreed very well up to the end of 50 kcycles. After that there are 200 kcycles difference in lifetime between them. The shortest life came from the ASME model (50 to 70 kcycles) and the longest life from the Iida model using SC1 and the BSI model (around 160 to 220 kcycles). The lives of the Iida model with the SC2 was about 100 kcycles. The proportion of tensile loading had a greater effect on the predicted lives. Overall the fatigue life of 80% tensile loading case is longer than that of 100% tension case, as shown in Table 3.1.

3.4.2 100% bending , and 50% bending plus 50% tension cases

The predicted method and the experimental results are compared in Figure 3.7 for pure bending case. The experimental results under pure bending loads showed that the initial aspect ratio increased from 0.47 to 0.55 as a/T reached 0.2, and then the value of a/c remained constant around 0.55 when a/T varied from 0.2 to 0.44. After the coalescence, the aspect ratio dropped to the lower value of around 0.3. From the observation of fracture surfaces, it indicated that the crack growth exhibited semi-elliptical crack growth.

The predicted shape of the Iida model with the SC2 growth showed good

agreement with the experimental aspect ratio in Figure 3.7. The Iida model using the SC1 with a higher aspect ratio of up to 0.65 had better agreement with the experimental shape after the coalescence while the ASME model only fitted with the experiments before coalescence. Because the BSI model predicts crack shape as a straight fronted crack when the bending loads are over 20%, the comparison for this model is only shown in the diagram of *a versus N*.

It can be seen that the growth rate of the ASME model is not comparable to the experiments. It is because after the coalescence finished at around 100 kcycles, the growth rates in *a* and *c* directions almost stopped, producing much longer lives. The Iida models with the SC2 shows that predicted growth rates in two directions were faster than that of the experiments. Improved prediction was obtained by the Iida model with the SC1 growth in which the cracks were recharacterised upon contact. It predicted 501 kcycles propagation life compared to the experiments of 438 kcycles, ie., +14.4% in difference. The ASME had a large overestimation which life was 653 kcycles at the same crack geometries as that of the experiments at the final failure, +49% difference in lifetime. The other two, the Iida model with the SC2 model and BSI model obtained the under-estimated results with -21% and -86% difference to the experimental life, respectively. The most conservative estimates of fatigue life from the BSI model is only 58 kcycles predicted life. The reason for this is that the BSI simulated the crack shape as two dimensional straight fronted crack while the real crack shapes are semi-elliptical. The life of the straight fronted crack growth is very short due to the higher stress intensity factors at the crack front.

It can be concluded that under pure bending loads, the predicted lives of the Iida model using the SC1 and SC2 growth are closer to the experimentally obtained lives. The ASME model which uses the same constant aspect ratio through the entire fatigue life gives an unconservative assessment to fatigue propagation life. This is very important because if the design code is to be used as a tool for evaluating the safe life of structures, a conservative prediction is required. The assumption of the BSI model that the defect should be regarded as an edge crack (SFC) is extremely pessimistic and results in an overly conservative fatigue life.

The predicted results for 50% bending plus 50% tension case, shown in Figure 3.8, were remarkably similar to the pure bending case except for the ASME model. Due to 50% tensile stresses present, the crack growth rate increases with increased tensile stress so that the lives under this loading case were shorter than those of pure bending. No experimental data was available in this loading case for comparison. The predicted lives compared to that of other loading cases are listed in Table 3.1 as well.

3.5 Comparing the Experimental Results with Predicted Models Subjected to Pure Bending at Welded 'T' Joint

In this section the predicted results of the welded 'T' joint specimen subjected to bending loads will be obtained from the computer program to study the effect of the presence of a weld on the crack initiation and coalescence. Due to the fact that cracks initiated at a large number of separate sites of the weld toe, they usually coalesced at a very small crack depth. For this reason, the amount of information available on the

coalescence and crack shape development processes was very limited. These experimental data were used to compare with the different predictive models.

The experimental data with crack depth a is plotted versus the corresponding number of cycles N obtained from Frise [30], where the weld geometry was simulated by a 135° vee-notch with a representative root radius of 0.2 mm under 200 MPa bending stress. The stress distributions through the notch root have been found to be similar to that through the weld toe region. There were two identical starters in each specimen and the development of the crack shape was measured by the ACPD technique and beachmarking.

The two different methods have been used to model crack shape development and simulate fatigue crack propagation life. One was based on using a single crack with empirical forcing function to simulate the multiple crack initiation and coalescence, the MC1 and MC2 shape model. The other used multiple coplanar crack growth with the coalescence models of the ASME, BSI and Iida models and the shape models of the SC1 and SC2. Bell's 3-D stress intensity equations for welded joints and Paris growth law are applied in the calculation.

From the diagram of *a/c versus a/T* for specimen 02F, as shown in Figure 3.9, it can be seen that the aspect ratio of the Iida model using the SC1 increased monotonically except during the coalescence process. However, the a/c value of the Iida model using the SC2 dropped to 0.2 after the coalescence. The ASME model kept a constant value throughout the fatigue life. For the forcing function models of the MC1 and MC2, the formation of an edge crack or constant crack shape is obtained once the aspect ratio decreases sharply to 0.2. This is represented by an almost vertical line in the figure of a/c

versus a/T because of the high stress intensity resulting from the small vee-notch radius (0.2mm). The MC models accounted for the possibility that multi initiation and coalescence occurs along the weld toe using a single crack The SC models, on the other hand, considered the interaction and coalescence processes of two independent cracks.

The specimens were assumed to fail when the crack depth was half through the plate thickness. With the high aspect ratio of the ASME model and Iida model with the SC1, as shown in Figure 3.9, the predicted lives are over-estimated by +54% to +108% with the experimental life of specimen 02F, shown in Table 3.2. The Iida model using the SC2 growth was better with +33.5% margin. The predicted lives of the MC2 and the BSI models give the most conservative prediction of 84 and 83 kcycles, respectively, compared with 230 kcycles obtained in the experiments. Only the MC1 model obtains a good fit to the experimental life with 224 kcycles of predicted life or about -2.6% difference in lifetime. As seen in Figure 3.9 of *a versus N*, none of the predicted models could not model the crack growth rate very well and over-predicted it through the thickness directions

The coalescence took place at 100 kcycles for the experiments compared with 113 kcycles for the ASME prediction, 157 kcycles for the Iida model using the SC2 and 207 kcycles for the Iida model using the SC1, listed in Table 3.2. The MC model and the BSI model could not model the specified coalesced points because they are based on the single or straight-fronted crack growth.

The similar growth pattern for specimens 02H and 02M are shown in Figure 3.10 and 3.11. To illustrate the differences among the models, Table 3.3 gave the predicted

propagation life for each specimen compared with the experimental lives. The results using empirical formulas with two distinct crack shape development regimes, obtained by Frise {30}, are also shown in the table for comparison.

Close observation of the fracture surfaces of some specimens showed that the failure initiated at more than 40 sites across the width of the specimen and this leads to earlier coalescence into a single straight fronted crack, {30}. It is clear that coalescence models with the forcing function, which can treat the coalescence of up to nine specified cracks, could not handle this kind of situation. However, the multiple crack models with empirical forcing function especially for the MC1 model gave reasonable agreement with the experiments. The empirical relationship based on Frise's two region forcing functions of the crack shape development gives good results as would be expected.

In the next chapter a new model for flat plates under bending load accounting for coalescence life will be introduced and it will be used for further study of the coalescence behaviour.

Table 3.1 Comparison of the propagation life of predicted models of flat plates under different loading conditions

		100% tension [kcycles]	20% bending + 80% tension [kcycles]	50% bending + 50% tension [kcycles]	100% bending [kcycles]		Notes
					Prediction	Experiment FPB6-6 (Ref. 71)	
Iida	SC1	168 (af=32.0 cf=51.0) *	203 (af=32.19 cf=56.53)	276 (af=29.9 cf=66.7)	501 ** (+14.4%)	438 (af=22.04 cf=76.18)	Total stress: S=175 MPa Stress ratio: R=0.05 Plate width: 2B=152 mm Plate thickness: T=32mm Crack1: a1=2mm c1=4mm @55mm Crack2: a2=5mm c2=5mm @80mm
	SC2	94 (af=22.0 cf=80.0)	114 (af=21.25 cf=77.06)	159 (af=22.1 cf=76.4)	344 (-21.5%)		
BSI		159 (af=32.0 cf=32.0)	220 (af=32.59 cf=32.59)	65 (af=75.5)	61 (-86%)		
ASME		57 (af=33.7 cf=57.6)	72 (af=32.20 cf=58.25)	131 (af=32.10 cf=60.25)	653 (+49.1%)		

* (af, cf represents the final crack geometry [mm])
** (% different between prediction and experiment)

Table 3.2 Comparison of the propagation life of predicted models of weld toe with experimental results (02F)

		Coalescence @ [kcycles]	Final failure @ [kcycles]	Difference with experiments	Experimental results (02F) {Ref. 30} [kcycles]	Notes
Iida	SC1	207	479 (af=19.51 cf=40.82)	+108%	230 Coal. @ 100	Bending stress: Sb=200 MPa Stress ratio: R=0.05 Plate width: 2B=160 mm Plate thickness: T=39 mm Inital geometries Crack 1: a1=0.6 mm c1=1.75 mm @ 70 mm Crack 2: a2=0.6 mm c2=1.75 mm @ 93 mm
	SC2	157	307 (af=19.52 cf=86.47)	+33.5%		
BSI		/	83 (af=21.40)	-64%		
ASME		113	355 (af=19.53 cf=43.30)	+54.3%		
MC1 (forcing function)		/	224 (af=19.59 cf=97.96)	-2.6%		
MC2 (forcing function)		/	84 (af=21.08)	-63.6%		

(af, cf represents the final crack geometry [mm])

Table 3.3 Comparison of the propagation life of predicted models of weld toe with experimental results

Specimens (Ref. 30)	LEFM Predicted Life [kcycles]							Experimental results (Ref. 30) [kcycles]
	Iida		BSI	ASME	Forcing function		Predicted life of two region forcing function (Ref.30)	
	SC1	SC2	SFC	SC2	MC1	MC2		
02F (ai=0.6 * ci=1.75 ss=23.0)	479 ** (+108%)	307 (+33.5%) a/c=0.45	83 (-64%)	355 (+54.3%) a/c=0.45	224 (+2.6%)	83 (-63.6%)	213 (-7.4%)	230
02H (ai=0.75 ci=2.5 ss=25.0)	457 (+126%)	303 (+50%) a/c=0.45	79 (-60.9%)	339 (+67.8%) a/c=0.45	219 (+8.4%)	79 (-60.9%)	163 (-19.3%)	202
02M (ai=2.5 ci=5.0 ss=17.0)	406 (+213%)	313 (+143.8%) a/c=0.6	51 (-60.8%)	431 (+232%) a/c=0.6	166 (+27.7%)	51 (-60.8%)	81 (-37.7%)	130

* (ai and ci represent the initial crack geometry, ss represents the spacing between the initial cracks [mm])

** (% difference between the predicted and experimental results)

All specimens subjected to pure bending of 200 MPa

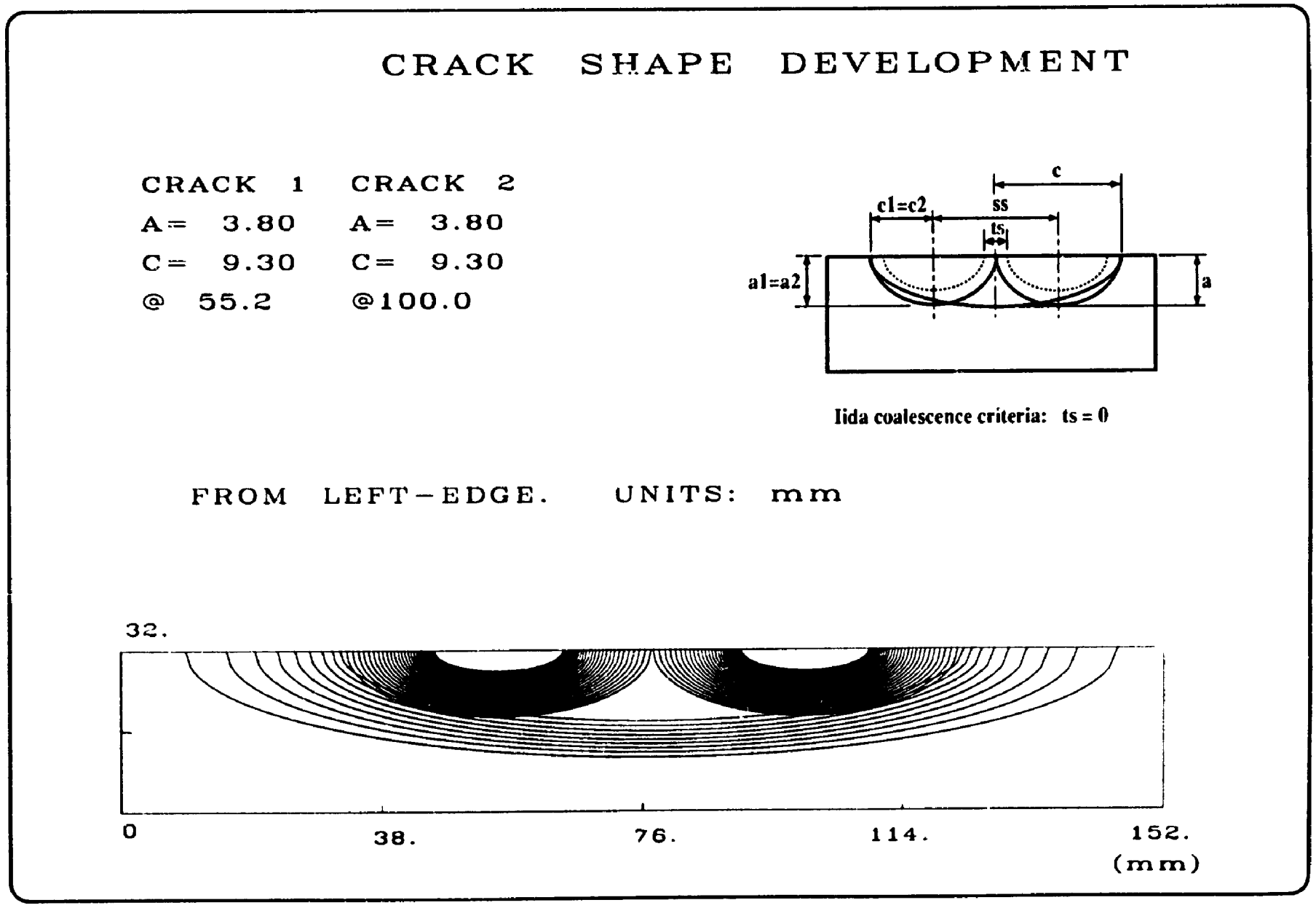

Figure 3.1 (a) Predicted crack profile using the Iida coalescence model with the SC1 shape growth

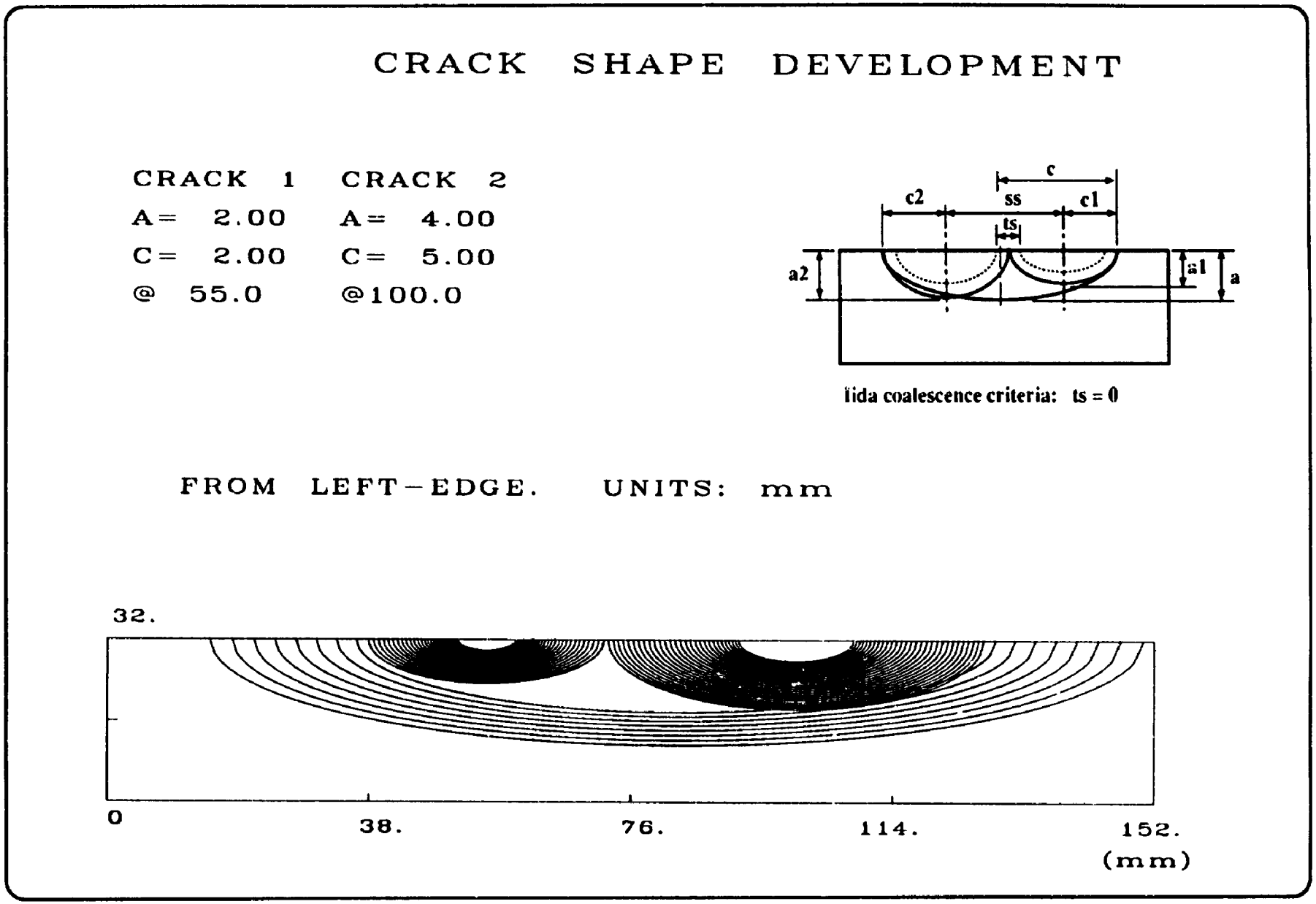

Figure 3.1 (b) Predicted crack profile using the Iida coalescence model with the SC2 shape growth

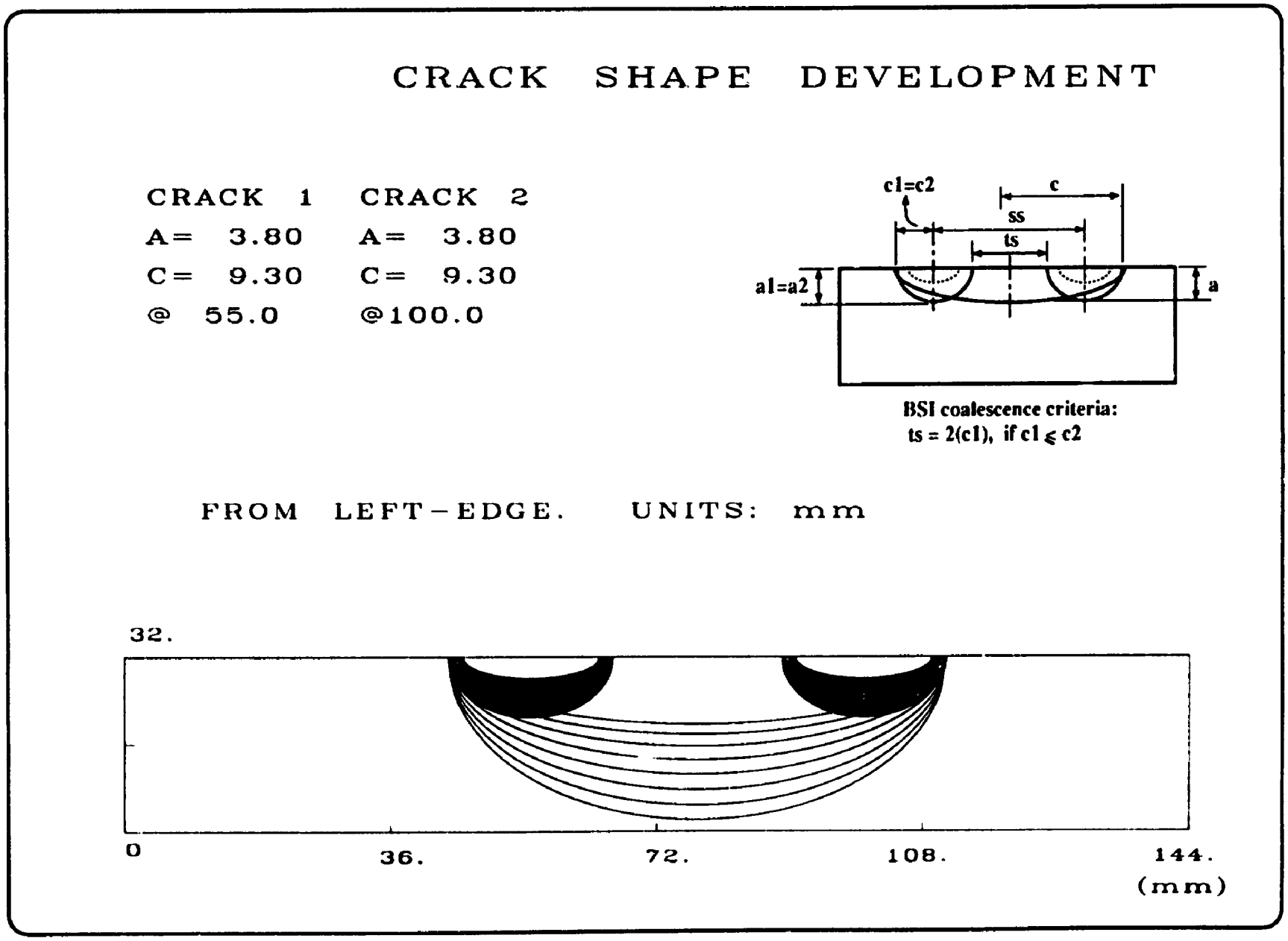

Figure 3.2 (a) Predicted crack profile using the BSI coalescence model under 20% bending plus 80% tension

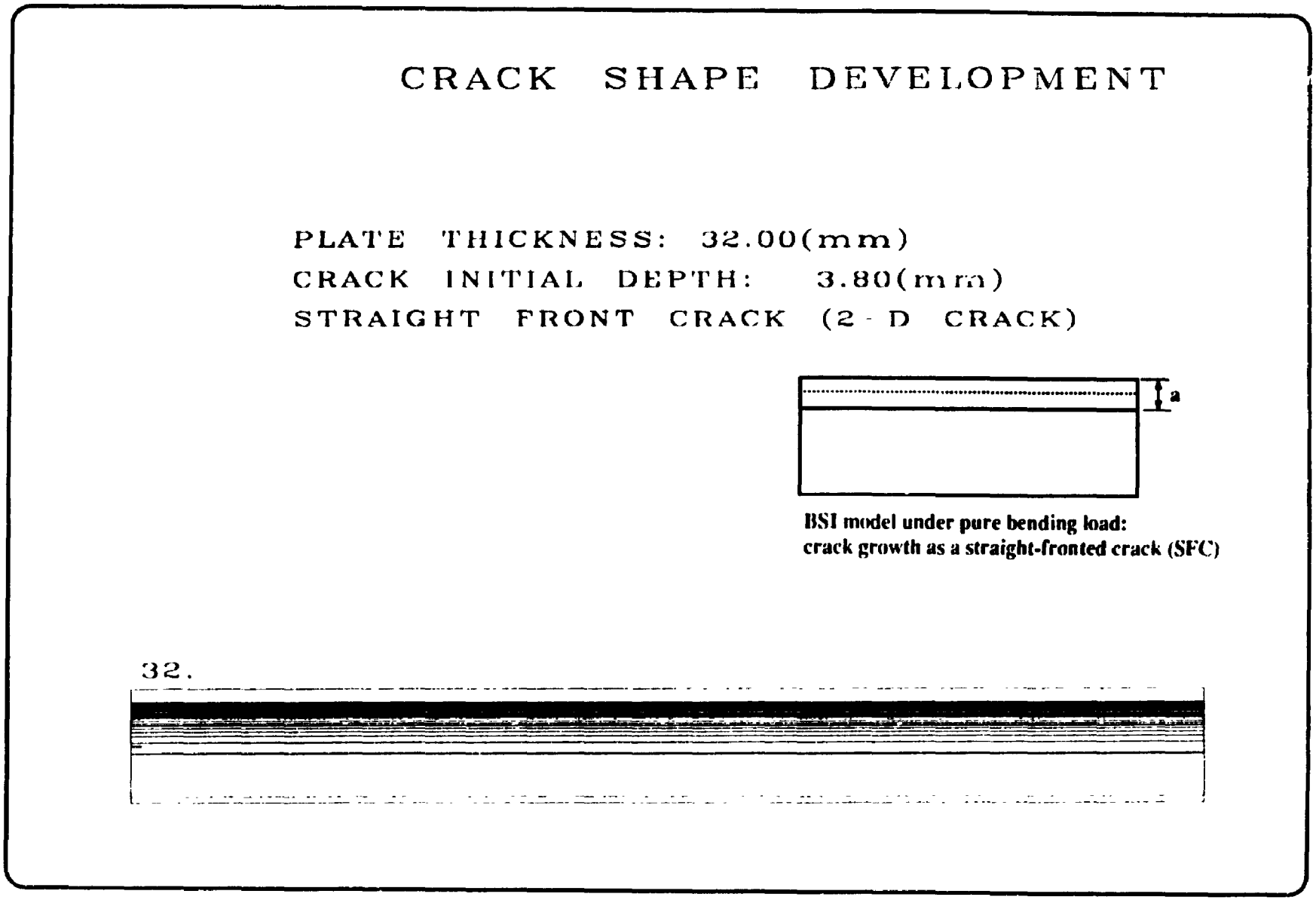

Figure 3.2 (b) Predicted crack profile using the BSI coalescence model under pure bending load

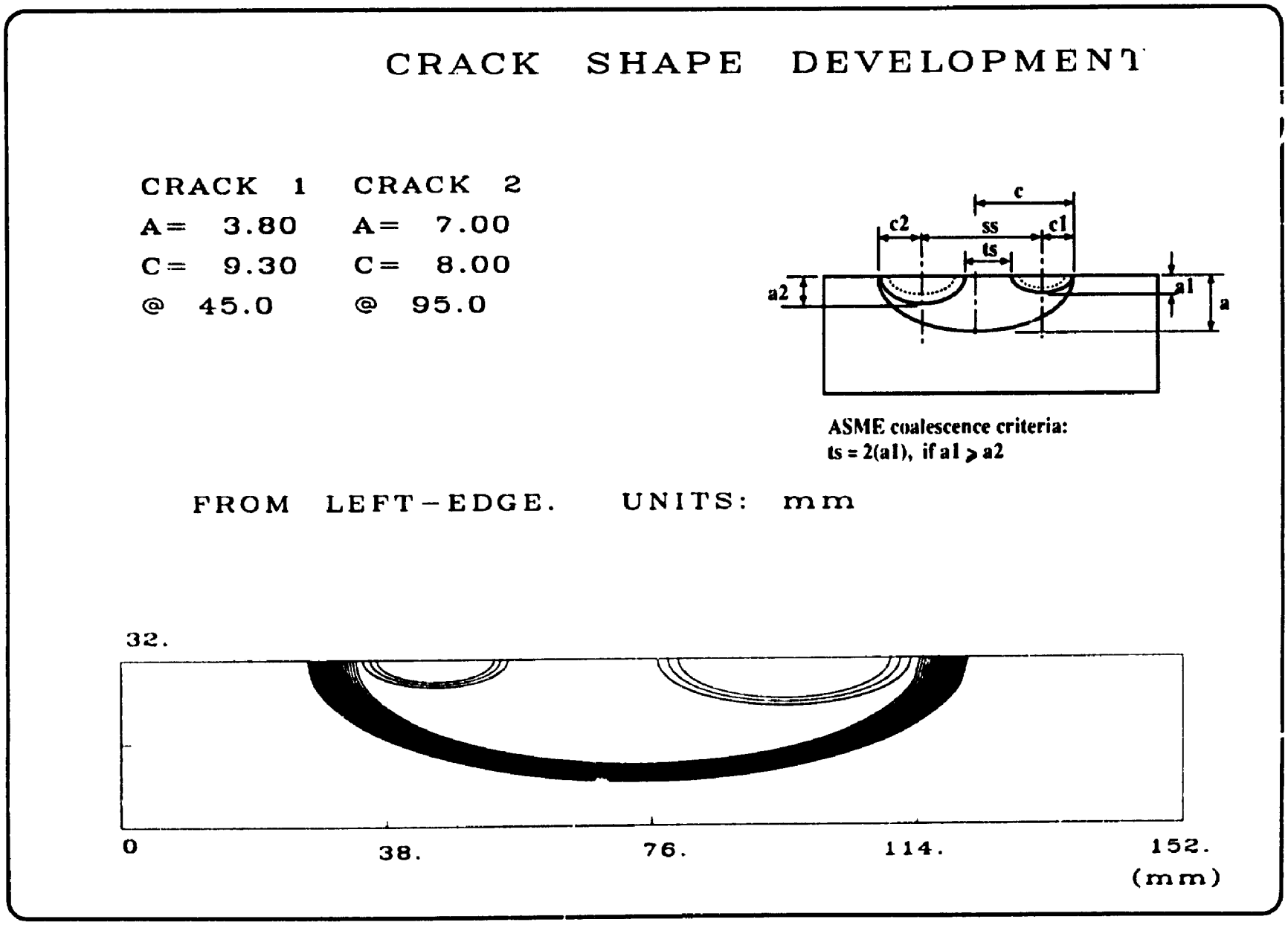

Figure 3.5 Predicted crack profile using the ASME coalescence model with the SC2 shape growth

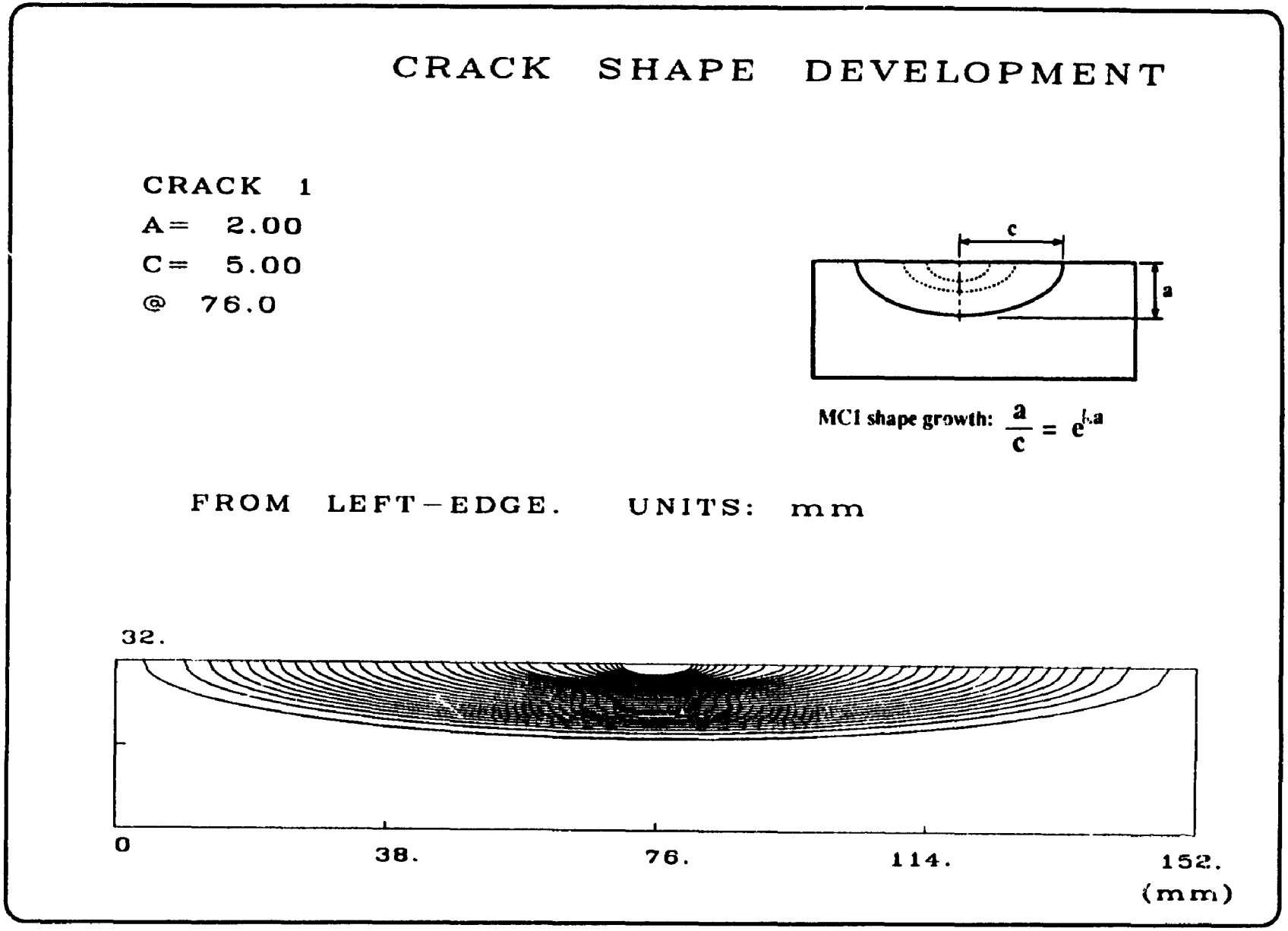

Figure 3.4 Predicted crack profile using the MC1 shape growth (forcing function)

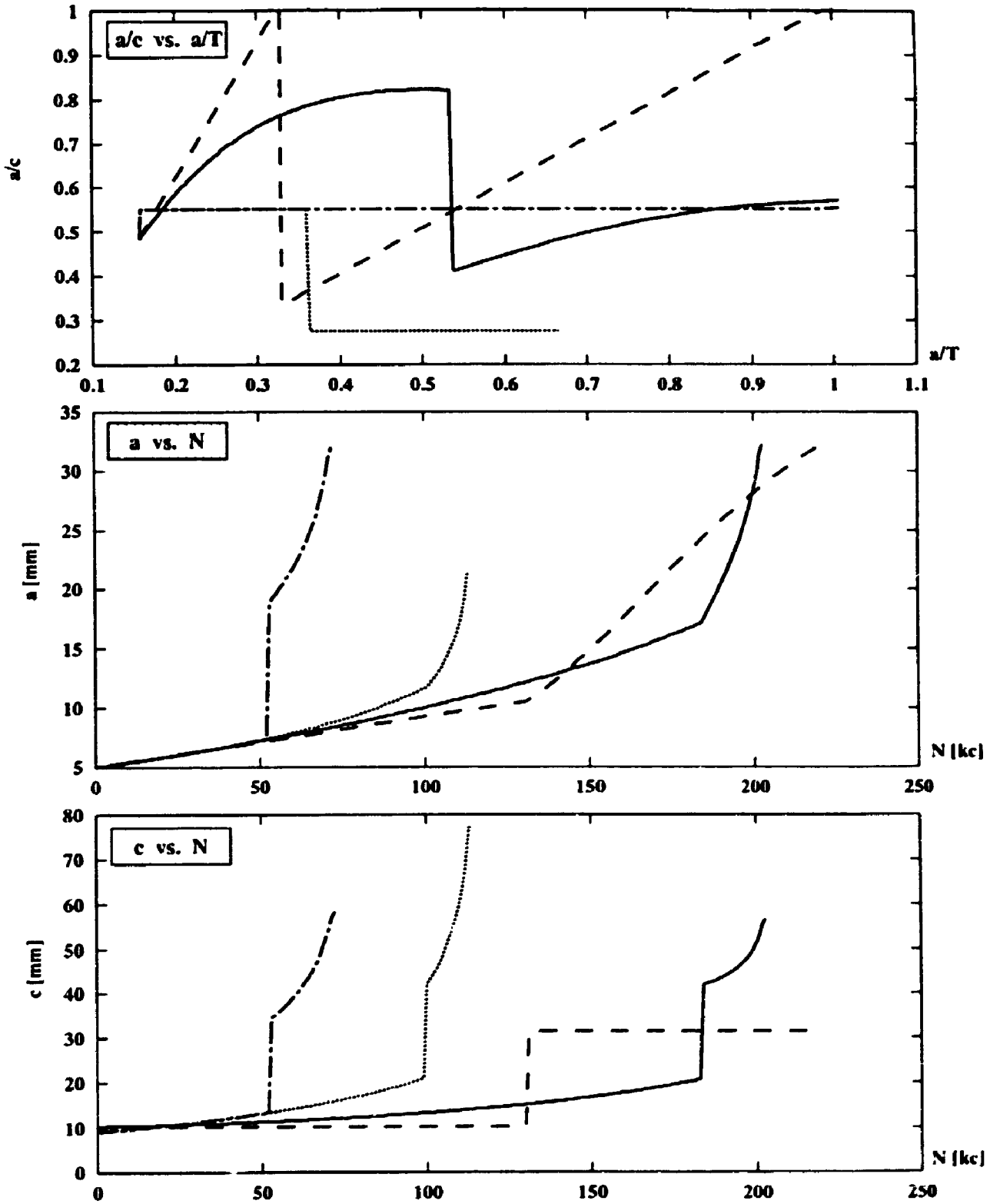

Figure 3.5 Comparison of crack shape development with different predictive models under 20% bending plus 80% tension

Iida with SC1	———	ASME	—·—·—
Iida with SC2	·····	BSI	— — —

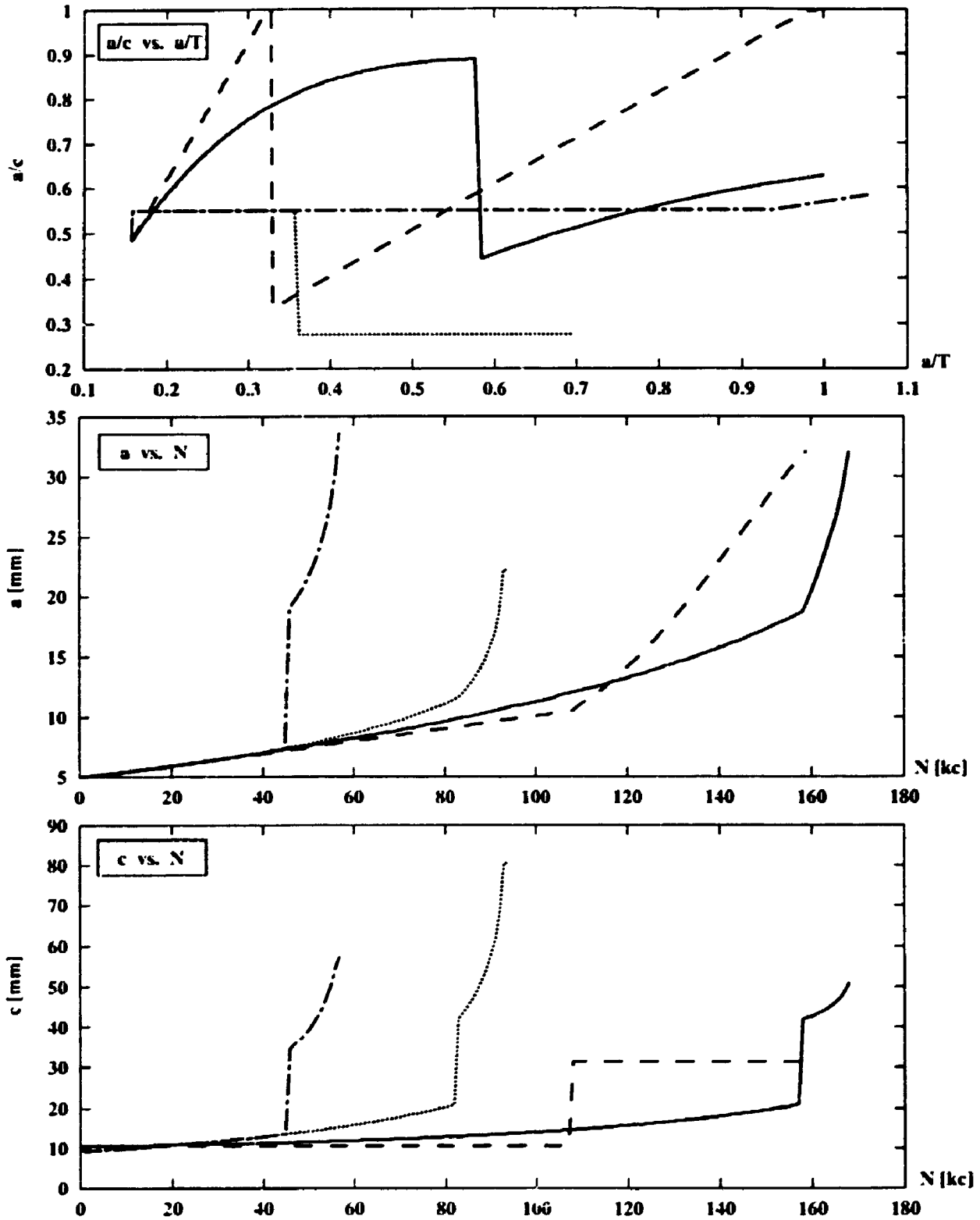

Figure 3.6 Comparison of crack shape development with different predictive models under 100% tension

Iida with SC1 ———	ASME —·—·—
Iida with SC2 ·····	BSI — — —

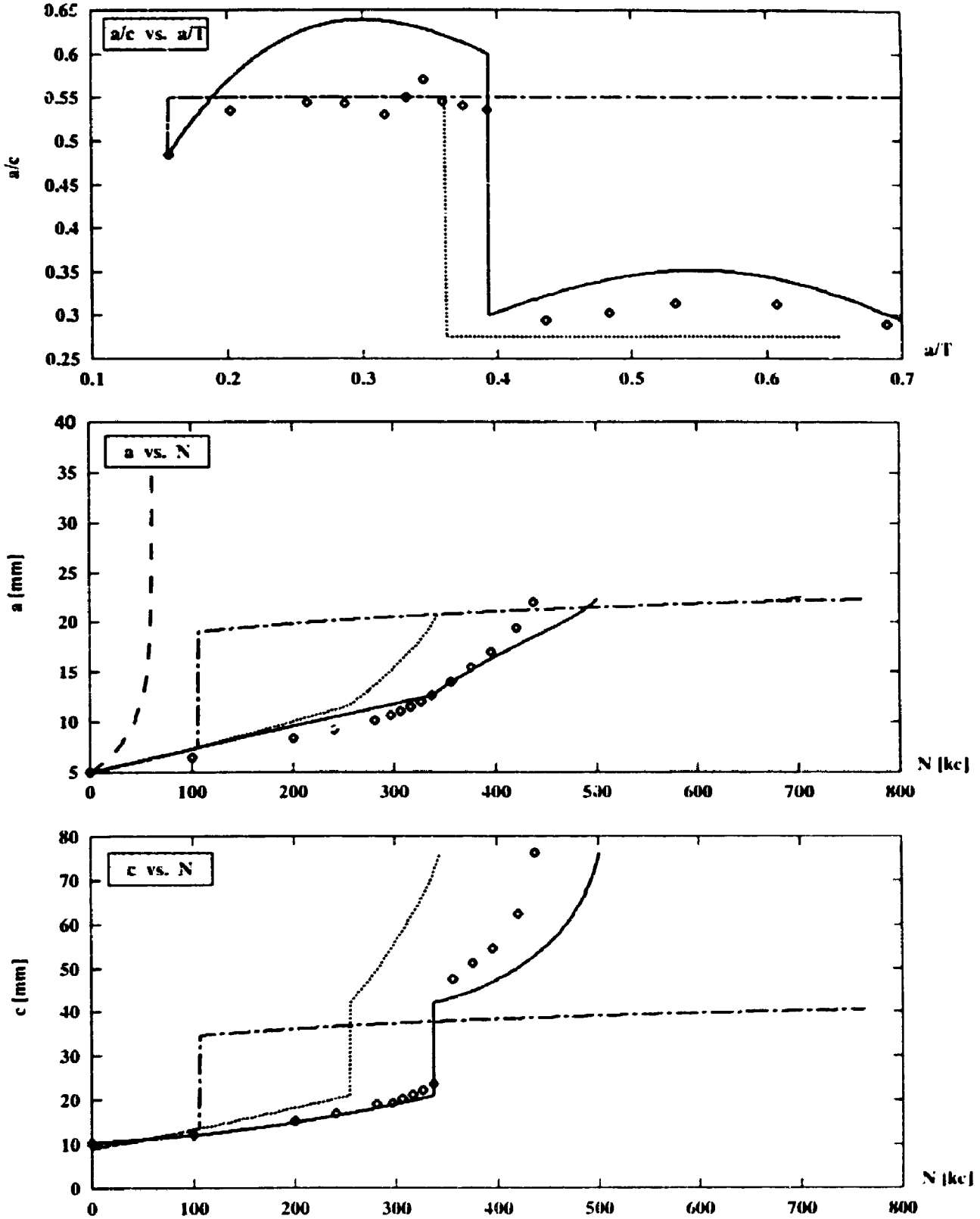

Figure 3.7 Comparison of crack shape development with different predictive models and experimental results under 100% bending

Iida with SC1	———	ASME	—·—·	Exp. data	○ (Ref. 71)
Iida with SC2	·····	BSI	— —		

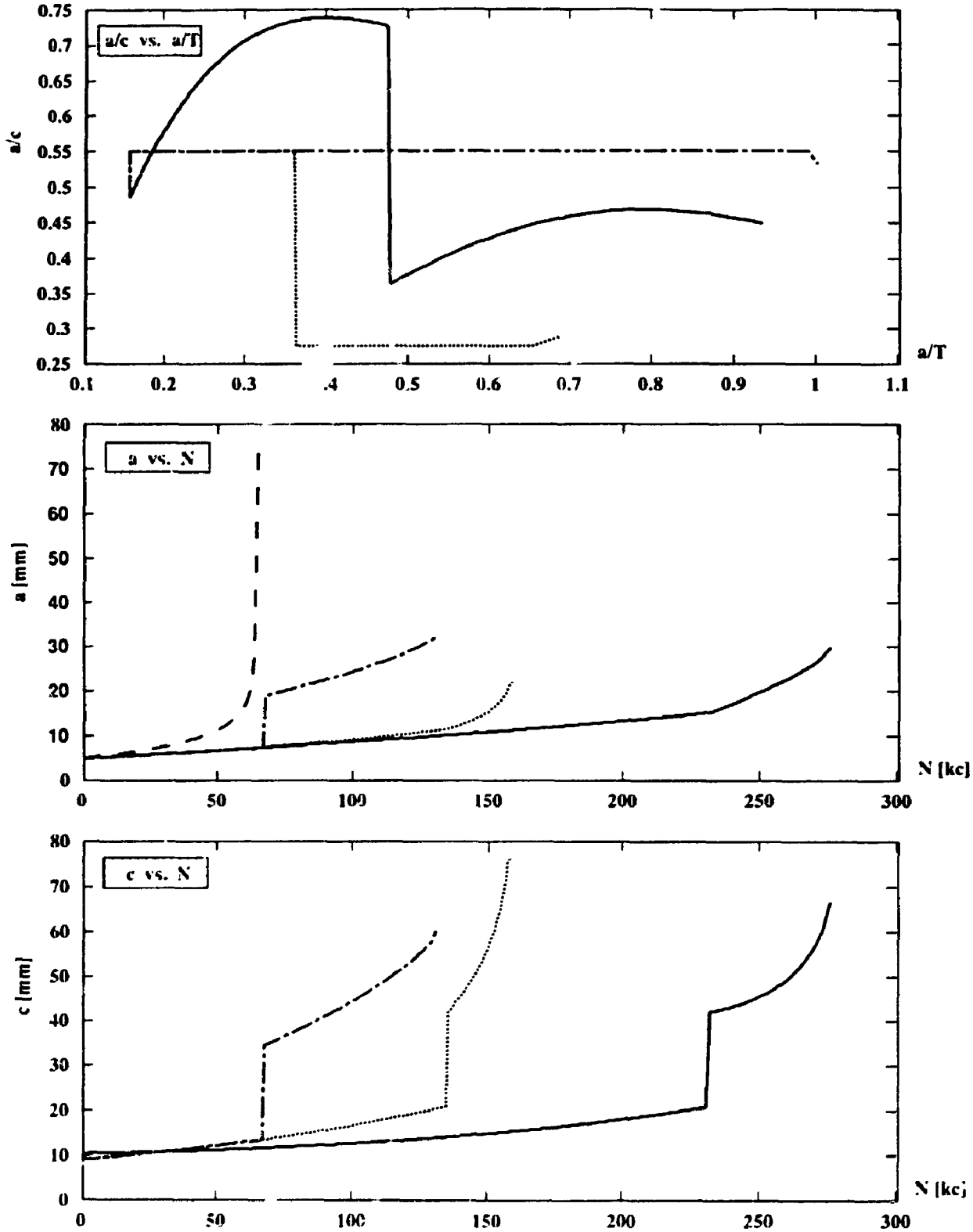

Figure 3.8 Comparison of crack shape development with different predictive models under 50% tension plus 50% bending

Iida with SC1 ———	ASME —·—·—
Iida with SC2 ·····	BSI — — —

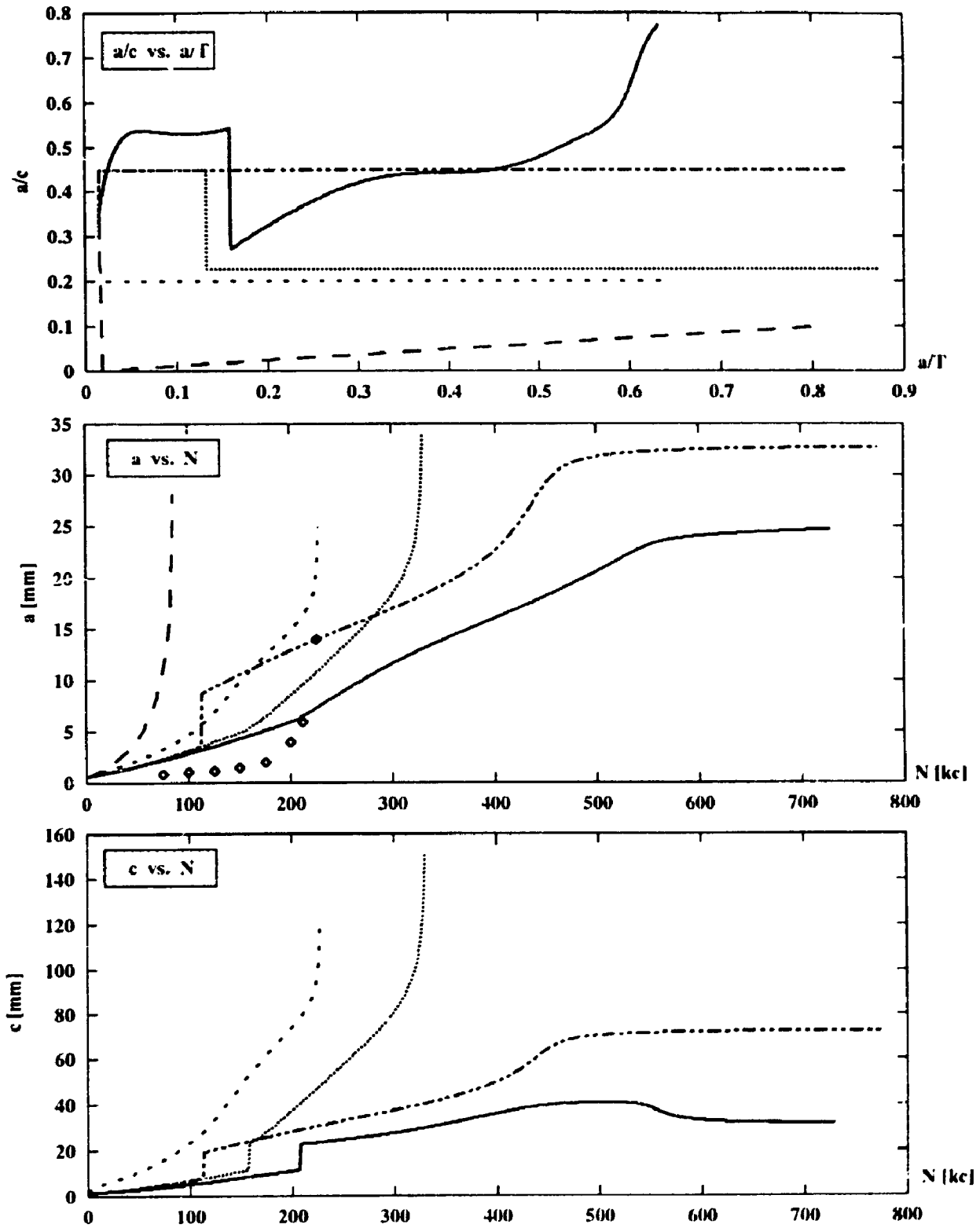

Figure 3.9 Comparison of crack shape development of the MC and SC models with the experimental results (02F) at the weld toe

Iida with SC1	———	MC1	· · · · · · ·
Iida with SC2	·····	MC2 & BSI	— — — —
ASME	—·—·—	Exp. data	○ (Ref. 30)

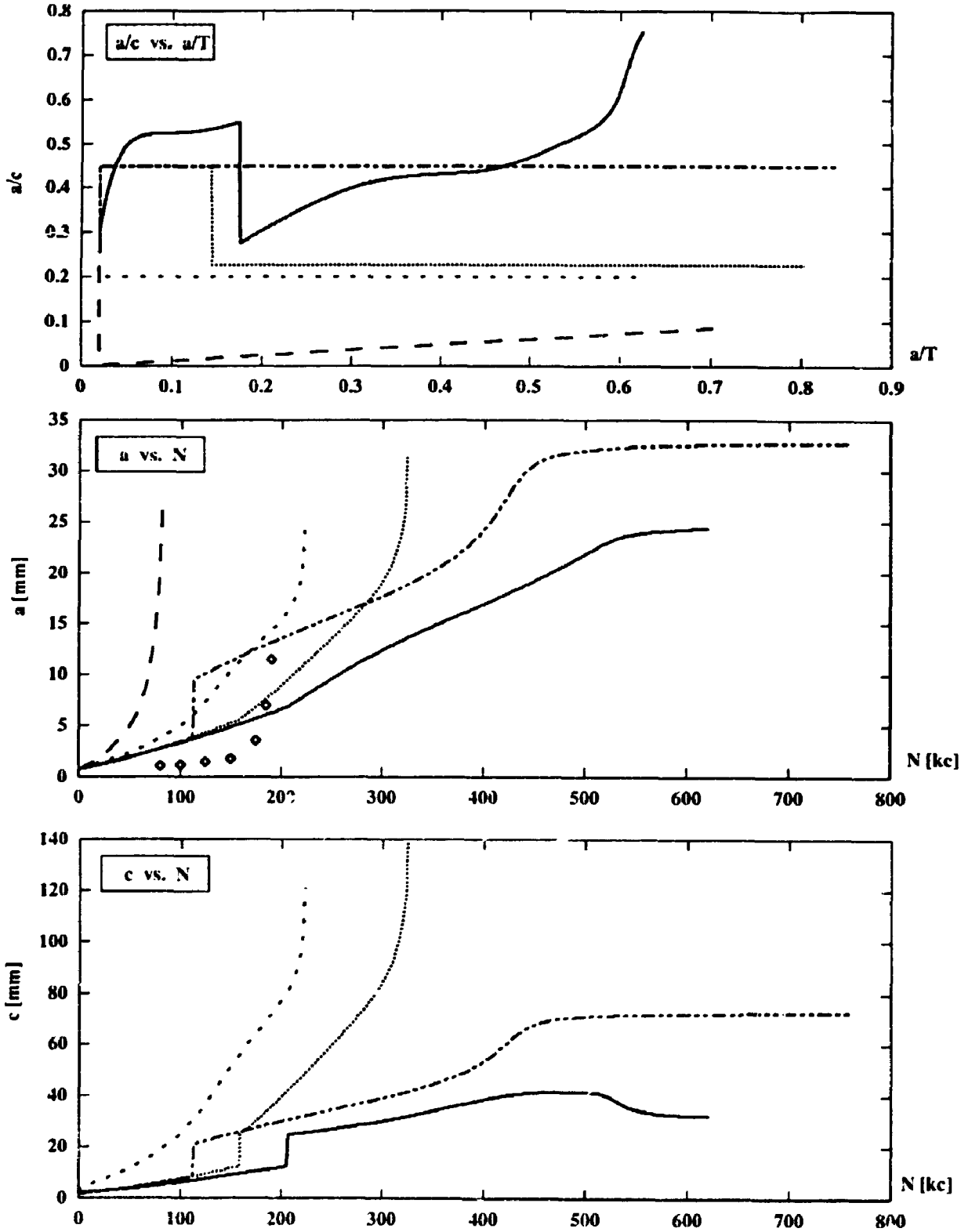

Figure 3.10 Comparison of crack shape development of the MC and SC models with the experimental results (02H) at the weld toe

Iida with SC1	———	MC1	· · · · · · ·
Iida with SC2	·····	MC2 & BSI	— — — -
ASME	—·· ---—···	Exp. data	◇ (Ref. 30)

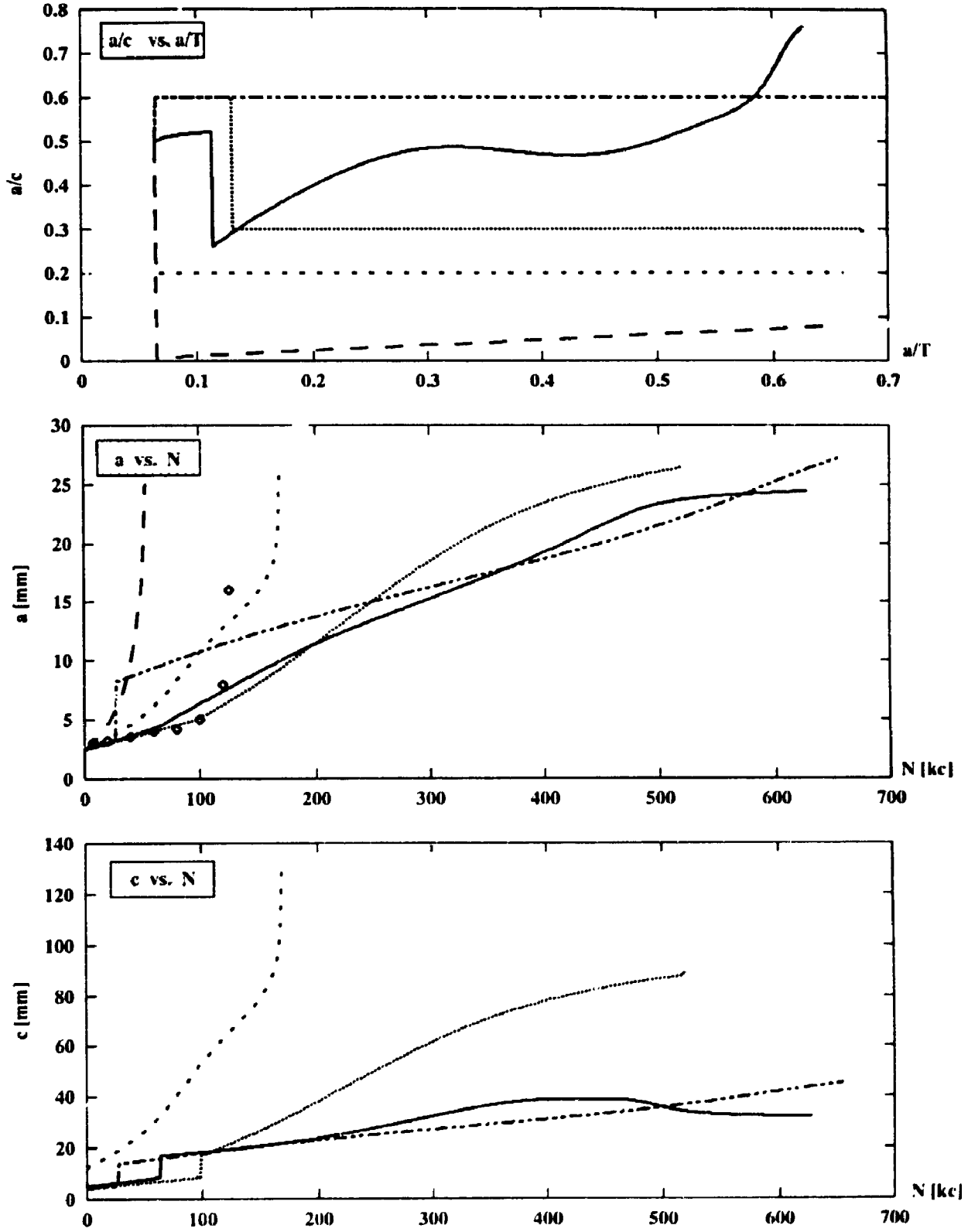

Figure 3.11 Comparison of crack shape development of the MC and SC models with the experimental results (02M) at the weld toe

Iida with SC1	———	MC1	- - - - - -
Iida with SC2	·····	MC2 & BSI	— — —
ASME	—·—·—	Exp. data	◇ (Ref. 30)

CHAPTER IV: The Coalescence Study

4.1 Introduction

According to the experimental data, a percentage of the total life is consumed in the coalescence period. However, the Iida, ASME, and BSI coalescence models assumed that the coalescence process is instantaneous so that once the two adjacent cracks begin to interact, they immediately become a large crack that embraces the previous cracks. Ignoring the coalescence life in many cases does not securately describe the whole fatigue process. The study of fatigue crack growth and coalescence behaviour of semi-elliptical surface cracks in flat plates will be carried out in this chapter. The various parameters governing the effect of parameters such as the coalescence, the interaction and aspect ratio during the crack growth will be demonstrated by the experimental results and crack growth calculations. New models will be generated to simulate the coalescence process in a realistic manner. Experimental data will be used to validate the predictive model.

In this chapter, the predicted initiation life is defined as the number of cycles required to make the starter notch grow into a stable crack shape. The coalescence life is the number of cycles required to grow cracks from the beginning of the crack

interaction to the disappearance of the cusp region. The propagation life is defined as the number of cycles between when a stable crack is formed and final failure occurs. The total fatigue life is the sum of the initiation life and the propagation life.

4.2 Comparison with Previous Experimental Work

The prediction results will be compared with the experimental work carried out by Harrington {71}. The four tests from {71}, designated as the specimen FPB6-3, FPB6-4, FPB6-6 and FPB6-7, will be used. The specimens were fabricated from Grade 350 offshore quality steel plate and were tested in four-point bending. The flat plate specimens had the geometry of 760 x 152 x 31 mm and had a pair of symmetric starter notches, perpendicular to the surface direction which were obtained by a saw cut of 0.15mm thickness. Fatigue tests were performed such that defects grew from these notches under sinusoidal loading of constant amplitude in a hydraulic test machine at a stress ratio of 0.05. The development of the crack front shape was monitored by a beachmarking technique and the DCPD method. The crack growth measurements were taken at the surface and at the maximum depth axes.

4.2.1 Experimental results

Specimen FPB6-3 was tested with low aspect ratio of two identical semi-elliptical starters placed 55mm apart under a stress range of 250 MPa. In the initial growth period, the defects had significant growth through the thickness direction from *2.10 mm* to *5.04* mm and less growth in their surface direction where the surface length increased only

from *18.50 mm* to *19.80 mm*. The data and graphical representation is shown in Table 4.1. Examining the crack growth profiles of the beach marks during this stage, it was found that the cracks grew as groups of semi-ellipses with almost the same major axis length on the surface direction but different minor axis length in the through thickness direction. This phenomenon can be explained as the cracks initially grew to smooth their crack front which had a rough profile produced by the saw cut. It usually developed 0.5 mm depth along the crack front. Then the cracks evolved from an unstable crack shape to a equilibrium stable crack shape, discussed in the section 2.4. The effect of the saw cut and the initiation growth on the crack growth rates can also be observed from the other specimens. After developing a stable crack shape, the cracks grew in the both directions.

Because the computer program can only predict crack growth in two directions, this abnormal growth in one direction and retardation in the other direction can not be simulated. The life of the crack growth during this period is incorporated into the initiation life. It results in 98 kcycles of initiation life and represents 39% of a total life of 253 kcycles. The actual crack dimensions at this time were therefore taken as the initial crack dimensions for computer input, that is, the initial sizes were chosen as the configuration of the first beach mark of specimen FPB6-3 where the cracks started to grow in both a and c directions. The crack coalescence consumed 14 kcycles or 5.5% of the total life according to the experimental data.

The other specimens were tested in a similar manner to that of specimen FPB6-3 except for the stress range. Specimen FPB6-4 and FPB6-7 were tested at the same stress range of 200 MPa. Experimental results and actual crack profiles for these specimens are

shown in Table 4.2 and 4.4. It can be seen that initially they had almost the same starter notches. The spacing between the starters was *44.8 mm* for the FPB6-4 and *43.9 mm* for the FPB6-7. After 140 kcycles and 240 kcycles initiation for the FPB6-4 and the FPB6-7, the crack growth stabilized and resulted in the different initial crack sizes used in the prediction program. Finally, the different propagation lives were obtained as 362 kcycles for specimen FPB6-4 and 310 kcycles for specimen FPB6-7. The experimental coalescence lives for both were around 30 kcycles, i.e., 5.5% to 6.0% of the total life.

Specimen FPB6-6 demonstrated very good results on elliptical crack growth and a well defined coalescence region with a total of 15 beach marks, as shown in Table 4.3. The two notches started at $a = 2.10mm$ and $2c = 18.61mm$ under the stress range of 175 MPa. The initiation life was 300 kcycles, or 40.7% of the total life. After initiation, the geometries were $a = 5.01\ mm$ and $2c = 20.69\ mm$. The crack growth was dominated by the semi-elliptical crack growth following a relatively short period of the crack coalescence. The coalescence life was 46 kcycles out of a total life of 738 kcycles, i.e., 6.23% of the total life. The test terminated when one of the crack surface points reached the edge of the plate and the other one was at half through the thickness of the plate. The very long life of this specimen was due to the relatively low stress level of the test.

4.2.2 Coalescence data generation

Prior to calculating the fatigue life with the prediction model, a study was carried out to obtain the crack geometries from the experimental data during the coalescence period. It can be seen that the coalescence behaviour leads to the complex changes in the

crack shapes. When the two crack tips began to contact or the intersection point of the cracks started to grow through the thickness direction, the crack surface length of the experimental data was measured by the total surface length of the coalescing cracks, that is, the distance between the outer tips of the two cracks. The depth of the cracks, however, was measured separately until the cusp profile was no longer present.

By carefully analyzing the actual crack profiles on the fracture surface of the specimens, it can be seen that two cracks did not immediately become a single crack as the approaching crack tips met. That means that the coalescence process is not instantaneous but a step by step process. It can be noted that after the cracks came into contact with each other, the two cracks still grew independently although their surface length merged like a single crack and the part of the crack fronts fused giving a cusp profile. The growth rate of the intersection point was faster at the beginning of the coalescence and gradually slowed down as the coalescence period progressed. Because the sharp cusp shape is unstable, the intersection region adjusts quickly to smooth this shape until it became a flat profile, as illustrated in Figure 4.1(a). Then the coalescing cracks became a single large crack.

The assumptions of the new coalescence model for a pair of the identical cracks are based on this observation, that is, the cracks contact and continue to grow independently until the intersection point of the two cracks reaches a certain depth. In order to be consistent with the predicted results in the same situation, the surface length of the experimental results during the coalescence period will be recalculated using the total surface length $2c'$ obtained from the beach marks and the initial notches spacing s,

defined as:

$$2c = 2c' - ss \tag{4.1}$$

Where $2c$ is the surface length of each crack obtained from the data generation. This relationship is shown in Figure 4.1(b).

The coalescence data from the experiments for specimen FPB6-6, for example, can be generated as ($ss = 42.1\ mm$):

Beach marks #	Data from beach marks	Coal. data generation
#7	2c' = 80.89 mm	2c = 38.79 mm
#8	2c' = 82.56 mm	2c = 40.46 mm
#9	2c' = 84.40 mm	2c = 42.30 mm
#10	2c' = 86.59 mm	2c = 44.49 mm
#11	2c' = 89.21 mm	2c = 47.11 mm

The coalescence life read from the experiments and beach marks (for specimen FPB6-6 and FPB6-7) can be defined as beginning when the cracks meet and finishing when the point A and B differ by less than 1mm as shown in Figure 4.1(c). Points A and B represents the depth of the crack and the depth of the intersection point of two consecutive beach marks, respectively. At this time the crack profile is relatively flat and the two cracks are assumed to join together.

The same data presentation for other specimens is adopted and are listed in Tables

4.1 to 4.4. Figure 4.2 shows the crack shape development of the four specimens according to this coalescence data generation. In the graph of *a/c versus a/T*, the point at the beginning of crack coalescence can not be distinguished from the fatigue process. But the point at the end of the coalescence can be easily identified where the aspect ratio dropped to a low value forming a single crack. For the measured range of crack depths at $0.2 \leq a/T \leq 0.5$, the aspect ratios were almost the same at about *0.53 to 0.58* for the crack shapes subjected to different levels of the stress. After coalescence, the aspect ratio dropped to and remained at a level of *0.28 to 0.34*. The figures of crack growth at the surface and through the thickness directions verified that high stress range caused short fatigue life and the relationship between fatigue life and stress level is non-linear.

4.3 The Coalescence Model

In this section, an attempt will be made to model the coalescence stage of the crack shape development. As mentioned above, the stress intensity factor in the cusp region of coalescing cracks rises rapidly at the beginning of the coalescence period and then decreases as the small cracks join to become a large single crack of lower aspect ratio. Due to the unstable sharp cusp shape, the stress intensity factor at the intersection point is difficult to describe by a simple formula. Using the Paris law, the new coalescence model attempts to modify the crack growth rate by introducing a coalescence coefficient.

4.3.1 The procedure of the kSC1 coalescence model

The modelling of fatigue crack shape during the coalescence period is mainly concerned with the rapid growth in the cusp region. A modified procedure for the fatigue crack growth evaluation will be proposed on the basis of the experimental results and the shape changes of the crack front is computed on a step by step basis. In order to represent the crack coalescence behaviour with a pair of identical cracks in the predicted model, the following assumptions are made:

(1) The surface cracks are regarded as semi-circular or semi-elliptical cracks. The initial crack sizes are given.

(2) The crack shape models are assumed to grow according to the SC1 - natural crack growth shape model. The increase in the crack depth and surface length is calculated by integration of Paris growth law. The material growth constants are those chosen by McFadyen [83] with the values of $m = 3.0$ and $C_a=5.36*10^{-12}$. The relation of C_a and C_c are assumed to be:

$$C_c = 0.9^m \, C_a \qquad [Ref.19] \tag{4.2}$$

(3) The stages of the coalescence can be described as follows:

(a) Before coalescence, the cracks grow independently in the surface and depth directions.

(b) Once the inner tips of the cracks contact, the calculated depth of the cracks at this time is a_t. Coalescence is assumed to start.

(c) Coalescence continues process as the cracks grow independently but the crack growth rate changes to the k times of the original growth rate, that is,

$$\begin{aligned} \left(\frac{da}{dN}\right)' &= k \left(\frac{da}{dN}\right) \\ \left(\frac{dc}{dN}\right)' &= k \left(\frac{dc}{dN}\right) \end{aligned} \tag{4.3}$$

Where the (da/dN) and (dc/dN) are the growth rates before coalescence from the step (a). The $(da/dN)'$ and $(dc/dN)'$ are the growth rates during coalescence. The factor k is termed as the coalescence coefficient. For each increment of the crack growth, the depth of the intersection point $M(X_0)$ is calculated.

(d) When the predicted depth of $M(X_0)$ is equal to or larger than the value of a_t from the step (b), the end of the coalescence process is assumed. The crack growth rates are again calculated as that before coalescence from step(a). Adjacent cracks are regarded as a single semi-elliptical crack enveloped by a known shape depth of which is assumed to be equal to the maximum depth of the two cracks, and the surface length is assumed to be equal to the distance between the outside tips of the two cracks. Those stages of the coalescence period are shown schematically in Figure 4.3.

This model is termed as the *kSC1* coalescence model and was programmed to simulate the crack growth of double semi-elliptical surface cracks. The predicted crack growth profiles using this model are shown in Figure 4.4.

4.3.2 The coalescence coefficient k

The coalescence coefficient describes the crack growth rate during the coalescence process. If the k is equal to 1.0, it means that when coalescence starts, the cracks will grow at the same growth rate as that before coalescence. At the end of the coalescence period, the coalescence life can be calculated and it is termed as N_{coal} (for $k = 1.0$). By using the experimental coalescence life N_{exp} discussed in the section 4.2.2, the ratio of N_{coal} to N_{exp} can be determined and the coalescence coefficient k defined as:

$$k = \frac{N_{coal}}{N_{exp}} \tag{4.4}$$

Where the N_{coal} is calculated by the computer program when $k = 1.0$. The N_{exp} is the real coalescence life obtained from the experimental data.

If k is obtained as, for example, $k = 2.0$, it implies that during the coalescence stage the crack growth rate both in the surface and through the thickness directions will be twice as fast as the normal growth rate at $k = 1.0$. Therefore, the coalescence

coefficient modifies the growth rate to account for the accelerated growth. With this factor the predicted coalescence life should be the same as the experimental result N_{exp} .

In order to compare the effect of different values of k on the fatigue life and the coalescence life, Table 4.5 shows the comparison with k range from 1.0 to 5.0. The larger the k value, the shorter the coalescence life and propagation life. It needs to be pointed out that whatever the value of k is, the crack geometries compared to the different value of k at the beginning and the end of the coalescence period are almost the same.

The empirical relationship for the k dependence on $\Delta\sigma$ has been derived from a series of tests and it very much depends on reading the coalescence life from the experimental data. The value of k is approximate due to the 10 to 100 kcycles interval between the nearby beach marks. The empirical values of k with different stress level are calculated as below:

Specimens #	N_{exp} [kcycles]	N_{coal} @ k = 1.0 [kcycles]	$k = N_{coal} / N_{exp}$
FPB6-3 ($\Delta\sigma$ = 250 MPa)	14	58	4.14
FPB6-4 ($\Delta\sigma$ = 200 MPa)	30	112	3.73
FPB6-7 ($\Delta\sigma$ = 200 MPa)	30	113	3.77
FPB6-6 ($\Delta\sigma$ = 175 MPa)	46	165	3.59

The values of k are range from 3.59 to 4.14 for the four specimens. It can be found that the coalescence coefficient had linear relationship with the stress range, as

2 of/de 2

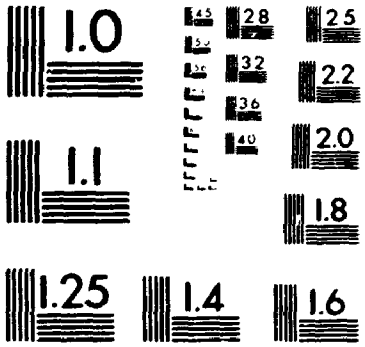

MICROCOPY RESOLUTION TEST CHART
NATIONAL BUREAU OF STANDARDS
STANDARD REFERENCE MATERIAL 1010a
(ANSI and ISO TEST CHART No. 2)

illustrated in Figure 4.5. For the stress levels considered, the relationship can be prescribed by least squares method as a best fit straight line which slope is equal to *0.00728* (standard deviation = 0.0087). It suggests that the stress level is linearly related to the coalescence life, or it is related to the crack growth rate during the coalescence.

4.3.3 The predicted crack shape and fatigue life for the kSC1 model

Figures 4.6 - 4.9 show the crack shape predicted by the kSC1 method for the four surface cracked specimens with the best fit value of k and the corresponding experimental data. The solid line represents the crack growth in the simulation and the dots show the experimental crack growth.

It is noted that the kSC1 predicted model has three distinct crack shape development regimes, one is before the coalescence, one is during the coalescence to account for the shape development and one is after the coalescence. The model changes from the first regime to the second at the point where the two cracks contact each other and from regime two to three at the time which the depth of intersection point is equal to or larger than the crack depth of the semi-elliptical crack at the beginning of the coalescence. This implies that the cracks grow significantly at the deepest and surface points during the coalescence period. It has been shown to be true by examination of the fracture surface of specimen FPB6-6. It is found that the predicted crack depth had significant growth from *12.63 mm* to *16.34 mm* compared to the experiments which showed growth from *10.30 mm* to *13.97 mm* during this period. The crack depth increments are *3.71 mm* for the prediction and *3.67 mm* for the experiments. This small

difference verifies that the assumptions of the kSC1 model which assumed the time at the beginning and the end of the coalescence is acceptable.

In Figure 4.6 of specimen FPB6-6, the predicted life are in good agreement with the test results where the experimental life was 438 kcycles compared to 454 kcycles of the prediction. The overall crack shape parameters for the experimental and predictive results are plotted in terms of *a/c versus a/T*. The aspect ratio for the predicted crack shape is over-estimated when $a/T < 0.4$. That is because the experimental crack depth at this time did not grow as quickly as prediction. Also the predicted time at the end of the coalescence period is greater than that shown in the experiment. It can be seen that the growth rate of the surface direction during 0 and 350 kcycles period is predicted very well. After this stage, the slope of the curve becomes steep representing the higher growth rate. Then the single crack instantaneously formed showing a straight vertical line in the diagram of *c versus N*.

Similar approaches were adopted for the specimen FPB6-7 and FPB6-4 for a stress range of 200 MPa. The crack shape development shown in Figure 4.7 and 4.8 for both specimens are well predicted with a slight over-estimation of the aspect ratio at the intermediate crack depth. The predicted fatigue lives are 324 kcycles for specimen FPB6-7 compared to 310 kcycles of the experimental result and 357 kcycles prediction life compared to 362 kcycles of the experimental life for specimen FPB6-4.

The kSC1 model used to simulate the fatigue life of specimen FPB6-3 is shown in Figure 4.9. The crack shape of the predictive model of *a/c versus a/T* shows some difference compared to the experiments. But the growth rate predictions in *a* and *c*

directions shows good agreement and the predicted life is about 163 kcycles compared to 155 kcycles for the experimental life, i.e. +5.2% difference.

Both the experimental results and the predicted model show that the coalescence life is approximately 5.5% to 6.2% of the total fatigue life for the stress range from 175 MPa to 250 MPa. That is small percentage of the total life for the flat plate. Table 4.6 shows that the kSC1 model produces the propagation life with the difference to the experimental results range from -1.4% to +5.2% for the four specimens. In the next section some parameters which are not included in the kSC1 model will be discussed.

4.4 Modifications to the kSC1 predictive model

4.4.1 The interaction effect

More careful investigation of the fracture surface showed that for the case of specimen FPB6-6 at beach mark #7, the surface length of each crack at the beginning of the coalescence stage is less than the spacing between the two cracks, that is, $ss = 42.1$ *mm* and $2c = 38.79$ *mm*. The calculation shows that they are still *3.31 mm* apart while the experimental data reported the start of the coalescence. This indicates fast crack growth just before the approaching crack tips meet at the interacting surface. The value named the interaction distance d_i is about one third of the crack depth of the same beach mark ($a = 10.66$ *mm*). It is very small compared to the crack surface length ($2c = 38.21$ *mm*) or the criteria from the ASME model (interaction distance is $2a = 20.26$ *mm*) and BSI model (interaction distance is $2c = 38.21$ *mm*). The same thing is observed from specimen FPB6-7 at the beach mark #10 which had the interaction distance about *2.62*

mm while the spacing between the cracks was *43.9 mm* and surface length of each crack was *41.28 mm*. The interaction distance was about one quarter of the crack depth (a = *11.48 mm*) at this time. Those experimental crack growth studies indicate the interaction effect is only significant when the cracks are nearly touching.

To obtain a better understanding of the whole process of the coalescence, interaction between the two adjacent cracks (for a pair of identical cracks) is built into the model. This model is termed the interaction model with the SC1 shape growth has the same assumption as the kSC1 model except for the definition of the beginning of the coalescence. Therefore, the differences are:

> When the distance between the inner tips of the two cracks is equal to or less than *0.29* times the crack depth (this number comes from the average of the interaction distance shown above), the crack inner tips jump instantaneously to where they contact each other but the outer tips of the cracks remain at the same positions. The interaction distance is described as:
>
> $$d_i \leq 0.29\ a \tag{4.5}$$
>
> The new crack dimension is calculated as the surface length of the cracks is equal to the existing surface length plus half of the interaction distance d_i , i.e.
>
> $$2\ c = 2\ c' + \frac{1}{2}\ d_i \tag{4.6}$$
>
> The depth of the crack at this time remains the same and it is called a_i. The surface length change results in the centres of the two cracks moving toward each other about one quarter of the interaction distance. It is also assumed that at this time coalescence begins. The calculation of the crack growth rates and the coalescence coefficient will be similar to that of the kSC1 coalescence model.

The interaction model also has three stages of the coalescence as shown schematically in Figure 4.10 and the predicted crack shape is shown in Figure 4.11.

The fatigue lives of the interaction model with the SC1 shape growth are

illustrated in Figure 4.12 to 4.15 for the four specimens with the specified k as used previously in the kSC1 model. In the diagrams of crack shape development *a/c versus a/T*, the two vertical line step by step, one of which at the high aspect ratio represents the jump of the surface points at the beginning of the coalescence - the interaction effect, where the aspect ratio changes from *0.6 to 0.55*. The other one at the end of the coalescence represents the coalescence effect, where the aspect ratio changes from 0.5 to 0.3. The crack shapes of the interaction model show a better fit to the experiments than that of the kSC1 model. But the crack growth rate through the thickness direction is still over-predicted. In the surface direction this prediction has good agreement with the test results during the whole propagation life, especially for specimen FPB6-6 and FPB6-7 which have more beach mark data for the comparison.

Some finite element studies on semi-elliptical fatigue cracks have been indicated that the stress intensity factor increases gradually as the cracks approach each other but increase steeply when the cracks overlap, Miyoshi *et al* {64}. The interaction model simulates this process since it is a result of the increase of the growth rate at the time before and during the coalescence period.

The comparisons of the kSC1, the interaction and Iida models with the SC1 shape growth with the corresponding experimental data and relative errors are shown in Table 4.6 and Figure 4.16. Because of the interaction effect, the fatigue lives are shorter than that of the kSC1 coalescence model. The differences between the model and experiments are around -4.7% to +1.3% for the four specimens.

It is clear that fatigue crack interaction appears to be a small portion of crack

growth before the coalescence. The interaction model is applicable for the crack growth simulation due to considering the approaching and overlapping crack growth process and it leads to better predicted fatigue life.

4.4.2 The kSC2 coalescence model

As mentioned earlier, the experimental data show that the crack shapes tend toward the a constant value of *0.53* to *0.58* for the four specimens before the end of the coalescence process, as shown in Figure 4.1. After coalescence the aspect ratios of the cracks decrease to a lower value of *0.27* to *0.35*. As a result of this observation a model designated the kSC2 model was tested by this computer program.

It is known that the different crack shape models of the kSC1 and kSC2 will produce a different coalescence life N_{coal} at $k = 1$. Therefore, the coalescence coefficient k for the shape model of the SC2 needs to be recalculated in the same way as before. The results are listed as follows:

Specimens #	N_{exp} [kcycles]	N_{coal} @ k = 1.0 [kcycles]	$k = N_{coal} / N_{exp.}$
FPB6-3 ($\Delta\sigma$ = 250 MPa)	14	100	7.14
FPB6-4 ($\Delta\sigma$ = 250 MPa)	30	174	5.8
FPB6-7 ($\Delta\sigma$ = 200 MPa)	30	164	5.47
FPB6-6 ($\Delta\sigma$ = 175 MPa)	46	212	4.61

The linear relationship of best fit k with different stress range using least squares method has a slope of 0.0323 (standard deviation = 0.090), as shown in Figure 4.17. The predicted crack shape with this model is shown in Figure 4.18.

The simulated propagation behaviour for each specimen using this model is displayed in Figure 4.19 to 4.22 for comparison with the experimental results. In the diagram of *a/c versus a/T*, the constant aspect ratio is chosen to be 0.55 - an average value before the coalescence. After coalescence, the aspect ratio is development by the geometries of a single crack it formed from the two coalescing cracks. The predicted crack shapes agree with the experimental data very well throughout the fatigue life, but the model over-predicts the growth rates in the a and c directions. However, the final predicted life is close to the experimental life. From Table 4.7, it is found that the predicted fatigue lives of the four specimens are conservative in all cases. The differences range from *-3.2% to -5.5%*. Combining the SC2 shape growth with the interaction model, the predicted life can be expected to be more conservative than that of the kSC2 model.

It is clear that the simulated crack growth behaviour with the SC2 shape model is unable to match the experimental results since the errors in the growth rate are large, despite the fact that the crack shape development is modelled very well. The earlier coalescence in the predictions leads to conservative results.

It can be concluded that a good prediction of the crack shape described by the aspect ratio of *a/c versus a/T* gave conservative growth rates in the a and c directions in this case. Therefore, the simulated fatigue life must depend not only on the crack shape development (*a/c versus a/T*) but also on the crack growth rate alone the crack front

(*a versus N* and *c versus N*). The predictions for specimen FPB6-3 using the kSC1 model discussed in the section 4.3.3, gave a good prediction in the surface and through the thickness directions but does not agree with the experimental crack shapes, which are opposite to the present kSC2 case.

4.4.3 The saw cut and initiation effect

In the section 4.2.1 it was noted that the saw cut and initiation effect on the cracks allowed growth in one direction and retarded growth in another. In general, there appears to be significant effect on fatigue life predictions when this behaviour is ignored. Figure 4.23 shows the difference of -18.7% in total life for specimen FPB6-6 although the crack shape *a/c versus a/T* still fits the experiments very well. The recommended procedure is to model the initiation behaviour and stable crack during the initial load cycle using the experimental data and beach marks which give a very clear picture of the crack growth history.

4.4.4 Other effects

There are some other factors which may affect fatigue life prediction. From the fracture surfaces of the specimen, it can be observed that there are some deviations (called shear zone) located between the two cracks as the two cracks overlap from slightly different planes. This can be seen in the actual crack profile of specimen FPB6-7. The deviation of the crack plane is a very complex problem resulting from stress level, loading conditions, initial crack growth and so on. This phenomenon affects the fatigue life.

Another effect is that in the experimental test had two starter notches which were a slightly different in size and gradually grew toward differently, even if the difference is small compared to the overall geometry of the cracks. In the prediction method the crack sizes are chosen to be the average size of the two notches and two identical cracks are used in all models.

The experimental data provided the coalescence life. The coalescence coefficient is calculated from the experimental data for the geometries tested. Whether this coalescence factor can be used in the different geometries, different loading conditions and under different stress ranges needs further study.

4.5 Conclusions

In this chapter the crack coalescence processes were investigated and the kSC1, kSC2 and interaction model with the SC1 shape growth were developed. The results illustrate the importance of crack shape development in the accurate modelling of the fatigue crack propagation of flat plates during the coalescence period. The modelling also indicated that the coalescence and failure criteria need to consider stable crack growth after initiation and crack growth during the interaction and coalescence life in order to provide a long design life than more conservative estimates.

The predictive evaluations show that it is satisfactory to assume that the cracks will grow independently of each other until neighbouring cracks interact at which point they coalesce. Then they grow independently with a faster growth rate until the coalescence process finishes. The models used a similar parameter which was defined as

the coalescence coefficient. Further, the interaction model considered the interaction effect before coalescence using the interaction distance. The crack shape development in the simulation tends to over-predict the experimental aspect ratio, leading to faster crack growth behaviour in the through thickness direction. But the predicted propagation life gave in a small error.

Table 4.1 Experimental results and actual crack profiles for specimen FPB6-3 {Ref.71}

Beachmark #	Life N [kc]	Depth a [mm]	Length 2c [mm]	Coal. data generation		
				Life	a	c
notch	0	2.01	18.5			
1	98	5.04	19.8	0	5.04	9.9
2	155	8.12	28.1	57	8.12	14.05
3	185	9.94	33.8	87	9.94	16.9
4	215	12.72	91.2	117	12.72	22.45
5	245	18.86	111.4	147	18.86	55.7
failure	253	21.26	136.0	155	21.26	68.0

General information:

Plate:
width 2B = 152.3 mm
thickness T = 31.6 mm

Stress:
bending stress = 250 MPa
stress ratio R = 0.05

Notches:
# of starter notch = 2
notch spacing ss = 46.3 mm

Fatigue life:
coalescence life = 14 kcycles
total life = 253 kcycles

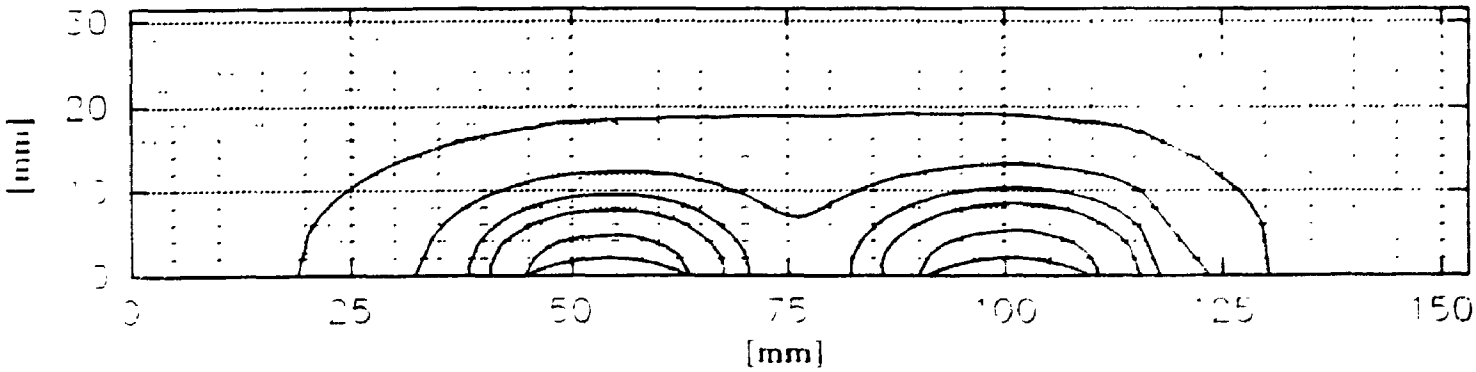

Table 4.2 Experimental results and actual crack profiles for specimen FPB6-4 {Ref. 71}

Beachmark #	Life N [kc]	Depth a [mm]	Length 2c [mm]	Coal. data generation		
				Life	a	c
notch	0	2.06	18.6			
1	140	3.80	18.6	0	3.80	9.3
2	190	4.89	19.8	50	4.89	9.9
3	240	6.06	21.5	100	6.06	10.75
4	290	7.34	25.8	150	7.34	12.9
5	340	8.81	30.9	200	8.81	15.45
6	390	10.52	38.4	250	10.52	19.2
7	440	13.53	94.3	300	13.53	24.75
8	490	19.21	123.9	350	19.21	61.85
failure	502	21.40	142.6	362	21.40	71.3

General information:

Plate :
width 2B = 152.4 mm
thickness T = 31.7 mm

Stress:
bending stress = 200 MPa
stress ratio R = 0.05

Notches:
# of starter notch = 2
notch spacing ss = 44.8 mm

Fatigue life:
coalescence life = 30 kcycles
total life = 502 kcycles

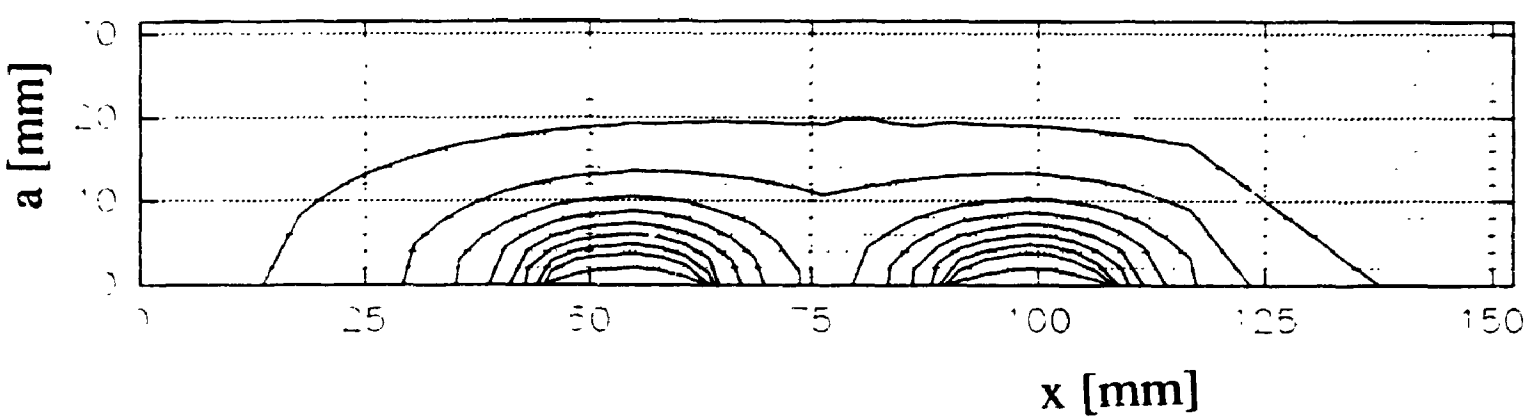

Table 4.3 Experimental results and actual crack profiles for specimen FPB6-6 {Ref. 71}

Beachmark #	Life N [kc]	Depth a [mm]	Length 2c [mm]	Coal. data generation		
				Life	a	c
notch	0	2.1	18.61			
1	200	3.8	18.61			
2	300	5.01	20.69	0	5.01	10.345
3	400	6.48	24.27	100	6.48	12.135
4	500	8.30	30.54	200	8.30	15.27
5	540	9.18	33.79	240	9.18	16.895
6	580	10.13	38.21	280	10.13	19.105
7	596	10.66	80.89	296	10.66	19.395
8	606	11.05	82.56	306	11.05	20.23
9	616	11.52	84.40	316	11.52	21.15
10	626	11.99	86.59	326	11.99	22.25
11	636	12.59	89.21	336	12.59	23.56
12	656	13.97	94.96	356	13.97	47.48
13	676	15.48	102.20	376	15.48	51.10
14	696	17.04	108.83	396	17.04	54.415
15	721	19.43	124.62	421	19.43	62.13
failure	738	22.04	152.37	438	22.04	76.185

General information:

Plate:
width 2B = 152.4 mm
thickness T = 31.6 mm

Stress:
bending stress = 175 MPa
stress ratio R = 0.05

Notches:
# of starter notch = 2
notch spacing ss = 42.1 mm

Fatigue life:
coalescence life = 46 kcycles
total life = 738 kcycles

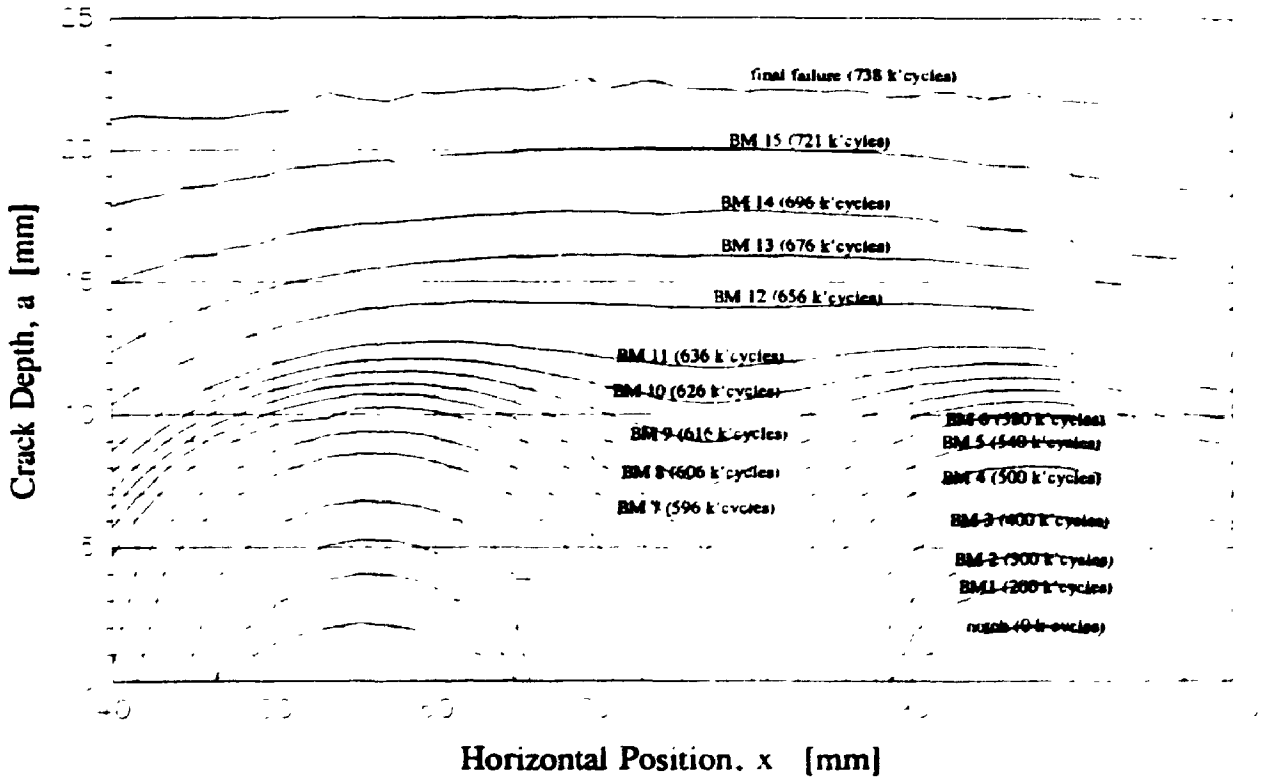

Table 4.4 Experimental results and actual crack profiles for specimen FPB6-7 {Ref.71}

Beachmark #	Life N [kc]	Depth a [mm]	Length 2c [mm]	Coal. data generation		
				Life	a	c
notch	0	2.17	18.71			
1	140	3.31	18.71			
2	190	4.02	18.71			
3	240	4.81	19.32	0	4.81	9.66
4	290	5.84	21.21	50	5.84	10.61
5	340	7.03	24.36	100	7.03	12.18
6	390	8.35	28.66	150	8.35	14.33
7	440	9.76	34.69	200	9.76	17.35
8	460	10.44	40.49	220	10.44	20.25
9	470	10.88	41.34	230	10.88	20.67
10	480	11.48	85.18	240	11.48	20.64
11	490	12.34	88.56	250	12.34	22.33
12	505	14.00	95.01	265	14.00	25.56
13	525	16.45	107.12	285	16.45	53.56
failure	550	21.33	144.01	310	21.33	77.01

General information:

Plate:
width 2B = 152.3 mm
thickness T = 31.7 mm

Stress:
bending stress = 200 MPa
stress ratio R = 0.05

Notches:
# of starter notches = 2
notch spacing ss = 43.9 mm

Fatigue life:
coalescence life = 30 kcycles
total life = 550 kcycles

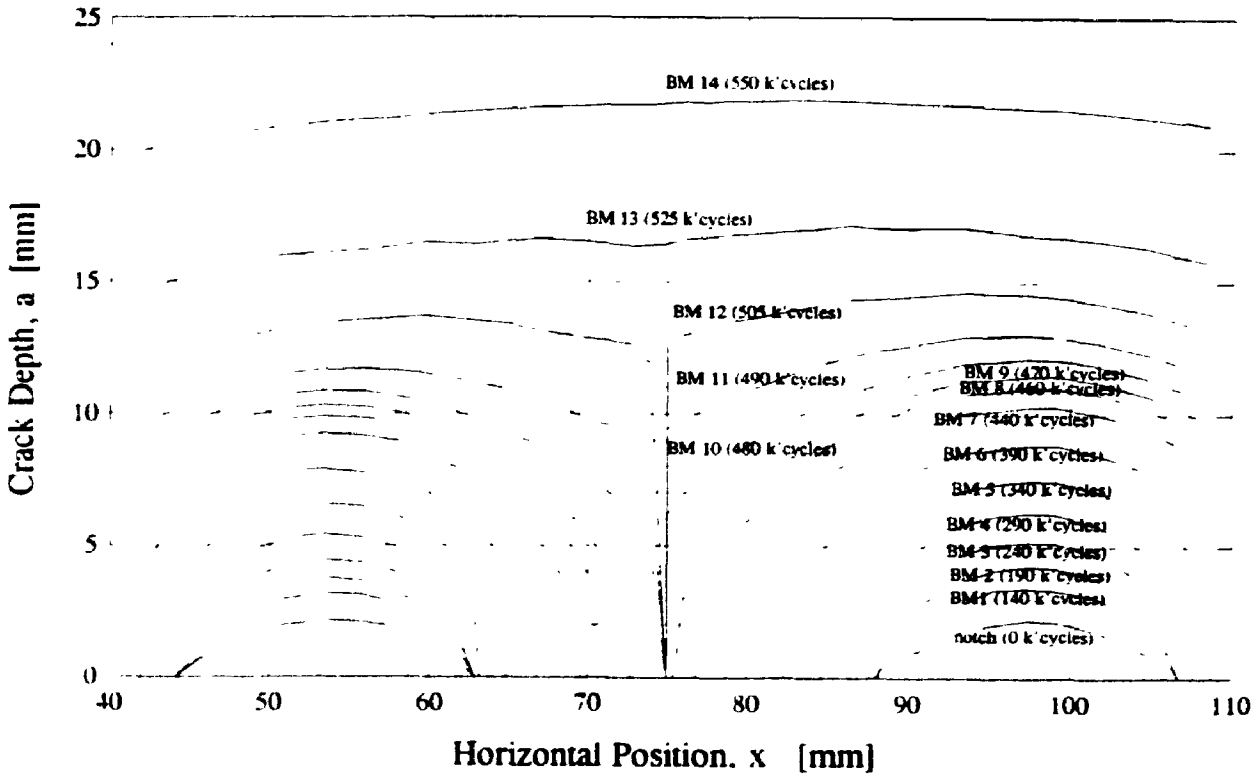

Table 4.5 Comparison of the predicted and experimental lives of the kSC1 model with various values of k

Specimen #	Coal. factor k	Coal. starts @ [kc]	Coal. starts geo. [mm]	Coal. ends @ [kc]	Coal. ends geo. [mm]	Predicted coal. life [kc]	Predicted propagation life [kc]	Experimental coal. life [kc]	Experimental propagation life [kc]
FPB6-6 $\Delta\sigma = 125$ MPa	k = 1.0	338	a = 12.63 c = 21.10	503	a = 16.34 c = 54.28	165	574	46	438
	k = 2.5			405		67	474		
	k = 3.0			394		56	463		
	k = 4.0			380		42	449		
FPB6-4 $\Delta\sigma = 200$ MPa	k = 1.0	291	a = 13.15 c = 22.43	403	a = 16.85 c = 58.22	112	439	30	362
	k = 2.5			336		45	367		
	k = 3.0			329		38	359		
	k = 4.0			320		29	349		
FPB6-7 $\Delta\sigma = 200$ MPa	k = 1.0	255	a = 12.98 c = 21.95	368	a = 16.70 c = 57.06	113	407	30	310
	k = 2.5			300		45	339		
	k = 3.0			293		38	332		
	k = 4.0			284		29	322		
FPB6-3 $\Delta\sigma = 250$ MPa	k = 1.0	134	a = 13.45 c = 23.32	192	a = 17.20 c = 60.75	58	207	14	155
	k = 3.0			154		20	164		
	k = 4.0			149		15	159		
	k = 5.0			146		12	156		

Table 4.6 Comparison of predicted models with experimental results

Specimen #	Coal. coeff. (least squares) k	kSC1 model		Interaction model with the SC1 growth		Iida coal. model with the SC1 growth		Exp. results
		coal. life [kc]	Np [kc]	coal. life [kc]	Np [kc]	coal. life [kc]	Np [kc]	Np [kc]
FPB6-6 $\Delta\sigma$ = 125 MPa	k = 3.585	46	454 (+3.7%)	46	438 (0%)	0	501 (+14.4%)	438
FPB6-4 $\Delta\sigma$ = 200 MPa	k = 3.767	30	357 (-1.4%)	30	345 (-4.7%)	0	387 (+6.9%)	362
FPB6-7 $\Delta\sigma$ = 200 MPa	k = 3.767	30	324 (+4.5%)	30	313 (+1.0%)	0	356 (+14.8%)	310
FPB6-3 $\Delta\sigma$ = 250 MPa	k = 4.131	14	163 (+5.2%)	14	157 (+1.3%)	0	180 (+16.1%)	155

(% different between prediction and experiments)

Table 4.7 Comparison of the predicted life of the kSC2 model

Specimen #	Coal. factor (least squares) k	Coal. starts @ [kc]	Coal. starts geo. [mm]	Coal. ends @ [kc]	Coal. ends geo. [mm]	Predicted coal. life [kc]	Predicted propagation life [kc]	Experimental propagation life [kc]
FPB6-6 $\Delta\sigma$ = 125 MPa	k = 4.72	255	a = 11.59 c = 21.07	300	a = 16.41 c = 50.89	45	419 (-4.3%)	438
FPB6-4 $\Delta\sigma$ = 200 MPa	k = 5.53	238	a = 12.33 c = 22.42	270	a = 17.50 c = 54.22	32	342 (-5.5%)	362
FPB6-7 $\Delta\sigma$ = 200 MPa	k = 5.53	192	a = 12.11 c = 22.02	222	a = 17.15 c = 53.13	30	299 (-3.6%)	310
FPB6-3 $\Delta\sigma$ = 250 MPa	k = 7.145	104	a = 12.77 c = 23.21	118	a = 18.11 c = 56.09	14	150 (-3.2%)	155

(% difference between prediction and experiments)

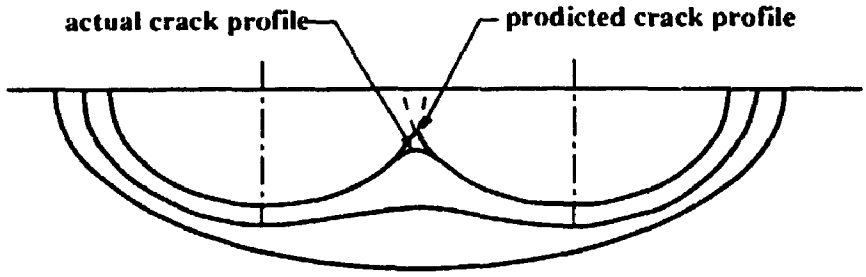

(a) Predicted crack profile vs. actual crack profile

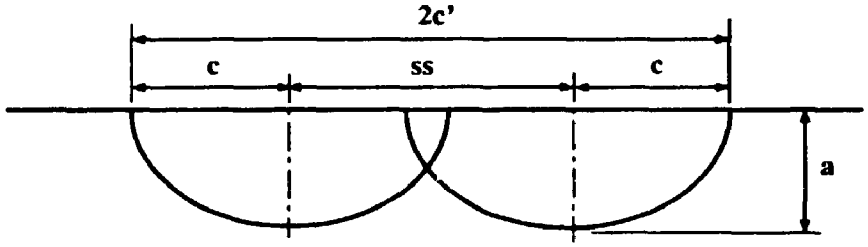

$2c = 2c' - ss$

Where:

2c' is the surface length obtained by the experimental work
ss is the spacing between the adjacent cracks
2c is the surface length obtained from the data generation

(b) The experimental coalescence data generation

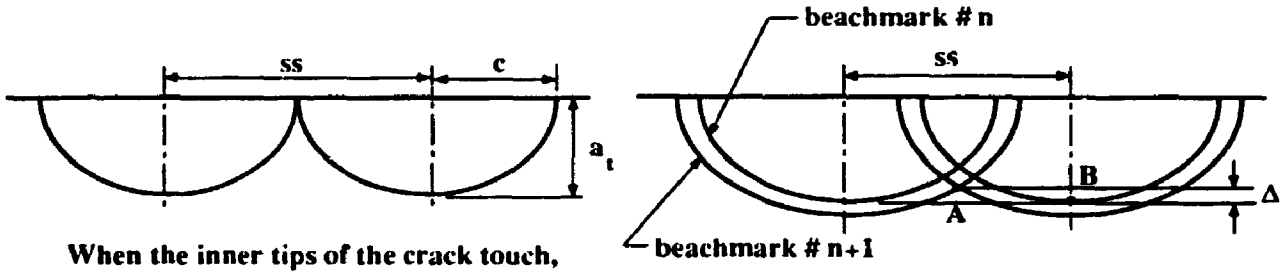

When the inner tips of the crack touch, the beginning of the coalescence.

When $\Delta < 1$ mm, the end of the coalescence.

(c) The coalescence life reading

Figure 4.1 Experimental coalescence data generation

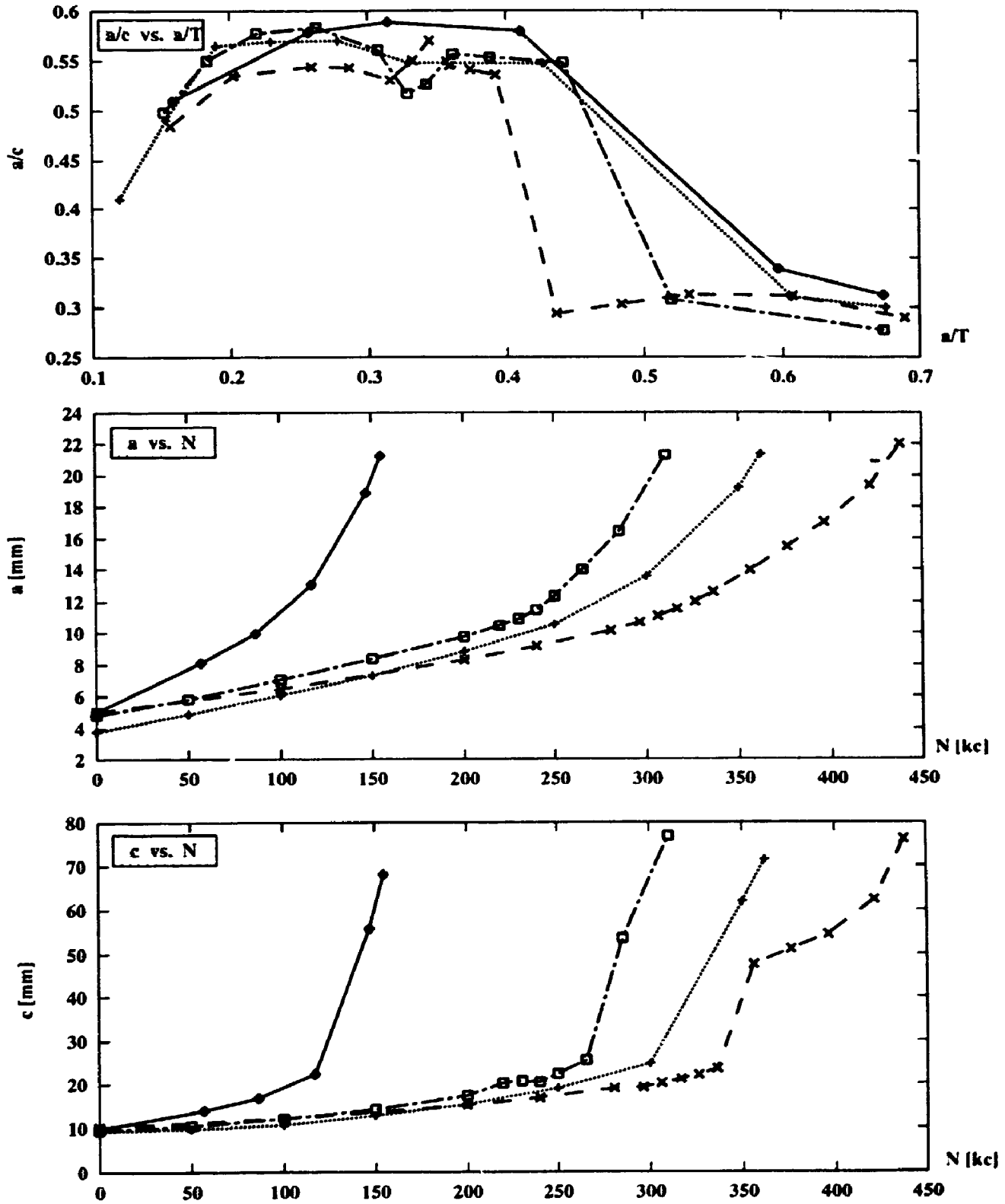

Figure 4.2 Experimental results

FPB6-3: 250 MPa
FBP6-4: 200 MPa
FPB6-7: 200 MPa
FPB6-6: 175 MPa

(a) Before coalescence

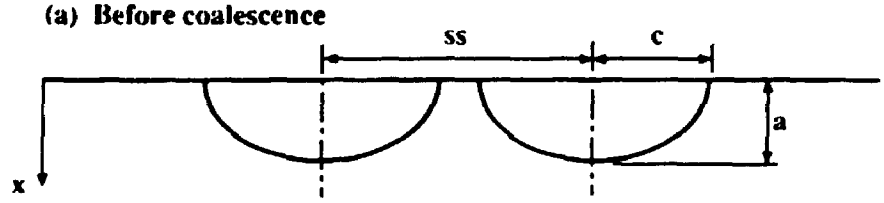

$$\frac{da}{dN} = C_a \Delta K^m \qquad \frac{dc}{dN} = C_c \Delta K^m$$

$$C_c = 0.9^m C_a$$

(b) During coalescence

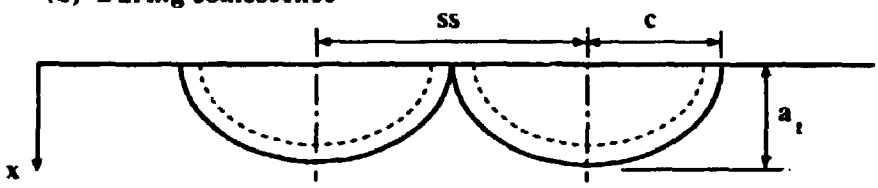

When two cracks touch, the coalescence process begins. The cracks continue to grow independently in the surface and through the thickness directions.

$$\frac{da'}{dN} = k\frac{da}{dN}$$

$$\frac{dc'}{dN} = k\frac{dc}{dN}$$

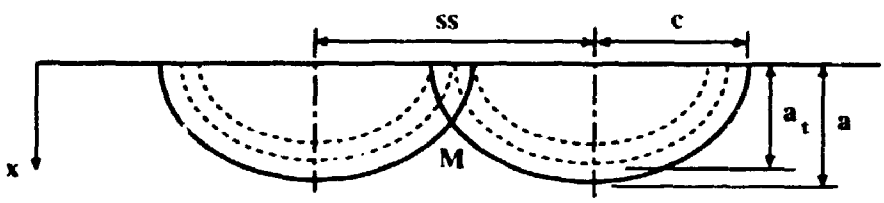

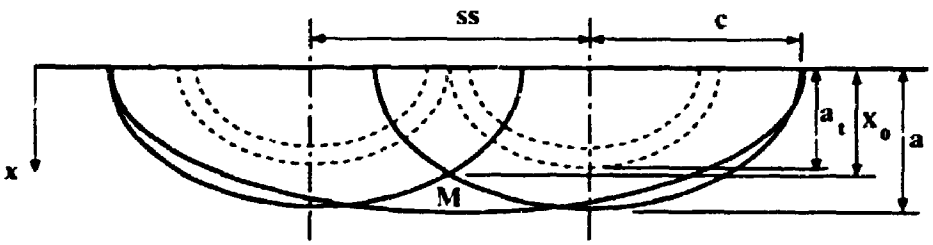

When $X_0 > a_t$, it is assumed the end of the coalescence process.

(c) After coalescence

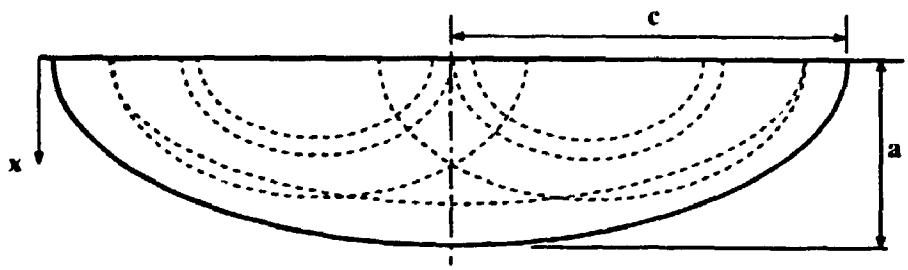

A single large crack forms.

$$\frac{da}{dN} = C_a \Delta K^m \qquad \frac{dc}{dN} = C_c \Delta K^m$$

$$C_c = 0.9^m C_a$$

Figure 4.3 The three stages of coalescence - kSC1 model, schematically (The dotted lines represent the previous states of the crack growth profile)

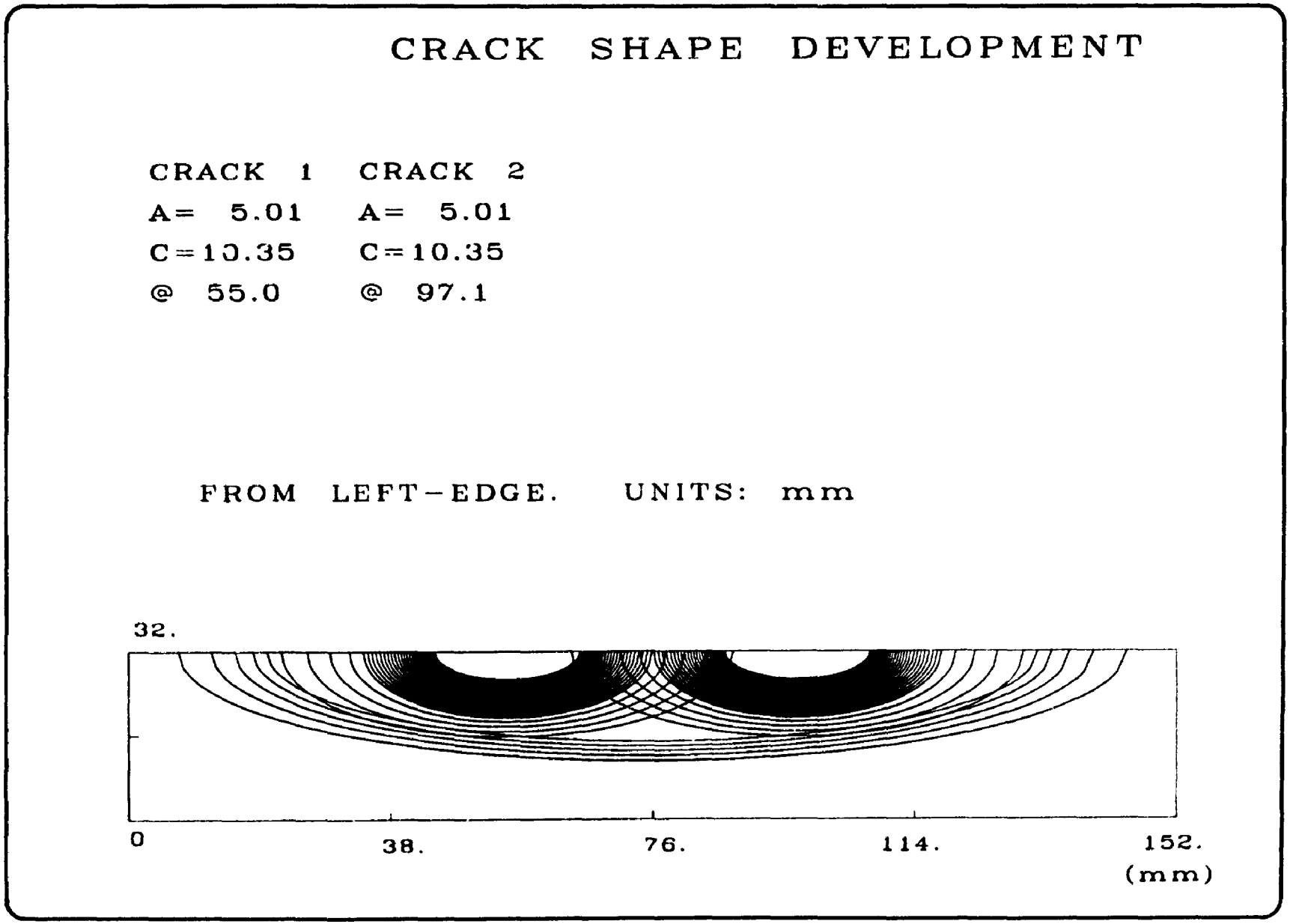

Figure 4.4 Predicted crack growth history of the kSC1 model

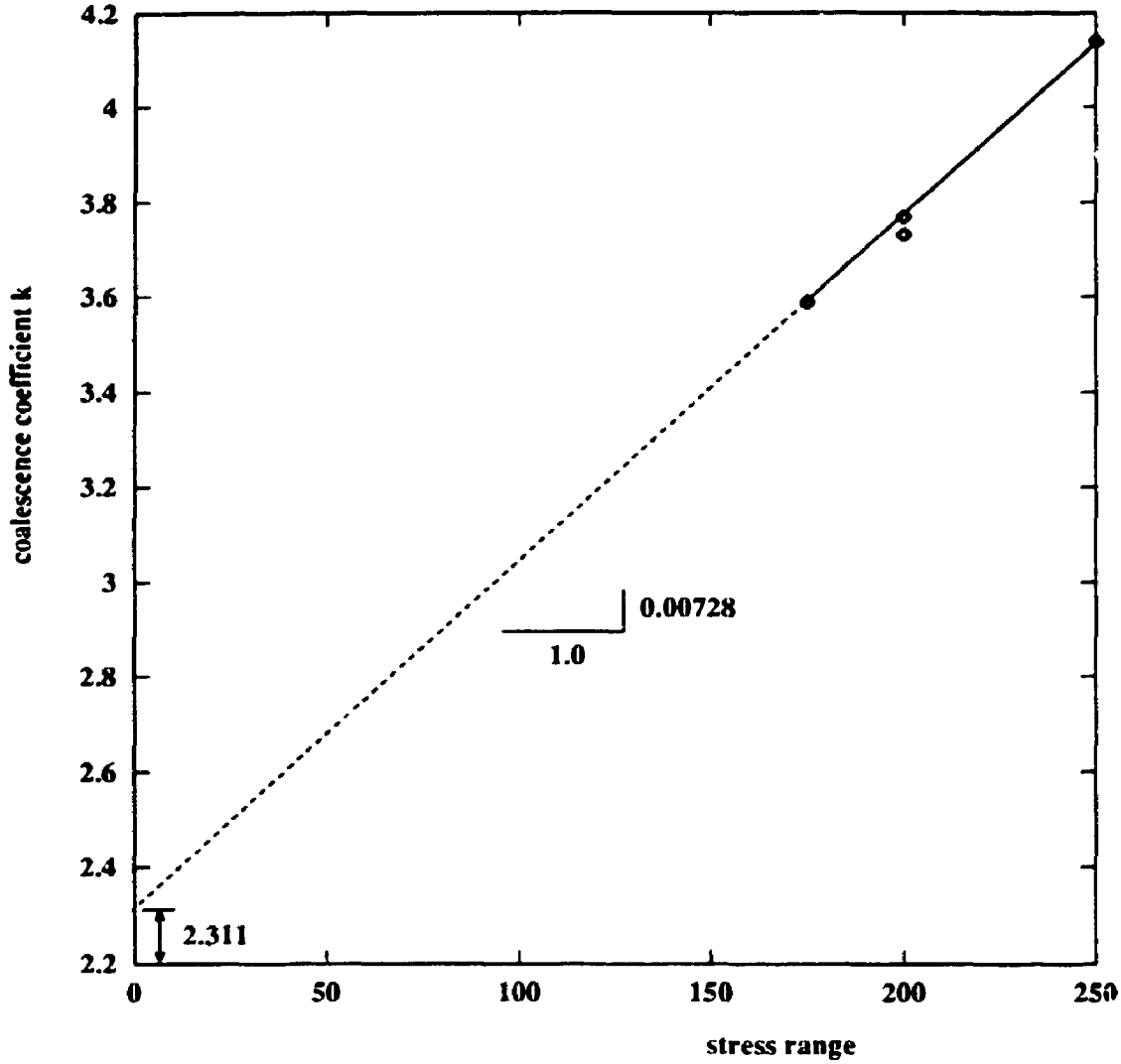

Figure 4.5 The coalescence coefficient related to the stress range for the kSC1 model and the interaction model with the SC1

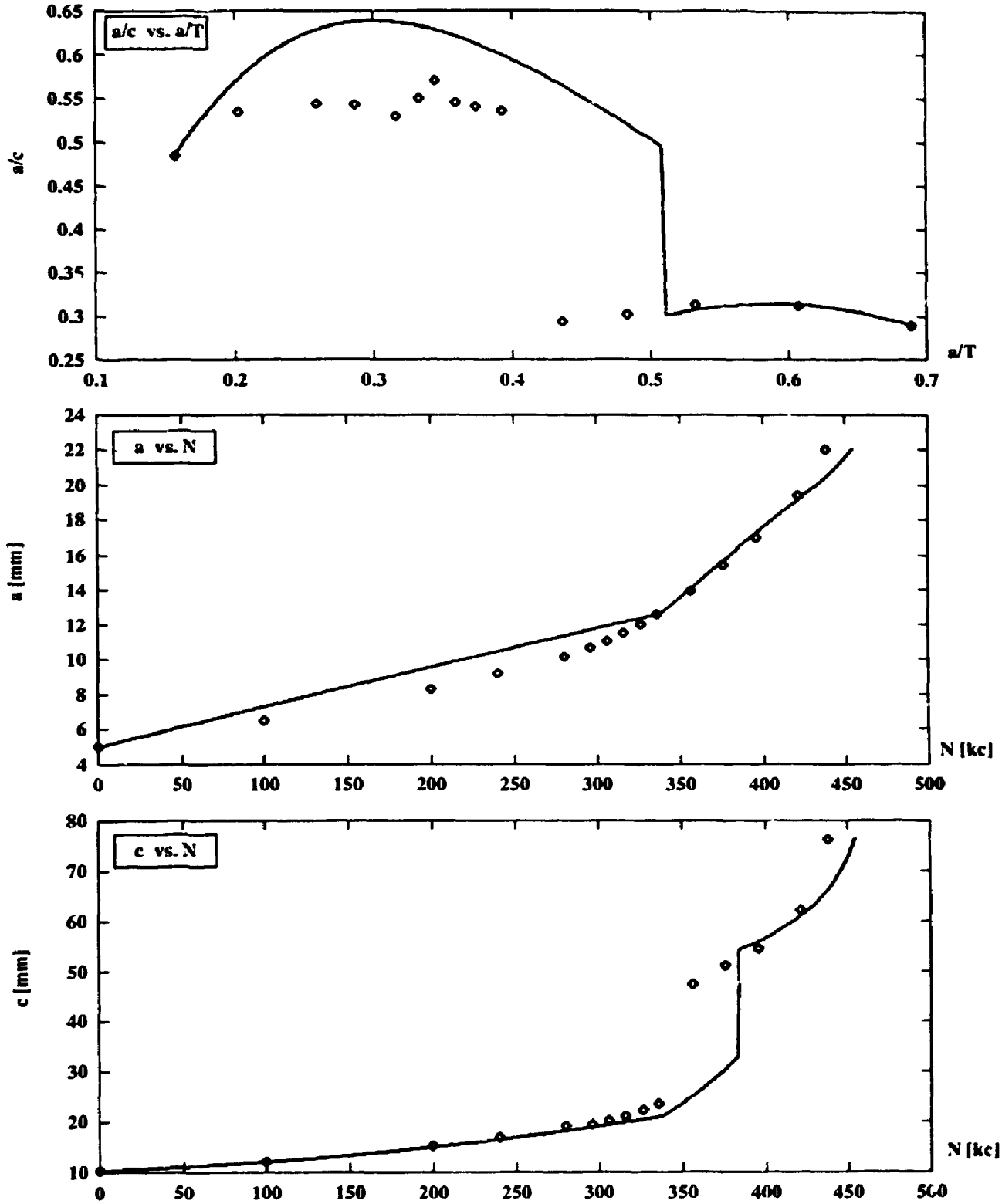

Figure 4.6 Crack shape development of the kSC1 model for specimen FPB6-6

FPB6-6: kSC1 model
Experimental data (Ref. 71)

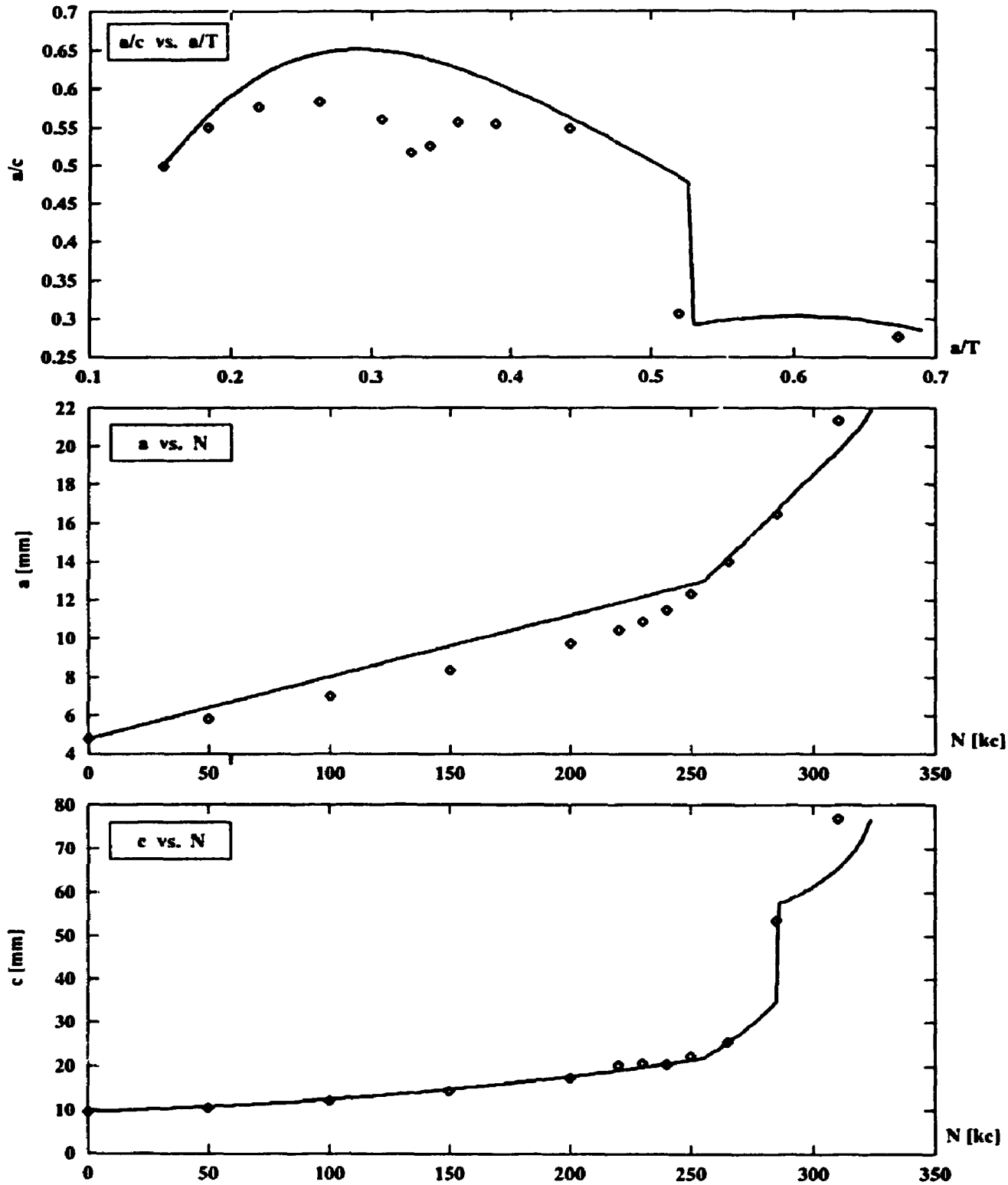

Figure 4.7 Crack shape development of the kSC1 model for specimen FPB6-7

FPB6-7: kSC1 model	———
Experimental data (Ref. 71)	◆

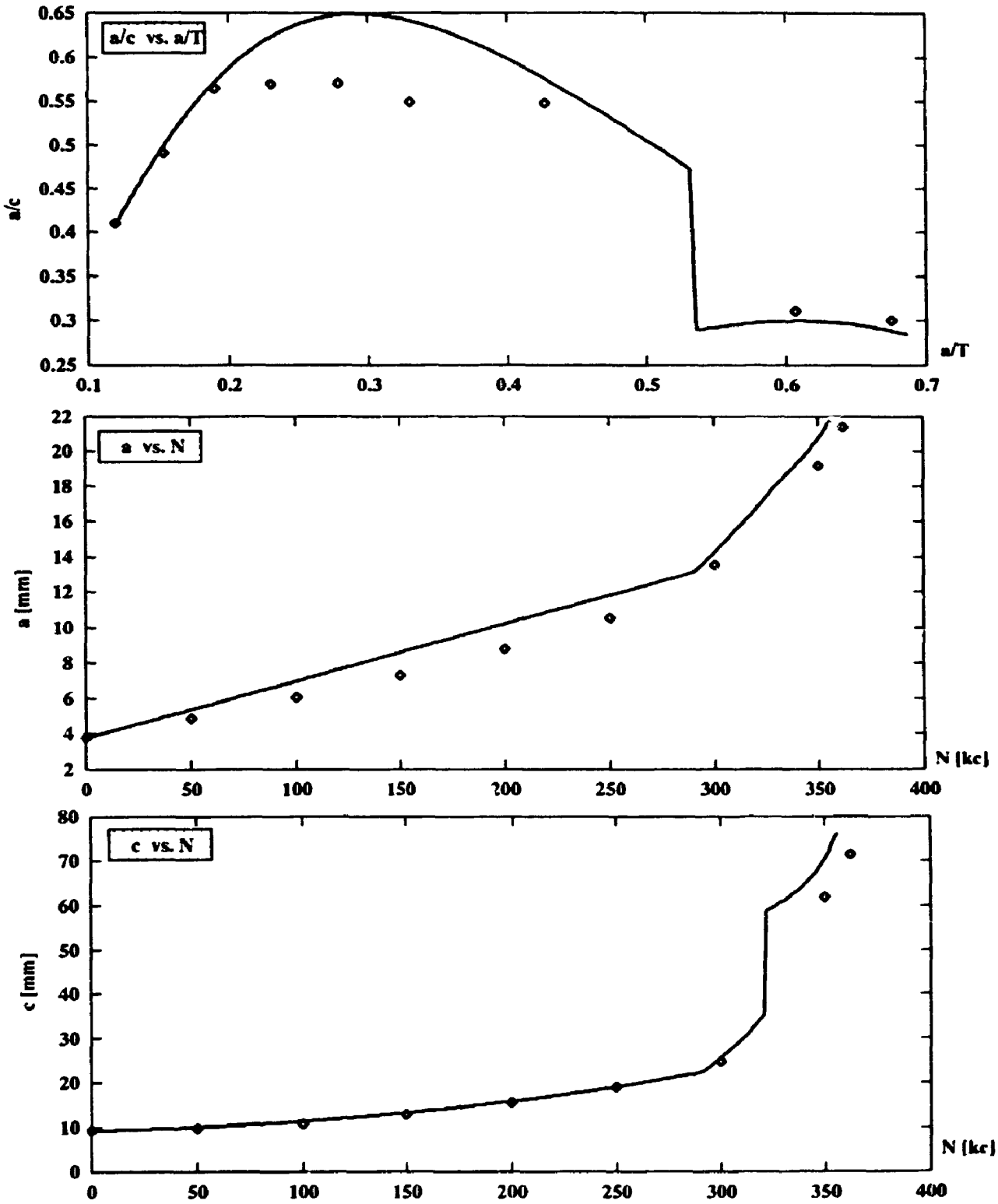

Figure 4.8 Crack shape development of the kSC1 model for specimen FPB6-4

FPB6-4: kSC1 model ——
Experimental data (Ref.71) ◇

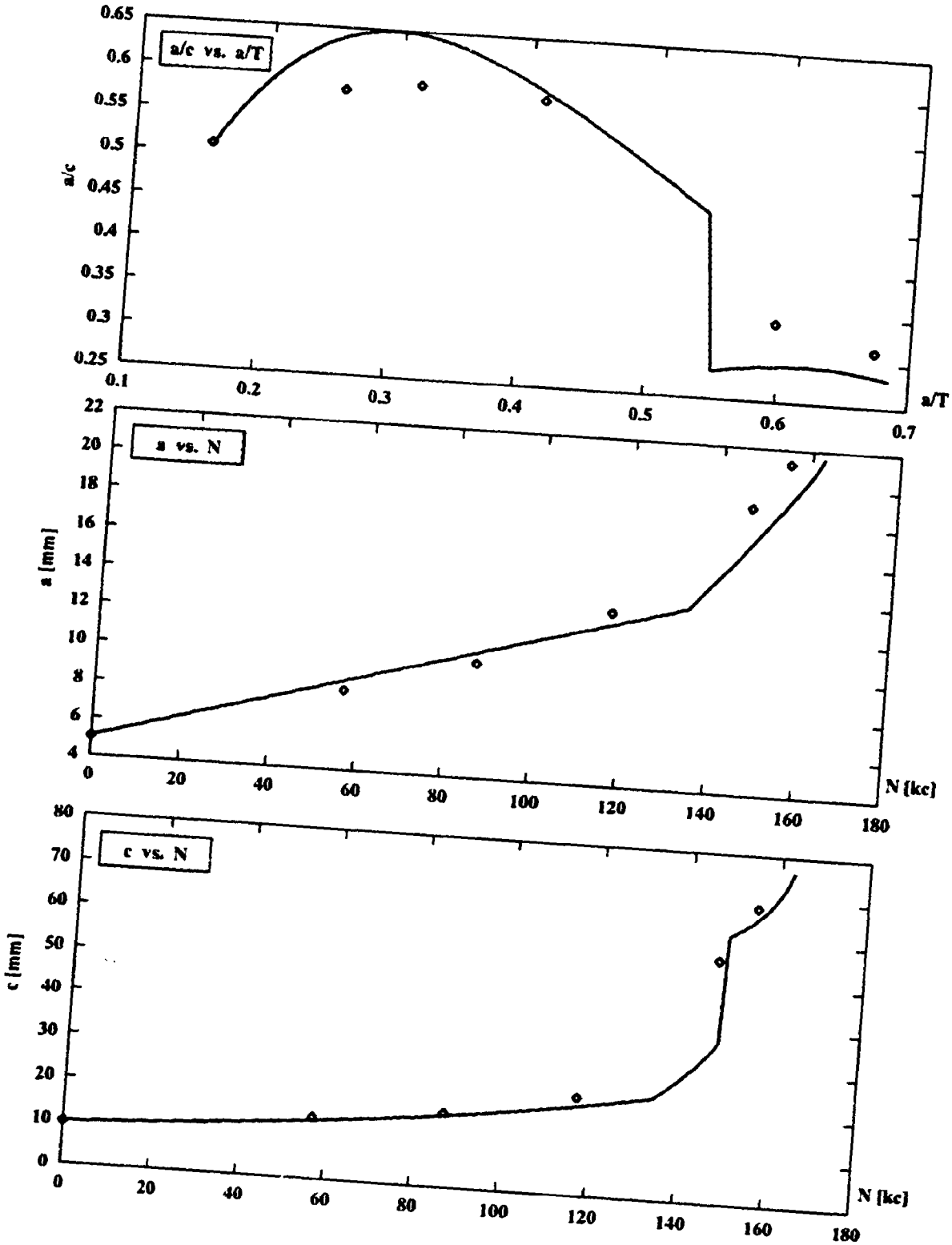

Figure 4.9 Crack shape development of the kSC1 model for specimen FPB6-3

FPB6-3: kSC1 model ——
Experimental data (Ref.71) ◇

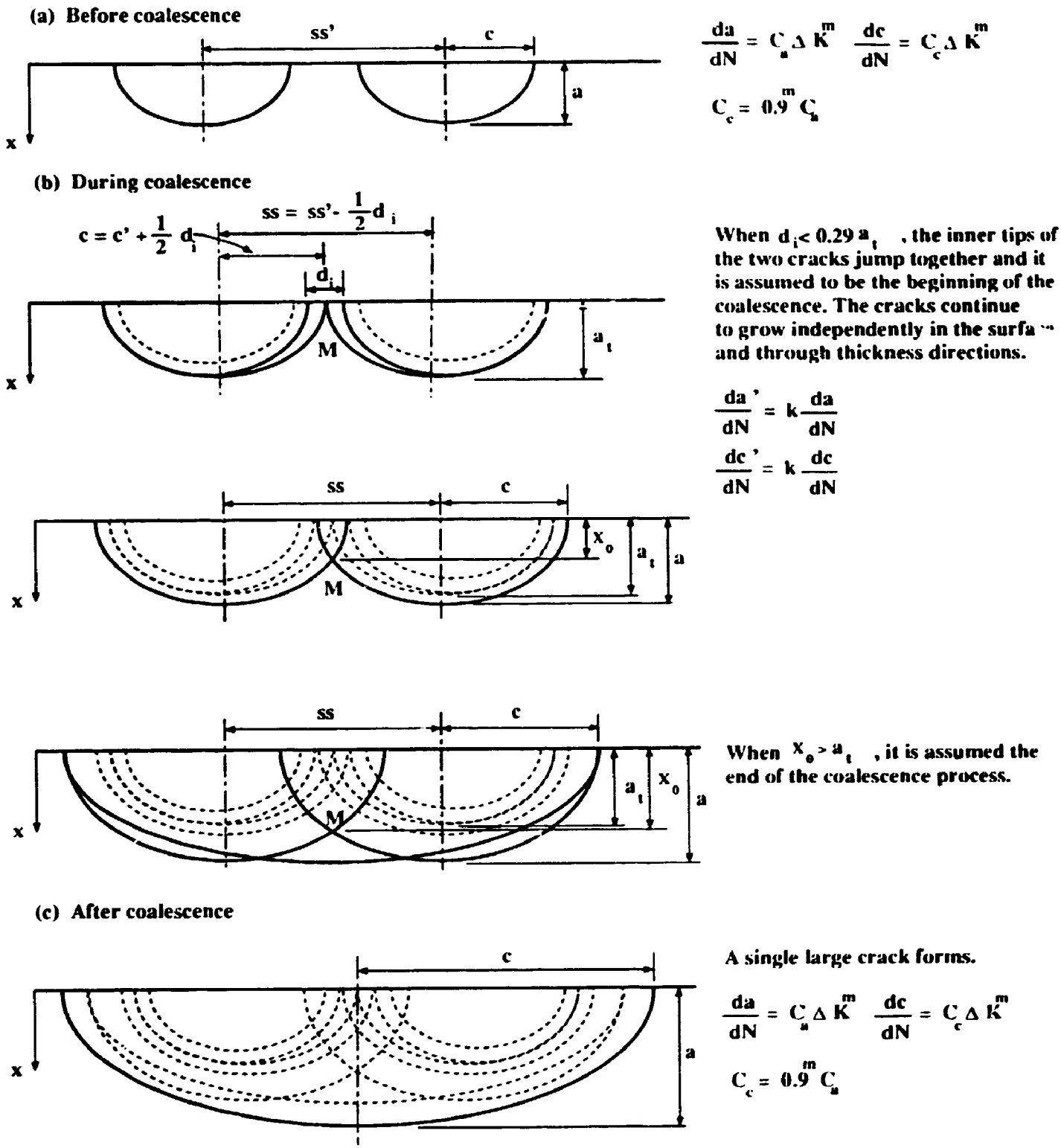

Figure4.10 The three stages of coalescence - the interaction model, schematically (The dotted lines represent the previous states of the crack growth profile)

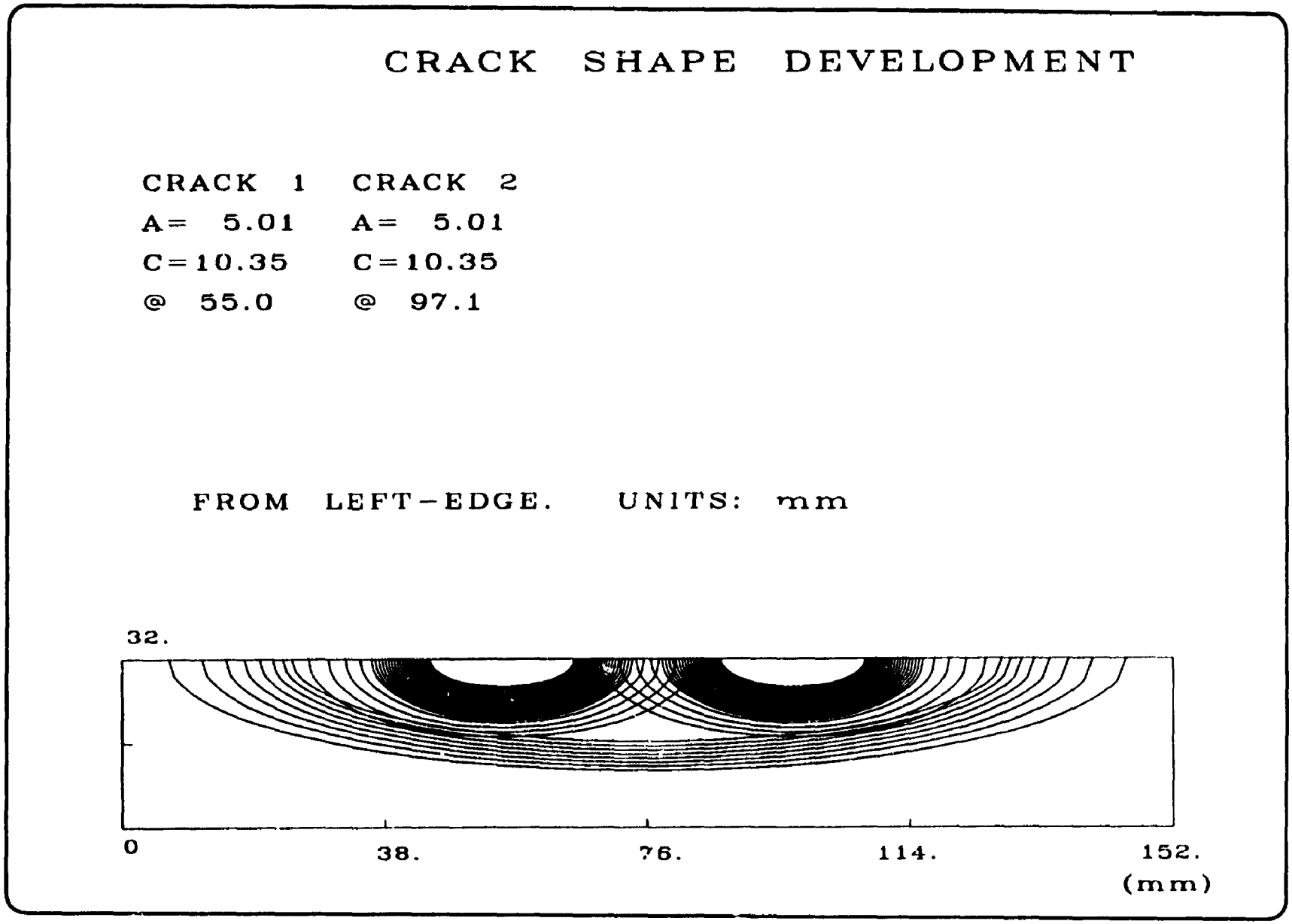

Figure 4.11 Predicted crack growth history of the interaction model with the SC1 shape growth

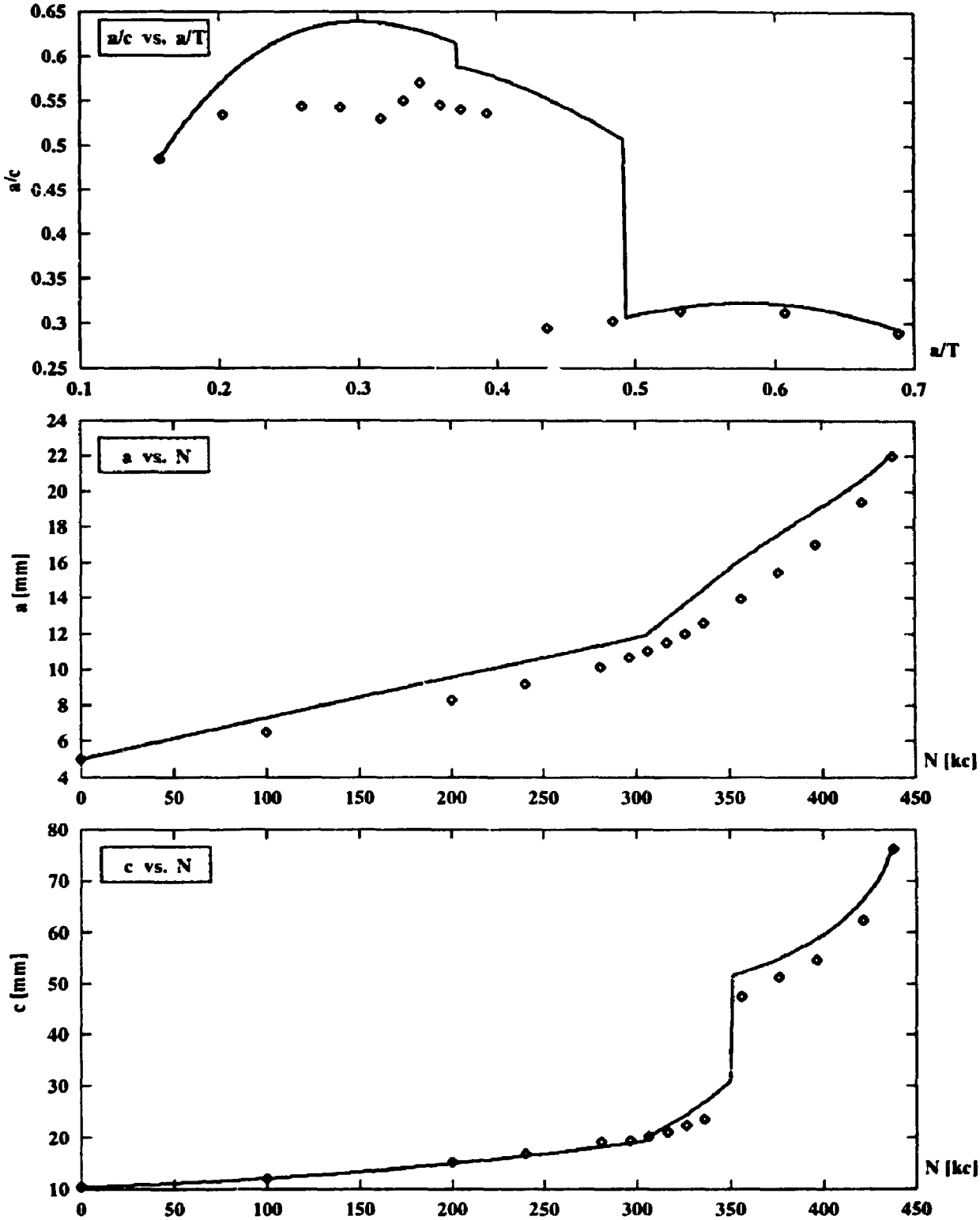

Figure 4.12 Crack shape development of the interaction with the SC1 growth model for specimen FPB6-6

FPB6-6: the interaction with SC1 model	———
Experimental data (Ref.71)	○

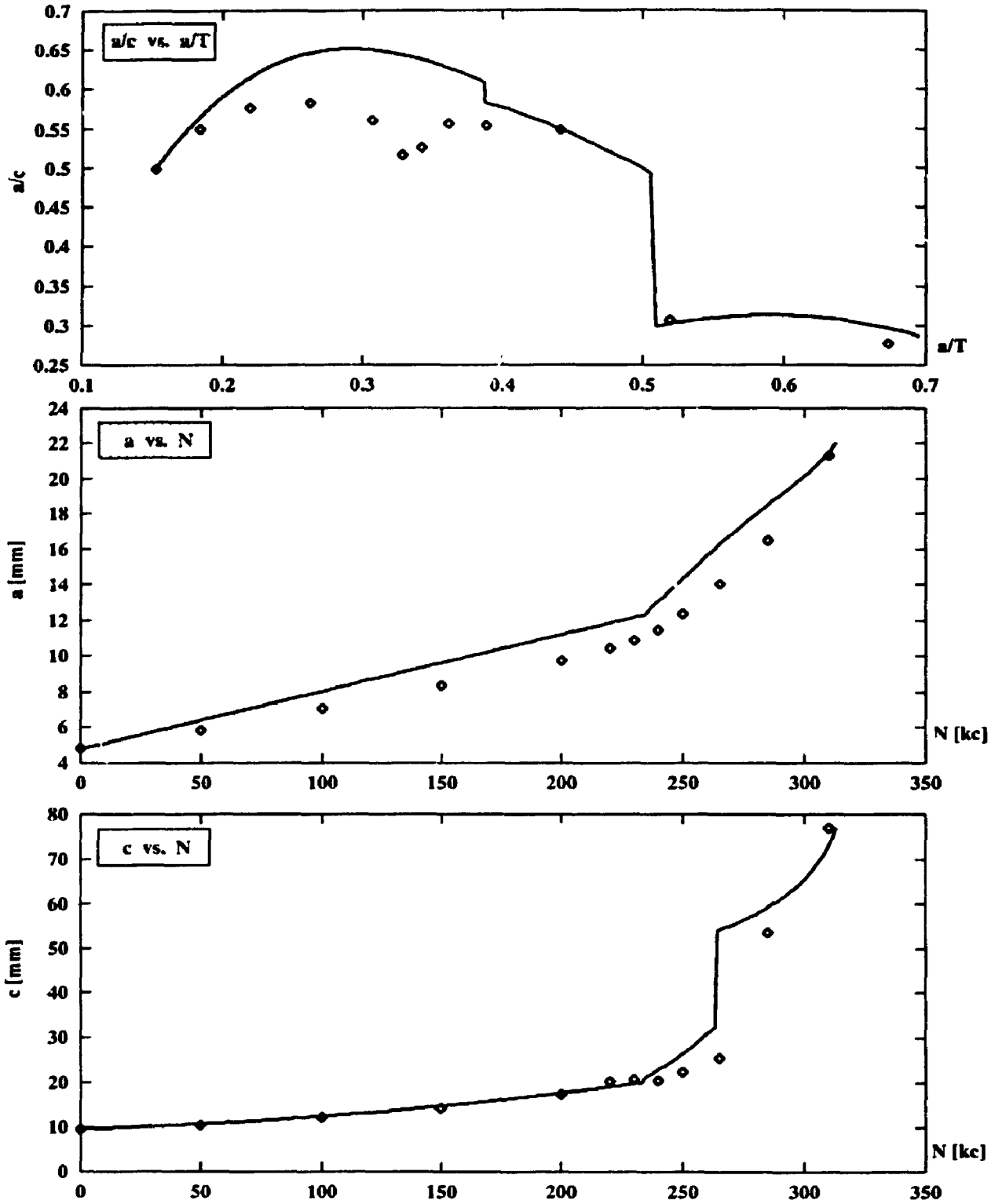

Figure 4.13 Crack shape development of the interaction with the SC1 growth model for specimen FPB6-7

FPB6-7: the interaction with SC1 model	———
Experimental data (Ref.71)	◇

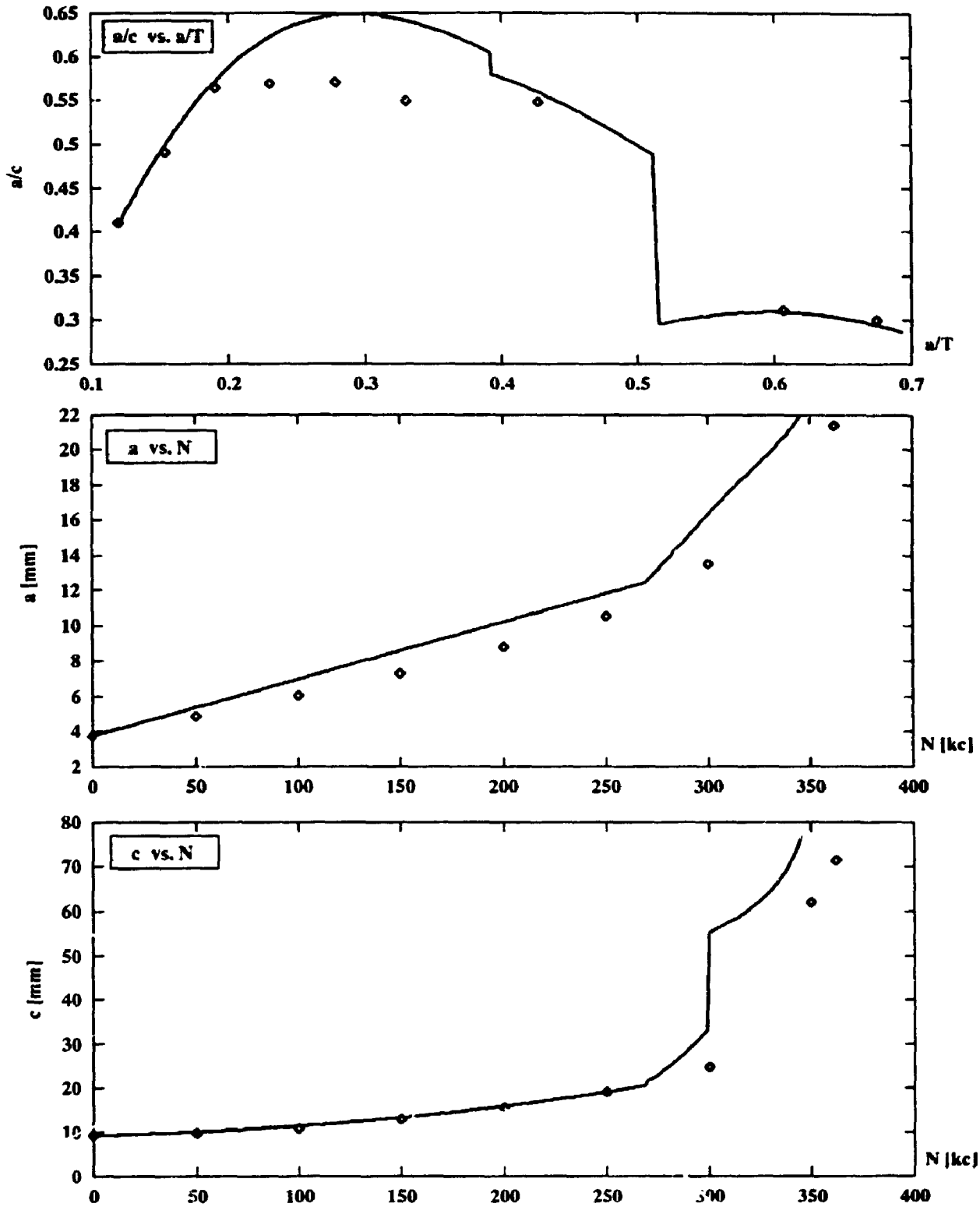

Figure 4.14 Crack shape development of the interaction with the SC1 growth model for specimen FPB6-4

FPB6-4: the interaction with SC1 model	———
Experimental data (Ref.)	◆

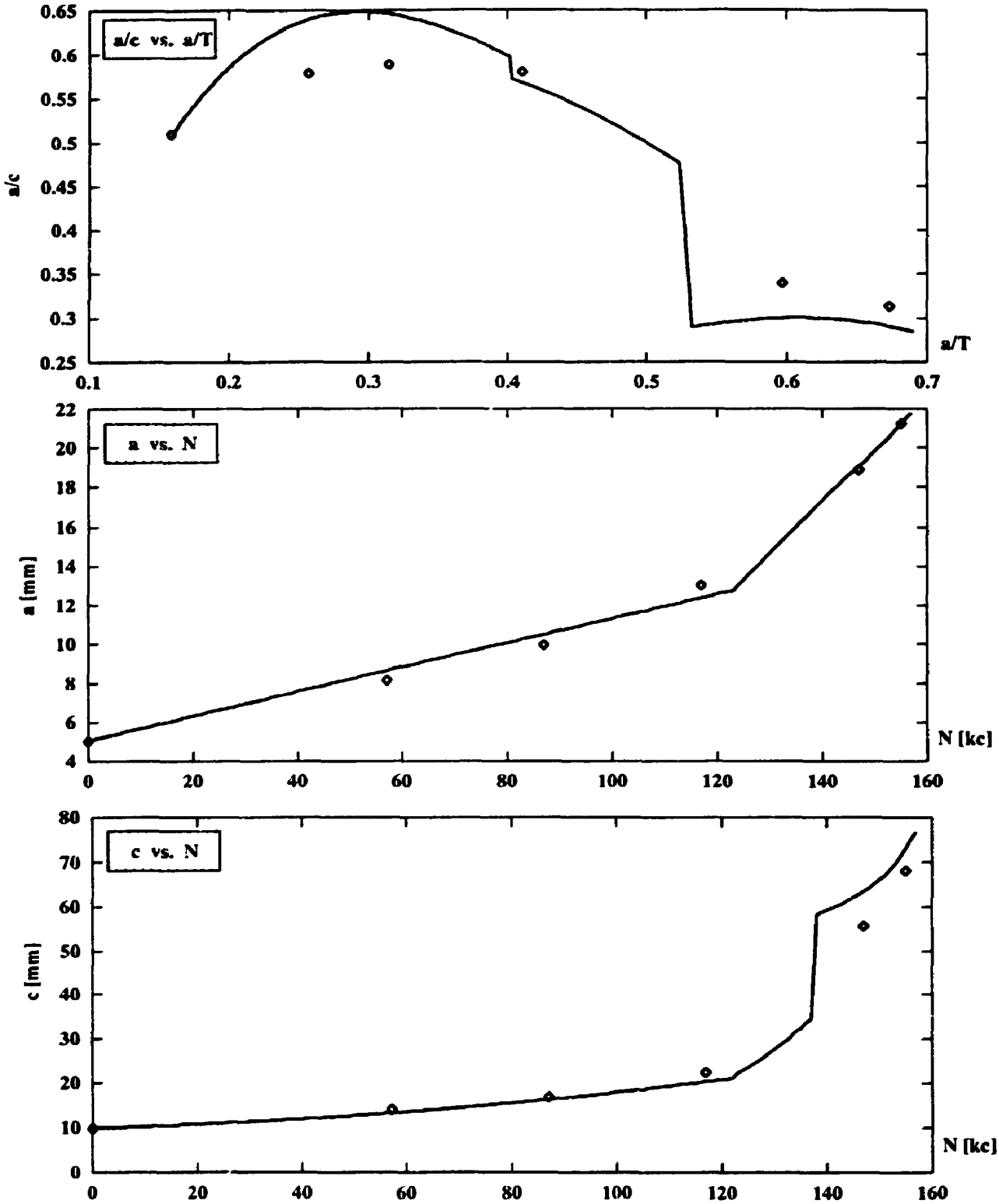

Figure 4.15 Crack shape development of the interaction with the SC1 growth model for specimen FPB6-3

FPB6-3: the interaction with SC1 model	——
Experimental data (Ref.71)	◆

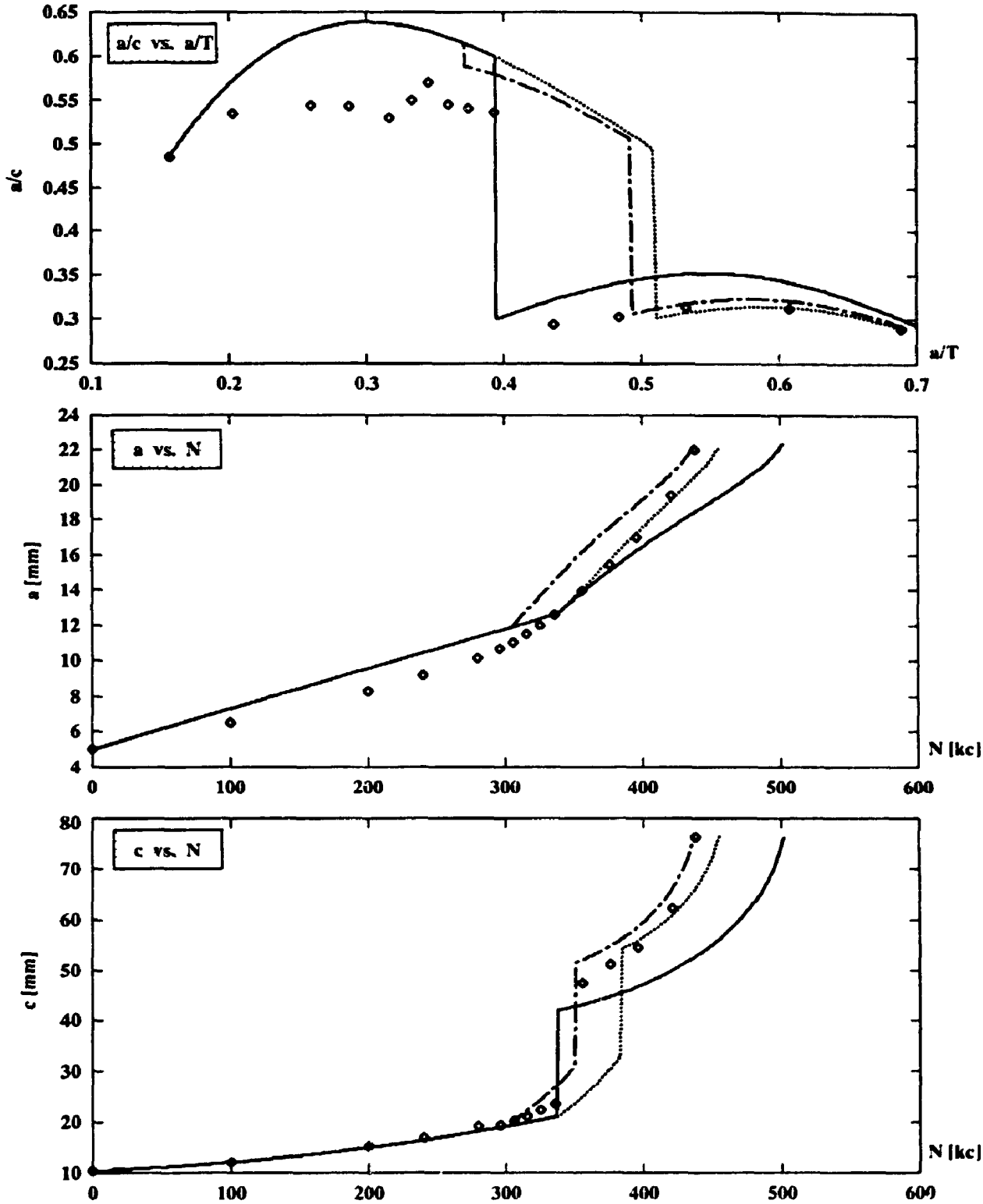

Figure 4.16 Comparison of the crack shape development of the kSC1 model, the interaction and Iida models with the SC1 for specimen FPB6-6

The Iida with the SC1 model	———
The kSC1 model	·····
The interaction with the SC1 model	—·—·—
Experimental data (Ref.71)	◇

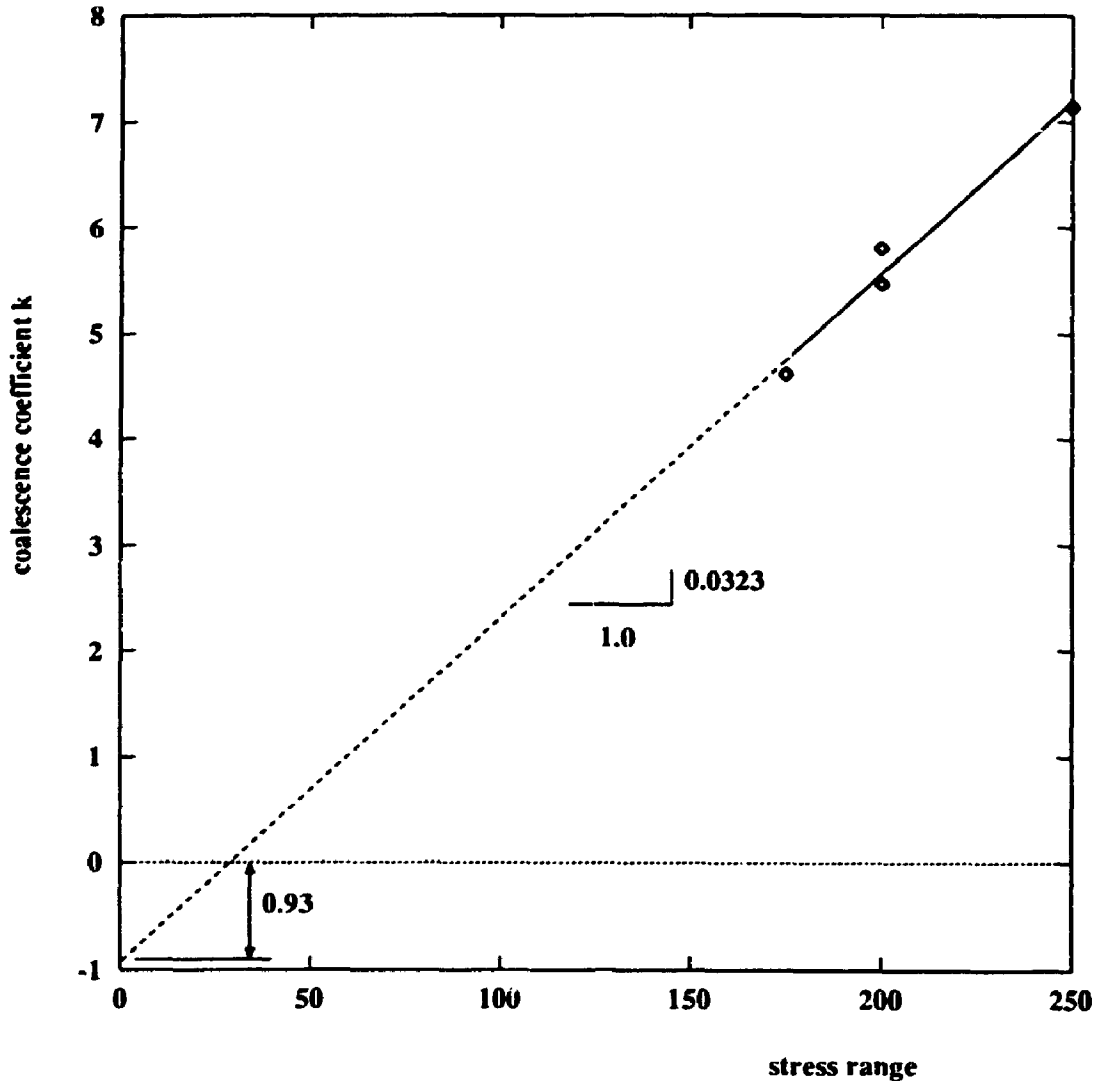

Figure 4.17 The coalescence coefficient related to the stress range for the kSC2 model

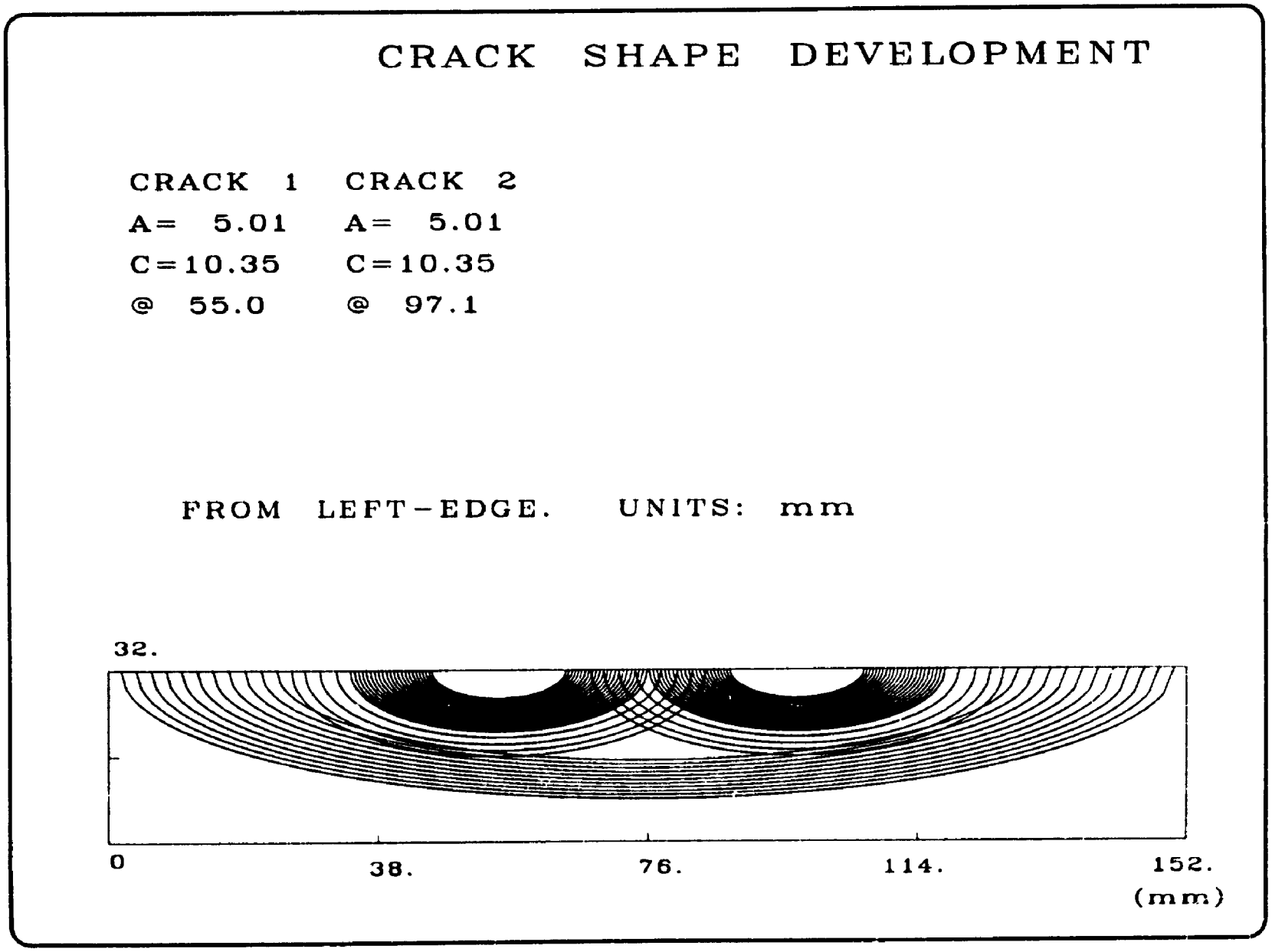

Figure 4.18 Predicted crack growth history of the kSC2 model

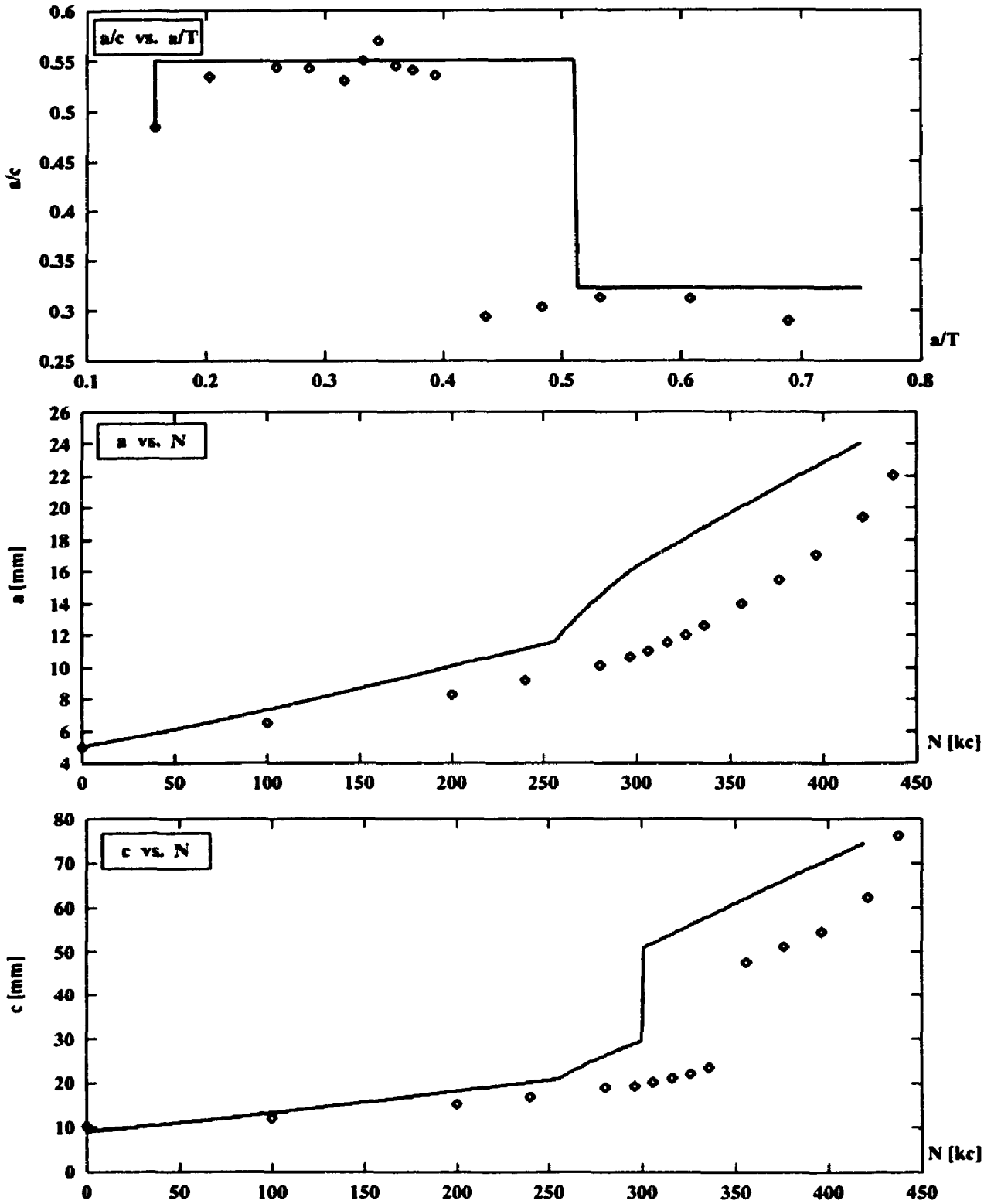

Figure 4.19 Crack shape development of the kSC2 model for specimen FPB6-6

FPB6-6: the kSC2 model ——
Experimental data {Ref.71} ◇

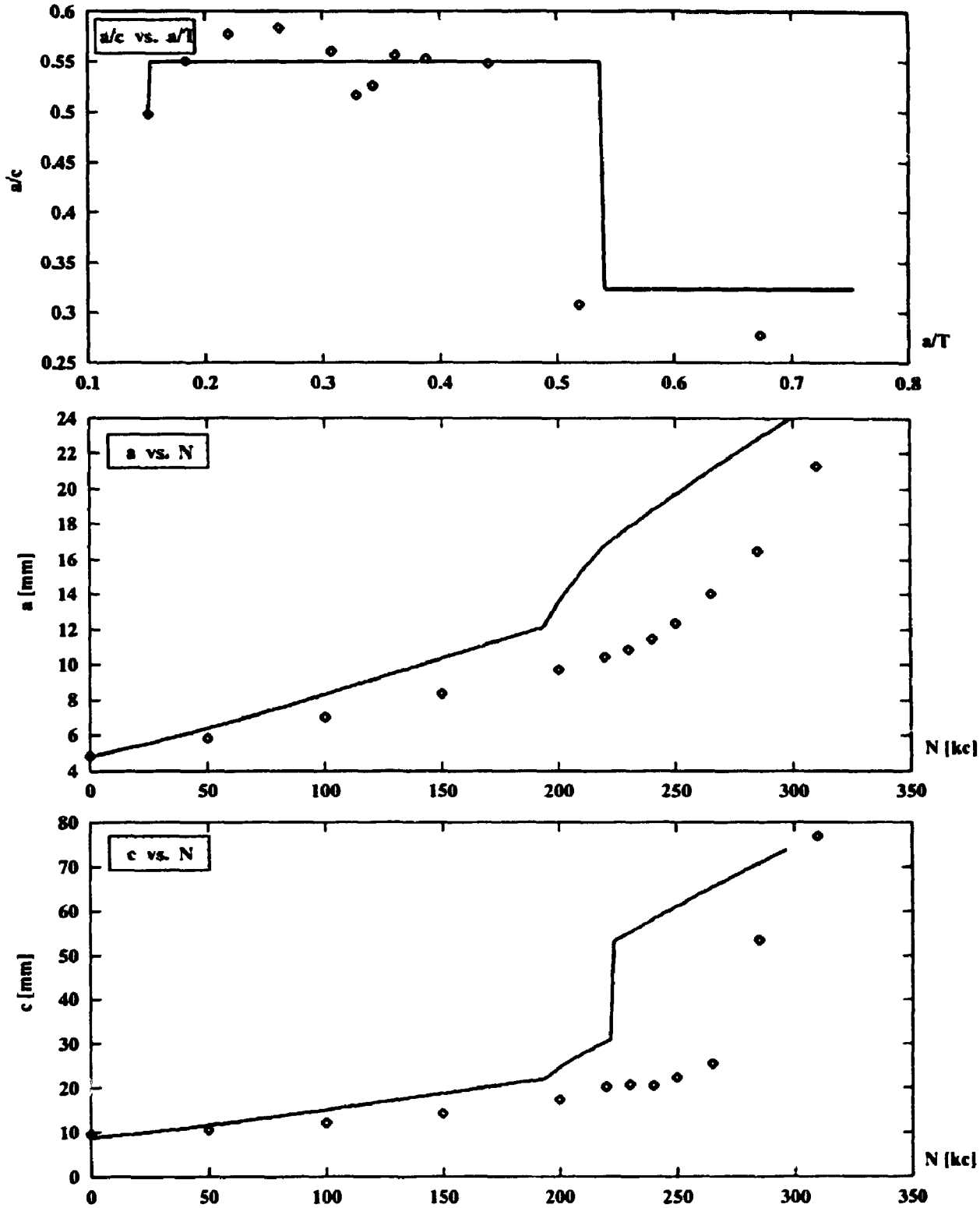

Figure 4.20 Crack shape development of the kSC2 model for specimen FPB6-7

FPB6-7: the kSC2 model	———
Experimental data (Ref.71)	◇

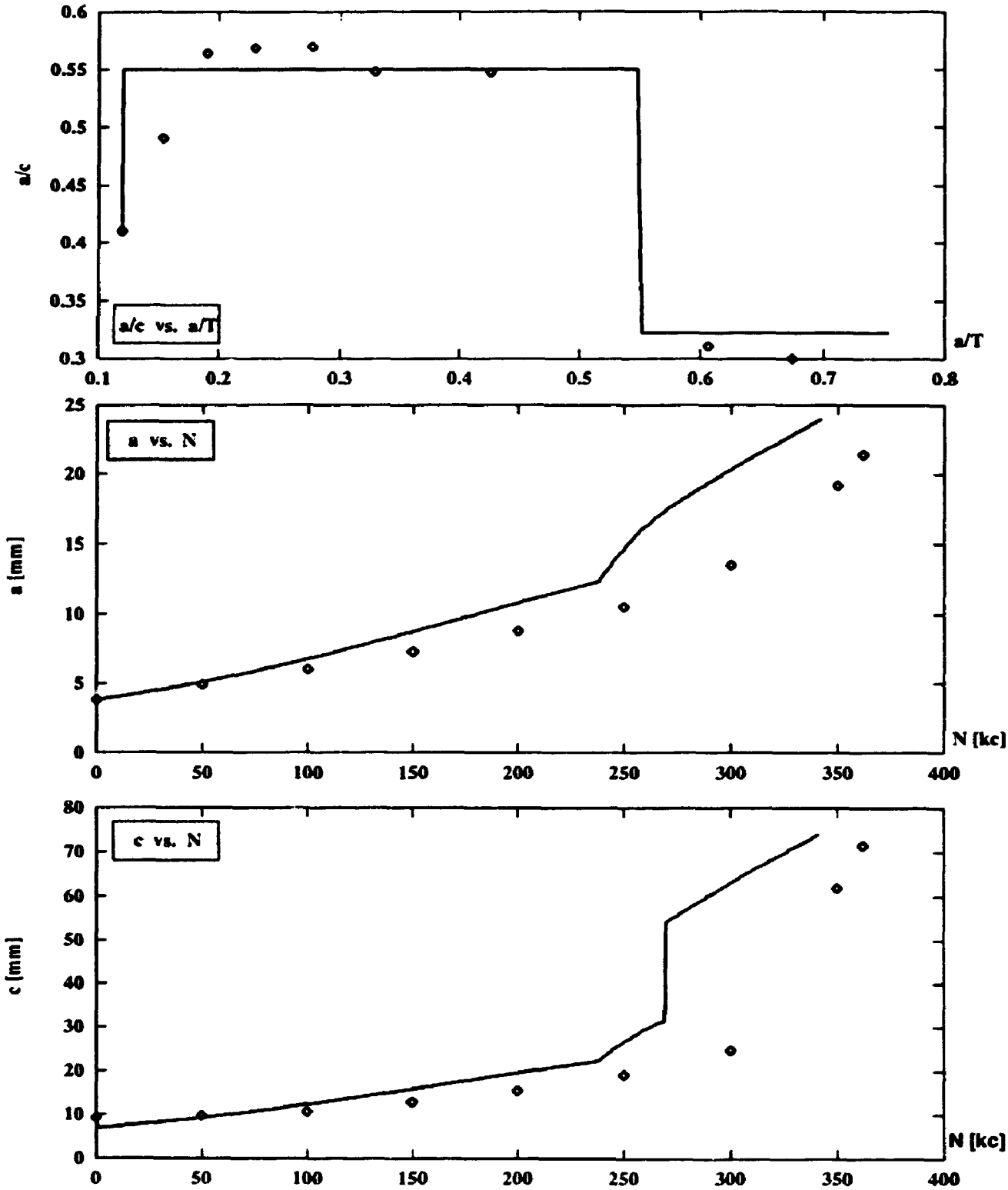

Figure 4.21 Crack shape development of the kSC2 model for specimen FPB6-4

FPB6-4: the kSC2 model	———
Experimental data (Ref.71)	◇

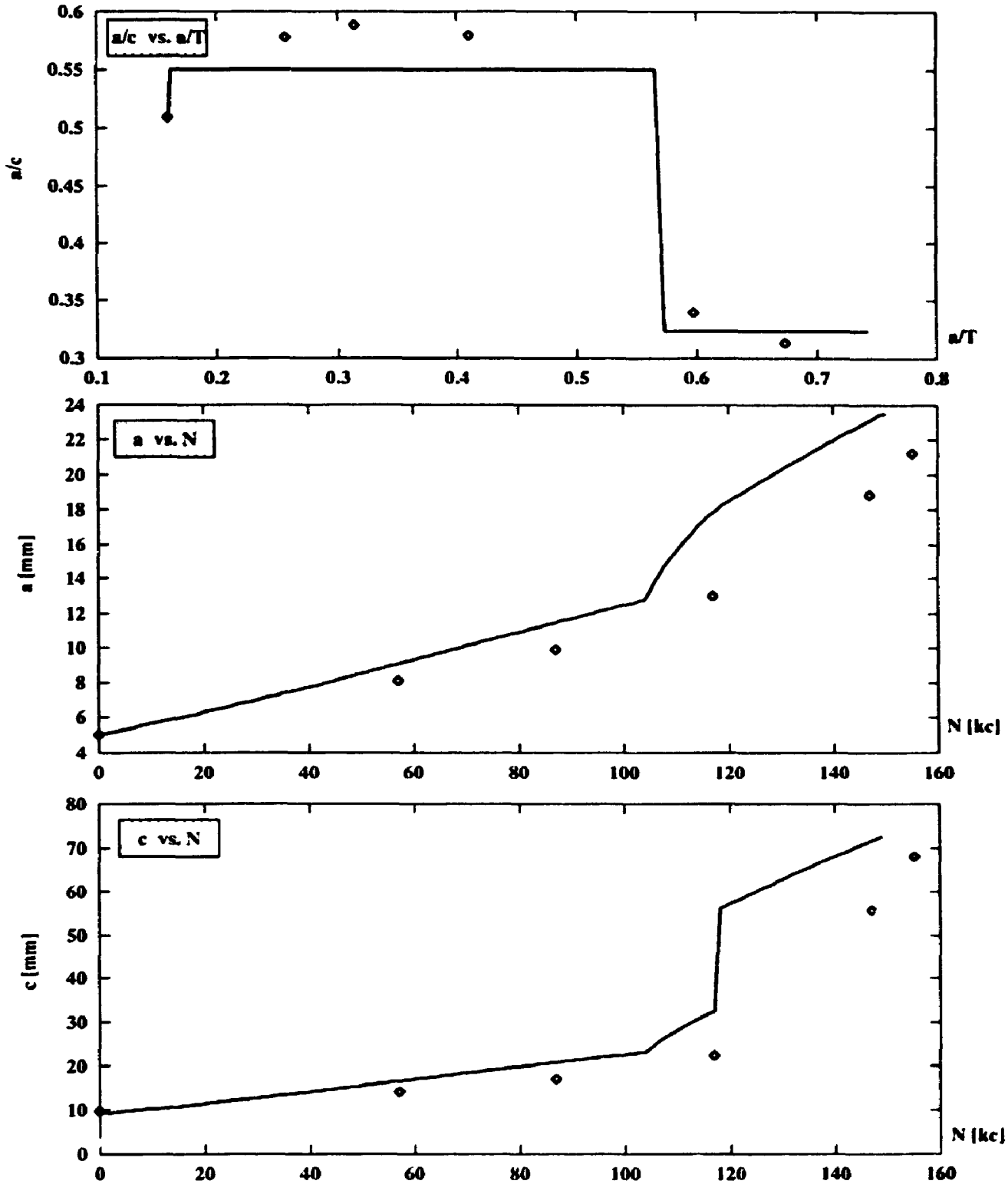

Figure 4.22 Crack shape development of the kSC2 model for specimen FPB6-3

FPB6-3: the kSC2 model	———
Experimental data (Ref.71)	◆

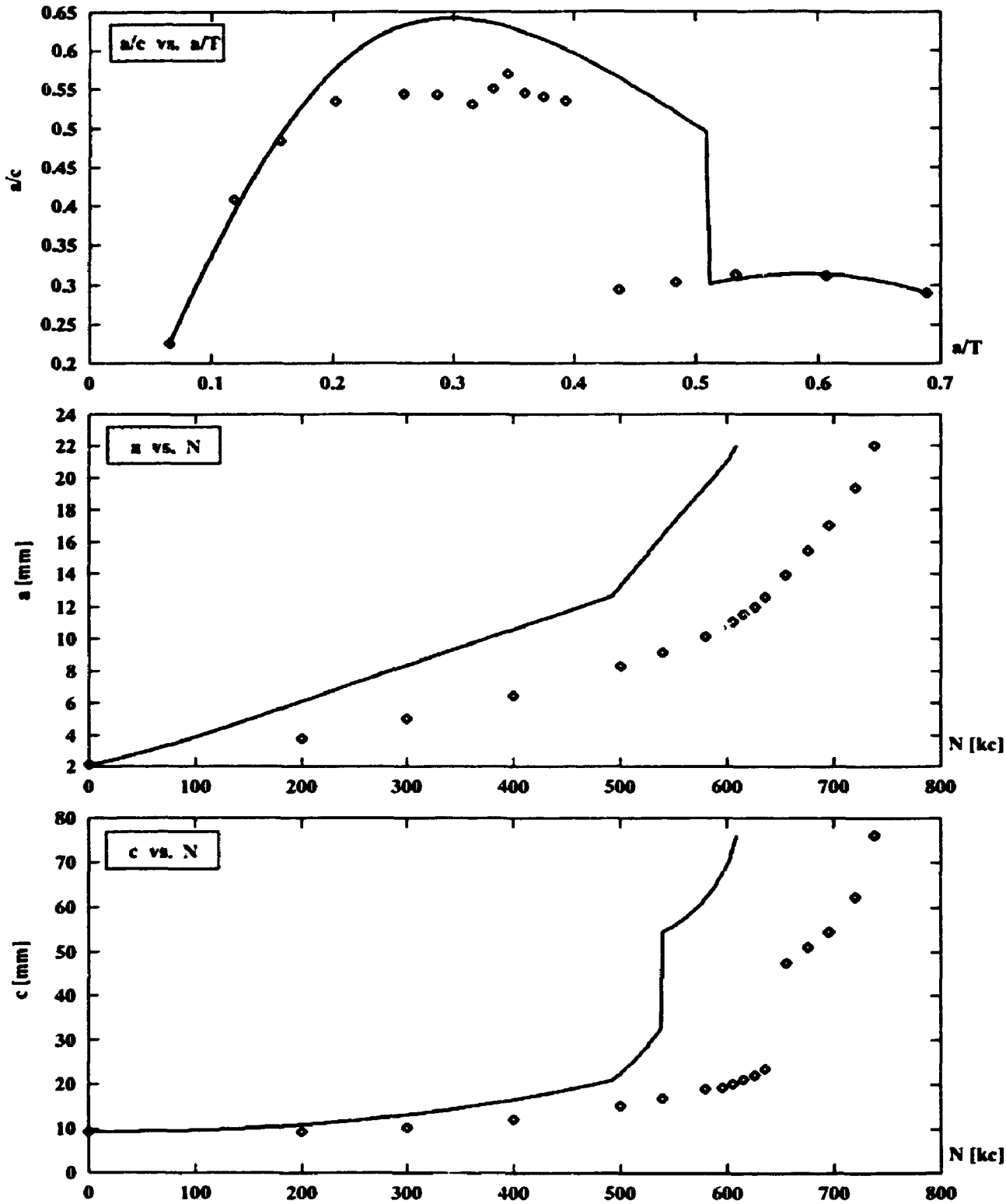

Figure 4.23 Saw cut and initiation effects on the fatigue life of the kSC1 model for specimen FPB6-6

FPB6-6: the kSC1 model	———
Experimental data (Ref.71)	◇

CHAPTER V: Conclusions and Future Study

5.1 Conclusions

For the objectives in Section 1.2, the following conclusions are made:

1. Modifications to the computer program (COALESCENCE) have been made. It can model single crack growth, multiple crack initiation and coalescence at weld toe and multiple collinear crack growth. The computer graphic output gives on explicit pictorial view of the predicted crack profile.
2. Comparison of the fatigue life using predictive models such as the ASME, BSI, and Iida coalescence model combined with the SC1, SC2 shape model under tensile and bending loads of flat plate has been made. It has been found that the ASME and BSI models predictions are unsatisfactory under the pure bending case. The Iida model with the SC1 provides better simulation of crack shape development and good estimation of fatigue life with +15% difference (specimen FPB6-6) in lifetime.
3. Comparison has been made of the fatigue life of the coalescence models combined with the SC1, SC2 and MC models with the experimental results under pure

bending of the weld specimen. It was found that the ASME, BSI and Iida coalescence models with the Bell 3-D stress intensity equations for welded joints could not model the multi-crack initiation and coalescence at weld toe. But the MC1 shape model with the empirical forcing function and Bell 3-D SIFs gives a better life prediction of the 'T' plate welded joints to within +30% difference to the experimental results.

4. An important objective of this thesis was to model the fatigue crack growth through the coalescence period using fracture mechanics techniques. By using the coalescence factor, the kSC1 model accounts for the crack extension in the coalescence region. Furthermore, the interaction model improves the kSC1 model by accounting for the crack shape change of the interaction effect. Both models based on experimental observations represent a significant improvement in fatigue life prediction to within ±5%. Errors in the prediction of crack shape development can occur due to variability as a consequence of crack initiation on different planes or due to simplify using identical cracks in the prediction.

5. The sensitivity of analyses to the saw cut and initial crack growth was examined. By ignoring this effect on the fatigue life, a reduction in fatigue life of 19% was observed. This result demonstrates the importance of accurate crack growth prediction. It is clear that fracture mechanics is a powerful tool to investigate special influences on the fatigue behaviour of crack growth.

5.2 Recommendations for Future Study

1. The present computer program has a limitation in that it can only determine the twin-identical crack coalescence behaviour. For various crack geometries, there needs to be further study in the growth of cusp region where the intersection point of two cracks grows in two directions. Experimental data of this kind of crack growth is also required.

2. It is important to remember that the coalescence coefficient k and interaction distance d_i are empirical models of a phenomenon. Care should be used when extrapolating these empirical modification factors beyond the range of the loading or initial crack conditions used to generate them.

3. The finite element method can be used to evaluate the stress intensity factor at the ligament region and simulate the coalescence process.

As was pointed out in chapter II, coalescence is a very complex process. The more that can be learnt about this process, the better it will be able to predict fatigue performance in service conditions.

References

1. **R. Irwin**, J. Appl. Mech., 24, 361, 1957.

2. **H.M. Westergaard**, J. Apl. Mech., 61, A49, 1939.

3. **H. Tada, P.C. Paris and G.R. Irwin**, "The Stress Analysis of Cracks Handbook", Del Research Corporation, Hellertown, pennsylvania, 1973.

4. **G.C. Sih**, "Handbook of Stress Intensity Factors", Lehigh Univesity, Bethlehem Pennsylvania, 1973.

5. **D.P. Rooke and D.J. Cartwright**, "A Compendium of Stress Intensity Factors", HMSO, London, 1976.

6. **E.B. Shields, T.S. Srivatsan and J. Padovan**, "Analytical Methods for Evaluation of Stress Intensity Factors and Fatigue Crack Growth", Engineering Fracture Mechanics, Vol. 42, No.1, pp1-26, 1992.

7. **A. Hosseini and M.A. Mahmoud**, "Evaluation of Stress Intensity Factor and Fatigue Growth of Surface Cracks in Tension Plates", Engineering Fracture Mechanics, Vol. 22, No.6, pp.957-974, 1985.

8. **W.O. Soboyejo, K. Kishimoto, R.A. Smith and J.F. Knott**, "A Study of the Interaction and Coalescence of Two Coplanar Fatigue Cracks in Bending", Fatigue Fract. Engng Mater. Struct. Vol. 12, No.3, pp.167-174, 1989.

9. **W.O. Soboyejo, J.F. Knott, M.J. Walsh and K.R. Cropper**, "Fatigue Crack Propagation of Coplanar Semi-elliptical Cracks in Pure Bending", Engineering Fracture Mechanics, Vol. 37, No.2, pp.323-340, 1990.

10. **K. Iida, and M. Kawahara**, "Propagation and Coalescence of Fatigue Cracks Initiated from Collinear or Parallel Adjacent Surface Flaws", 4th International Conference on Pressure Vessel Technology, Vol.1, Materials, Fracture and Fatigue, 1980.

11. **K. Kishimoto, W.O. Soboyejo, R.A. Smith and J.F. Knott**, "A Numerical investigation of the Interaction and Coalescence of Twin Coplanar Semi-elliptical Fatigue Cracks", Int. J. Fatigue, March 1989.

12. **G.R. Irwin**, "Crack-Extension Force for a Part-Through Crack in a Plate", J. Appl. Mech. 29,651-654,1962.

13. **F.W. Smith and M.J. Alavi**, "Stress-Intensity Factors for a Penny Shaped Crack in a Half Space", Engng. Fracture Mech. 3, 241-254, 1971.

14. **A. Carpinter**, "Stress-intensity Factors for Semi-elliptical Surface Cracks Under Tension or Bending", Engineering Fracture Mechanics, Vol.38, No.4/5, pp.327-334, 1991.

15. **R. Bell**, "Stress Intensity Factors for Weld Toe Cracks in Welded 'T' Plate Joints", DSS Contract OST84-00125, Faculty of Engineering, Carleton University, Ottawa, May 1987.

16. **R. Bell and J. Kirkhope**, "Determination of Stress Intensity Factors for Weld Toe Defects", DSS Contract OSU82-00233, Phase I Report, Faculty of Engineering, Carleton University, Ottawa 1984.

17. **R. Bell**, "Determination of Stress Intersity Factors for weld Toe Defects", DSS Contract OST84-00125, Phase II Report, Faculty of Engineering, Carleton University, Ottawa, 1985.

18. **X. Niu and G. Glinka**, "Weight Functions for Edge And Surface Semi-elliptical Cracks In Flat Plates And Plates With Corners", Engineering Fracture Mechanics, Vol.36, No.3, pp459-475, 1990

19. **J.C. Newman and I.S. Raju**, "An Empirical Stress-intensity Factor Equation for the Surface Crack", Engineering Fracture Mechanics, Vol.15, No.1-2, pp.185-192, 1981.

20. **P.M. Scott and T.W. Thorpe**, "A Critical Review of Crack Tip Stress Intensity Factors For Semi-eilliptic Cracks", Fatigue of Engineering Materials and Structures, Vol.4, No.4, pp291-309, 1981.

21. **R.J. Hartranft and G.C. Sih**, " Method of Analysis of Crack Problems", pp179-283, Noordhoof, 1973.

22. **R. Koterazawa and S. Minamisaka**, "Stress Intensity Factors of Semi-elliptical Surface Cracks in Bending", J. Soc. Mater. Sci. Jap., 26, 1-7, 1977.

23. **S.J. Holbrook and W.D. Dover**, " The Stress Intensity Factor for a Deep Surface Crack in a Finite Plate", Engng. Fract. Mech. 12, 347-364, 1979.

24. **Y. Murakami and S. Nemat-nasser**, "Growth and Stability of Interacting Surface

Flaws of Arbitrary shape", Engineering Fracture Mechanics, Vol. 17, No.3, pp.193-210, 1983.

25. **R.J. Allen, G.S. Booth and T. Jutla**, "A Review of Fatigue Crack Growth Characteristion by Linear Elastic Fracture Mechanics (LEFM). Part I - Principles and Methods of Data Generation", Fatigue Fract. Engng. Mater. Struct. Vol.11, No.1, pp45-69, 1988.

26. **R.J. Allen, G.S. Booth and T. Jutla**, "A Review of Fatigue Crack Growth Characterisation by Linear Elastic Fracture Mechanics (LEFM). Part II - Advisory Documents and Applications Within National Standards", Fract. Engng. Mater. Struct., Vol. 11, No.2, pp71-108, 1988.

27. **P.C. Paris and F. Erdogan**, "A Critical Analysis of Crack Propogation Law", Trans. ASME, Journal of Basic Engineering, Vol.85, No.4, 1963.

28. **B. Liu and X. Zheng**, "Prediction of Fatigue Crack Growth Rate in Steels", International Journal of Fracture 55: R21-R31, 1992.

29. **T.R. Gurney**, " Fatigue of Welded Structures", The Welding Institute, Cambridge University Press, 2th Edition, 1979.

30. **P.R. Frise**, "Fatigue Crack Growth and Coalescence in a Notch Region", Ph.D. thesis Carleton University, Ottawa, September, 1990.

31. **R.G. Forman, V.E. Kearney and R.M. Engle**, "Numerical Analysis of Crack Propagation in Cyclic-loaded Structures", Trans. ASME, Journal of Basic Engineering, Vol.89, No.3, 1967.

32. **J.E. Collipriest**, "An Experimentalist's View of the Surface Flaw Problem. The Surface Crack: Physical Problems and Computational Solution", ASME, pp43-62, 1972.

33. **W. Schulz**, "Procedures for Prediction of Fatigue Life of Tubular Joints", International Conference on Steel in Marine Structures - Special and Plenary Sessions", Paris, 1981.

34. **D.S. Dugdale**, "Mechanic Physical Solids", 8-100, 1960.

35. **J.R. Rice**, J. Appl. Mech., Trans. ASME, 39, 1968.

36. **J.M. Ferreira**, "Influence of Fillet Weld Joint Geometry on Fatigue Crack Growth", Theoretical and Applied Fracture Mechanics, 15(1991) 131-142.

37. **O. Vosikovsky, R. Bell, D.J. Burns, and U.H. Mohaupt**, "Thickness Effect on Fatigue Life of Welded Joints - Review of the Canadian Program", Eighth International Conference on Offshore Mechanics and Arctic Engineering - Vol.III, ASME.

38. **J.L. Otegui, D.J. Burns, and U.H. Mohaupt**, "Growth and Coalescence of Fatigue Cracks at Weld Toes in Steel", Int. J. Pres. Ves. & Piping 48(1991) 129-165.

39. **T.H. McComb, J.E. Pope and A.F. Grant Jr**, "Growth and Coalescence of Multiple Fatigue Cracks in Polycarbonate Test Specimens", Engineering Fracture Mechanics, Vol. 24, No.4, pp.601-608, 1986.

40. **W.O. Soboyejo, R.C. Reed and J.F. Knott**, "On the Calibration of the Direct Current Potential Difference Method for the Determination of Semi-elliptical Crack Lengths", International Journal of Fracture, 44: 27-41, 1990.

41. **D.S. Harrington and R. Bell**, "A Mobile DCPD Probe Arrangement for Improved Crack Profile Measurement", to be published.

42. **H.G. Morgan**, "Interaction of Multiple Fatigue Cracks", Inter. Conf. "Fatigue of Welded Constructions", Brighton, England, 7-9 April 1987.

43. **S. Melin**, "Why do Cracks Avoid Each Other?", International Journal of Fracture, 23(1983) 37-45.

44. **D.R. Twaddle and J.W. Hancock**, "The Development of Cracks by Defect Coalescence", Coalescence Research Progress, London, September 1988.

45. **P.R. Frise and R. Bell**, "Modelling Fatigue Crack Growth and Coalescence in Notches", Int. J. Pres. Ves. & Piping 51 (1992) 107-126.

46. **ASME**, "Rules for Inservice Inspection of Nuclear Power Plant Components", ASME Boiler and Pressure Vessel Code Section XI Div.1, 1980.

47. **British Standards Institution**, "Guidance on Some Methods for the Derivation Acceptance Levels for Defects in Fusion Welded Joints", B.S.I., PD 6493, 1980.

48. **H.G. Morgan**, "Fatigue Crack Shape Development in Cracked Plates and Welded Joints", C142/86, IMechE 1986.

49. **L. Hodulak, H. Kordisch, S. Kunzelmann and E. Sommer**, "Growth of Part Through Cracks", ASTM STP 677, 399-410, 1979.

50. **M. Kawahara and M. Kurihara**, "Fatigue Crack Growth from a Surface Flaw", Fracture 1977, Vol 2, ICF4, Waterloo, Canada.

51. **S. Wu**, "Shape Change of Surface Crack during Fatigue Growth", Engineering Fracture Mechanics, Vol. 22, No.5, pp897-913, 1985.

52. **M.A. Mahmoud**, "Growth Patterns of Surface Fatigue Cracks under Cyclic Bending - A Quantitative Analysis", Engineering Fracture Mechanics, Vol. 31, No. 2, pp.357-369, 1988.

53. **M.A. Mahmoud**, "Surface Fatigue Crack Growth under Combined Tension and Bending Loading", Engineering Fracture Mechanics, Vol. 36, No.3, pp.389-395, 1990.

54. **M.D. Gilchrist, M.I. Chipalo and R.A. Smith**, "Shape Development of Surface Defects in Tension Fatigued Finite Thickness Plates", Int. J. Pres. Ves. & Piping 49 (1992) 121-137.

55. **B.J. Heath and A.F. Grandt Jr**, "Stress Intensity Factors for Coalescing and Single Corner Flaws along a Hole Bore in a Plate", Engineering Fracture Mechanics, Vol.19, No.4, pp665-673, 1984.

56. **O. Vosikovsky, R. Bell, D.J. Burns and U.H. Mohaupt**, "Fracture Mechanics Assessment of Fatigue Life of Welded Plate T-joints including Thickness Effect", Proceeding of the 4th International Conference on Behaviour of Offshore Structure, the Netherland, 1985.

57. **R. Bell, O. Vosikovsky, D.J. Burns and U.H. Mohaupt**, "A Fracture Mechanics Model for Life Prediction of Welded Plate Joints", Proceeding of the 3rd International ECSC Offshore Conference on Steel in Marine Structure, the Netherland, 1987.

58. **R. Bell and O. Vosikovsky**, "Fatigue Life Prediction of Welded Joints for Offshore Structures under Variable Amplitude Loading", 1991 OMAE - Volume III-B, Materials Engineering ASME - 1991.

59. **M. Klensnil and P. Lukas**, "Influence of Strength and Stress History on Growth and Stabilization of Fatigue Cracks", Engineering Fracture Mechanics, Vol.4, 1972.

60. **T.R. Gurney and G.O. Johnston**, "A Revised Analysis of the Influence of Toe Defects on the Fatigue Strength of Transverse Non-Load Carrying Fillet Welds", Welding Institute International, 9-3, 1979

61. **S.J. Maddox**, "The Effect of Plate Thickness on the Fatigue Strength of Fillet

Welded Joints", The Welding Institute, 1987.

62. **R. Yee, D.J. Burns, U.H. Mohaupt, R. Bell and O. Vosikovsky**, "Thickness Effect and Fatigue Crack Development in Welded T-joints", Journal of Offshore Mechanics and Arctic Engineering - Volume 112, November 1990.

63. **N.S. McFadyen**, "Fatigue Crack Growth in Semi-elliptical Surface Cracks", Carleton University, Master's thesis, 1987.

64 **T. Miyoshi, M. Shiratori and O. Tanabe**, "Stress Intersity Factors for Surface Crack with Arbitrary shapes in Plates and Shells", Fracture Mechanics 16th Symp., ASTM STP 868, 521-534, American.

65. **J.A. Battjes**, "Behaviour of Offshore Structures", Proceedings of the 4th International Conference on Behaviour of Offshore Structures (BOSS '85), Delft, The Netherlands, July 1-5, 1985.

66. **C. Noordhoek and J. de Back**, "Steel in Marine Structures", Proceedings of the 3rd International ECSC Offshore Conference on Steel in Marine Structures (SIMS '87), Delft, The Netherlands, June 15-18, 1987.

67. **M. Yoda**, "Growth and Coalescence of Two Collinear Indentation Cracks In Glass", Int. J. fatigue, No.11, pp429-432, 1989.

68. **T. Tanaka, T. Sakai and K. Okada**, "A Statistical Study on Fatigue Life Distribution Based on the Coalescence of Cracks from Surface Defects", Bulletin of JSME, Vol. 28, No.236, February 1985.

69. **P.R. Frise and R. Bell**, "Fatigue crack Growth and Coalescence at Notches", Int. J. Fatigue 14, No.1, pp51-56, 1992.

70 **T.R. Gurney**, "Some Comments on Fatigue Design Rules for Offshore Structures", Proceedings of 2nd International Symposium on Integrity of Offshore Structures, Applied Science Publishers, Barking, Essex, 1981.

71 **D.S.Harrington**, Private Conversations

END

21-07-94

FIN